8-2017

Targeting Epigenetic Regulators for the Treatment of Diffuse Large B-Cell Lymphoma

Aarthi Goverdhan

TARGETING EPIGENETIC REGULATORS FOR THE TREATMENT OF DIFFUSE LARGE B-CELL LYMPHOMA

by

Aarthi Goverdhan, B.S.

APPROVED:

_____
Mien-Chie Hung, Ph.D.
Advisory Professor

_____
Mark T. Bedford, Ph.D.

_____
Paul Chiao, Ph.D.

_____
Richard E. Davis, M.D.

_____
Min Gyu Lee, Ph.D.

APPROVED:

_____
Dean, The University of Texas
MD Anderson Cancer Center UTHealth Graduate School of Biomedical Sciences

TARGETING EPIGENETIC REGULATORS FOR THE TREATMENT OF DIFFUSE LARGE B-CELL LYMPHOMA

A

DISSERTATION

Presented to the Faculty of

The University of Texas

MD Anderson Cancer Center UTHealth

Graduate School of Biomedical Sciences

in Partial Fulfillment

of the Requirements

for the Degree of

DOCTOR OF PHILOSOPHY

by

Aarthi Goverdhan, B.S.
Houston, Texas

August, 2017

ACKNOWLEDGMENTS

This dissertation is dedicated to the wonderful people in my life who have always believed in me.

My family- I have endeavored to become the best version of myself because of them. As a medical professional, my father introduced me to the wonder and power of science when I was a kid, which started me along this path to study a terrible disease that has touched so many lives, including members of our own family.

My friends- for being there when I needed them. I especially want to thank my best friends Dr. Maitri Shah and Dr. Shubhi Randhawa. This long and tumultuous journey would not have been possible without their unconditional support and encouragement.

My lab colleagues- for helping me navigate through scientific problems and for molding my thought process through constructive criticism. I would especially like to thank an outstanding postdoctoral fellow in my lab, Dr. Heng-Huan Lee, for overseeing my dissertation projects and helping me troubleshoot problems along the way. Former and current lab members who mentored and supported me during the process: Dr. Yekaterina (Kat) Khotskaya, Dr. Shih-Shin Chang, Dr. Mariano Ponz-Sarvise, Dr. Wen-Hsuan (Rose) Yu, Dr. Seung-Oe Lim, and Dr. Chao-Kai Chou.

I am deeply grateful to my advisor Dr. Mien-Chie Hung for taking me in as a graduate student and for being an excellent mentor. I would also like to thank Advisory Committee members for their engaging discussion and guidance. Dr. Paul Chiao: for being on my committee from the first year of graduate school and for helping me through the candidacy exam and project transitions; Dr. Mark Bedford: for guidance throughout the PRMT project; Dr. R. Eric Davis:

for lymphoma discussions and being a co-mentor on the EZH2/BCR project; Dr. Min Gyu Lee: for help with troubleshooting and tackling conceptual problems.

I am thankful to the numerous mentors at GSBS and the Cancer Biology Program who went out of their way to assist me. I also want to thank my fellow students in the Cancer Biology graduate program for making this a fun journey.

TARGETING EPIGENETIC REGULATORS FOR THE TREATMENT OF DIFFUSE LARGE B-CELL LYMPHOMA

Aarthi Goverdhan, B.S.

Advisory Professor: Mien-Chie Hung, Ph.D.

Small-molecule inhibitors of the histone methyltransferase EZH2 hold great promise for the treatment of Germinal Center B-Cell-like Diffuse Large B-Cell Lymphoma (GCB-DLBCL). Compared to a 60% Objective Response Rate (ORR) in Phase I clinical trials, Phase II trial results for the EZH2 inhibitor EPZ-6438 reported an attenuation of response. Mechanisms contributing to lymphoma cell survival and growth after EZH2 ablation are poorly studied. In EZH2-mutant cells, we found that B-Cell Receptor (BCR) signaling was enhanced after EZH2 inhibitor treatment, and associated with an activated B-cell phenotype. Genetic manipulation of BCR, CD19 and CD79A greatly increased sensitivity to the EZH2 inhibitor EPZ-6438. Combination therapy with SYK, PI3Kδ and BTK kinase inhibitors was highly synergistic in multiple lymphoma cell lines, regardless of EZH2 mutation status. At the epigenetic level, prolonged treatment with EPZ-6438 increased global levels of Histone H4 Arginine-3 asymmetric di-methylation. In a subset of lymphoma cell lines, combination therapy with EZH2 and Type I PRMT inhibitors showed synergy. Interestingly, Type I PRMT inhibitors were also highly effective as a single-agent, and mediated apoptosis in lymphoma cells by transcriptionally down-regulating the anti-apoptotic protein BCL2. To summarize, we have identified ways to improve EZH2 inhibitor sensitivity in DLBCL cells and revealed a critical role for the arginine methyltransferase PRMT1 in the regulation of lymphoma growth and survival. Therefore, PRMT1 presents a novel and promising target for the treatment of this cancer type.

TABLE OF CONTENTS

LIST OF ILLUSTRATIONS

LIST OF TABLES

Chapter 1:

INTRODUCTION

1.1 Biology of Germinal Center B-Cells

1.1.1 T-cell-independent and -dependent humoral immunity

As part of our body's adaptive immunity, humoral immune responses stem from antibodies generated by B-cells in response to foreign antigens. Humoral immunity can be further subdivided into T-cell-dependent and -independent types. Athymic mice cannot form germinal centers due to the absence of thymus-derived T-cells. Therefore, Germinal Centers (GC) represent a T-cell-Dependent (TD) immune response. Two signals are required for B-cell activation after initial encounter with antigen. The first signal is binding of the protein antigen to the B-Cell Receptor (BCR), and the second signal is supplied by cognate help from T-cells. On the other hand, athymic mice maintain responsivity to nonprotein antigens, representing T-cell-Independent (TI) responses. TI Type-1 (TI-1) antigens can elicit responses in CBA/N mice, which lack functionality of Bruton's Tyrosine Kinase (BTK), while TI Type-2 (TI-2) antigens are not able to elicit responses in these mice (1). TI-1 antigens, such as gram-negative bacteria-derived Lipopolysaccharides (LPS) and CpG nucleotides, or virally-derived RNA and coat proteins, bind nonspecifically to the BCR and additionally provide a second signal through Toll-like Receptor engagement. TI-2 antigens are typically structurally repetitive, causing extensive crosslinking of the BCR and leading to strong and sustained downstream signaling mediated by BTK. TI-2 antigens are most often derived from bacterial capsular polysaccharides and viral capsids. Follicular B-cells are mainly responsible for TD responses, whereas TI responses are mediated by Marginal Zone (MZ) B-cells and peripheral B-1 cells. B-1 cells offer the earliest and fastest defense against bacterial infection by producing large amounts of IgM, the natural immunoglobulin. MZ B-cells swiftly differentiate into short-lived plasma cells after encountering TI-1 and TI-2 antigens. Although the traditional view has been that TI responses do not generate B-cell memory unlike TD responses, many recent studies have challenged such a view. It is now apparent that there are T-cell-dependent

but GC-independent ways to generate memory B-cells even in response to TI antigens. Rag1-deficient mice receiving B-1b cells from T-cell-deficient donor mice infected with B. hermsii were able to mount a swift immune response when challenged with the pathogen (2). In some cases, TI antigens can lead to the formation of GCs, albeit short-lived and involving very limited affinity maturation of GC B-cells.

1.1.2 The Germinal Center Reaction

The Germinal Center reaction is a T-cell dependent immune response. In secondary lymphoid organs, Dendritic Cells (DCs) in the interfollicular T-cell zone present antigen to naïve CD4+ T-cells, which then mature into Pre-Follicular Helper T-cells (Pre-T_{fh}). The GC reaction is initiated when pre-T_{fh} cells present antigen to naïve B-cells (3). B-cells enter the dark zone, where they undergo clonal expansion and mutate their antibody genes through the process of Somatic Hypermutation (SHM) (4). In this step, EZH2 is critical to maintain proliferation and suppress DNA damage checkpoints which may become activated during hypermutation (5). SHM is largely restricted to the antibody genes, but can sometimes spill over to other genes. Once the cells complete SHM, they move to the light zone, and EZH2 levels decrease. B-cells that have generated antibodies with improved affinity can bind to Follicular Dendritic Cells (FDC) coated with antigen (Figure 1). In turn, these B-cells receive positive selection signals from FDCs and T_{fh} cells (6). These signals are delivered through TNF-superfamily ligands like CD40L, BAFF and APRIL. Binding of these ligands to cognate receptors on the B-cells activate pathways that mediate cell survival, mainly the canonical and non-canonical NFκB pathways. In addition to cell survival, downstream effects of the NFκB pathway include activation of target genes that promote differentiation into different lineages: short-lived and long-lived plasma B-cells, and memory B-cells (7). Some of these cells may re-enter the dark zone to undergo more SHM and acquire antibodies with higher affinity for the antigen. The end result of the germinal center reaction is the generation of effector (plasma) B-cells that

secrete antibodies to clear the infection, and also the production of memory B-cells which remain dormant to fight future infections. Class-Switch Recombination (CSR) occurs in the light zone upon binding of the BCR to antigen. Coupled with CD40 engagement, this leads to IgM class-switching to IgG, IgA or IgE (8).

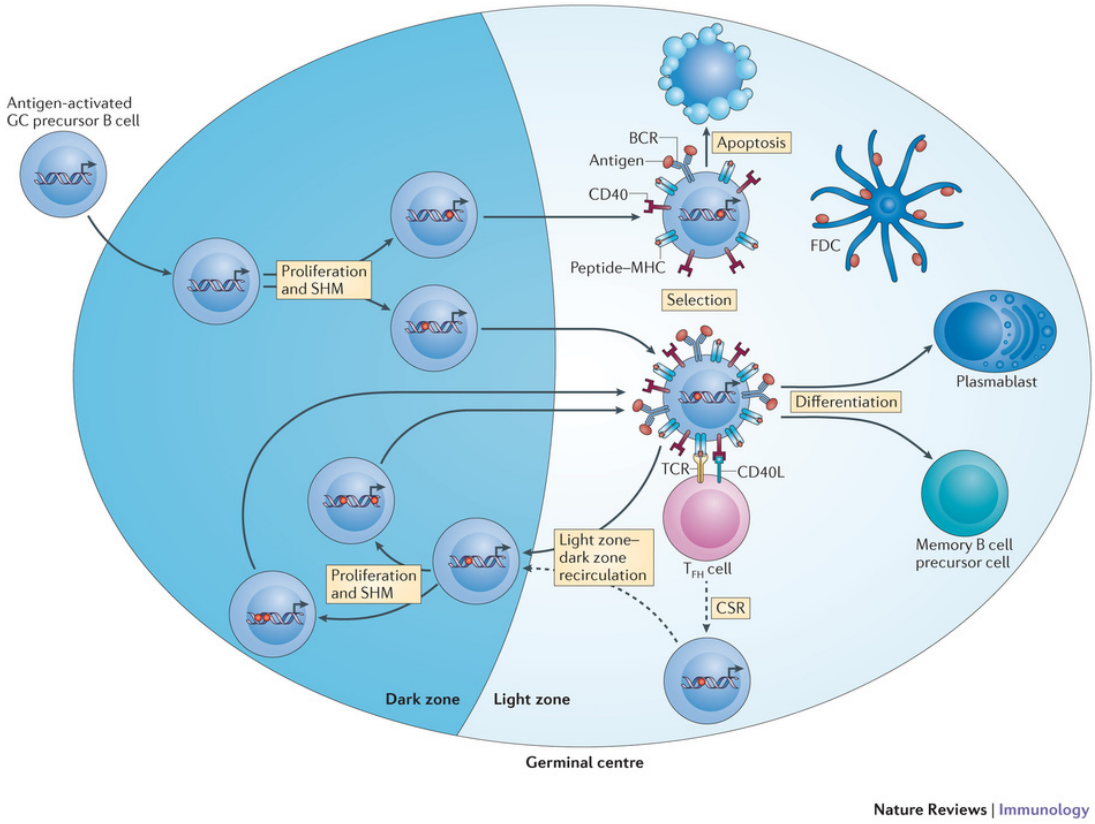

Figure 1. The Germinal Center Reaction. Exposure of naïve B-cells to foreign antigen leads to the formation of germinal centers in secondary lymphoid organs. Germinal Center B-cells proliferate extensively in the dark zone and undergo Somatic Hypermutation (SHM) to mutate their antibody genes. Upon exit to the Light zone, B-cells which have acquired higher affinity for the antigen receive survival signals from Follicular Dendritic Cells (FDC) and Follicular Helper T-cells (T_{FH}). These B-cells may cycle back to the dark zone to undergo further SHM, or differentiate into plasmablasts and precursors of memory B-cells. This image is published with permission from Nature Publishing Group, license number 4145491222880 (4).

1.1.3 Tonic and antigen-dependent B-Cell Receptor signaling

In the dark zone, GC B-cells called 'centroblasts' undergo somatic hypermutation and mutate their antibody genes to acquire higher affinity for the antigen presented to them. At this stage, the B-Cell Receptor is not active, but generates a basal low-level signal that promotes cell survival. This type of BCR signaling is called 'tonic signaling' (9). After SHM, when centroblasts exit the dark zone and enter the light zone, they become 'centrocytes' with active BCR. This is the zone where their specificity for antigen is tested by FDCs. When a BCR can bind to the presented antigen with moderate to high affinity, this activates downstream signaling pathways promoting cell proliferation and survival. At the highest level, BCR signaling is propagated via phosphorylation of the co-receptors CD79A and CD79B (formerly named Igα and Igβ). CD79A/B are phosphorylated on Immunoreceptor Tyrosine-based Activation Motifs (ITAM; consensus sequence YxxI/L$x_{6\text{-}12}$YxxI/L), by members of the SRC family of kinases (10). Phosphorylation of ITAM motifs attract the SYK tyrosine kinase, which then becomes activated through phosphorylation by a SRC family kinase, usually LYN. SYK phosphorylates an adaptor protein called BLNK, which brings together Bruton's Tyrosine Kinase (BTK) and Phospholipase-C gamma2 (PLCγ2). Additionally, LYN and SYK phosphorylate a positive co-receptor called CD19, which potentiates BCR signaling by activating PI3Kδ and increasing PIP2 to PIP3 conversion. PIP3 recruits Pleckstrin Homology-domain proteins like PKB/AKT and BTK to the inner leaflet of the plasma membrane to facilitate their activation (Figure 2). PLCγ2 converts PIP3 to the secondary messengers IP3 and DAG, which in turn activate calcium signaling via PKCβ. The significance of different co-receptors, adaptor proteins and kinases in the BCR signaling pathway can be deciphered through assessment of the phenotype of targeted knockout mice.

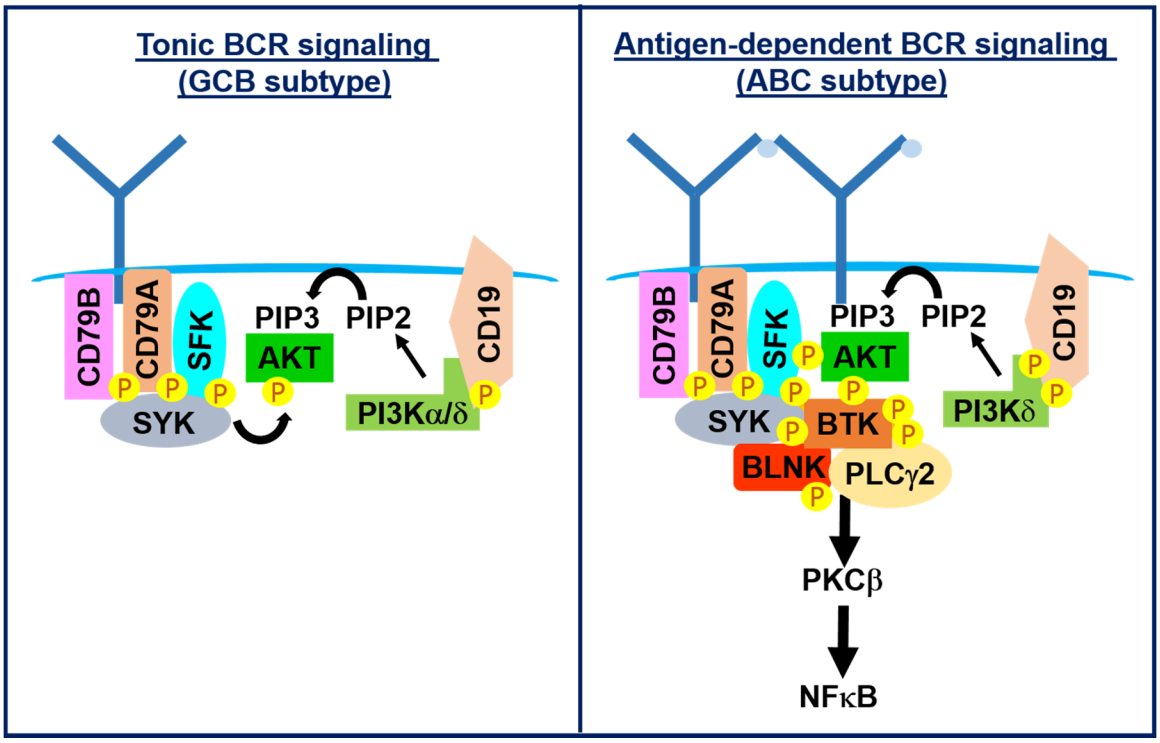

Figure 2. Tonic and antigen-dependent BCR signaling pathways engage different downstream effectors. Activation of BTK, PLCγ2, and calcium signaling can only be observed with antigen-type signaling. Both tonic and antigen-type signaling activate SYK and PI3K/AKT pathways. Tonic signaling can utilize PI3Kα and PI3Kδ isoforms interchangeably, whereas antigen-type signaling exclusively utilizes the PI3Kδ isoform (11).

LYN: B-cells in mice with LYN-/- maintain sensitivity to BCR ligation, suggesting that other SRC family kinases can compensate for the lack of LYN. In fact, these cells demonstrate hyperactivation of many downstream components like AKT and ERK, accompanied by enhanced calcium signaling. On the other hand, global tyrosine phosphorylation is delayed and reduced following BCR ligation. This phenomenon stems from deficient tyrosine phosphorylation of Immunoreceptor Tyrosine-based Inhibition Motifs (ITIM; consensus sequence S/I/V/LxYxxI/V/L) on negative co-receptors of the BCR, a phenomenon that is attributed to LYN. LYN-mediated feedback phosphorylation of ITIM motifs on CD22 and FcγRIIB1 are responsible for the recruitment of SHP1 and SHIP1 phosphatases that down-regulate BCR signaling (12). LYN-/- mice also display enhanced PI3K activity at the basal level and after BCR ligation. LYN promotes association of CSK with PAG (Phosphoprotein Associated with Glycosphingolipid-enriched microdomains) by phosphorylating multiple CSK-binding sites (13). CSK negatively regulates the activation of other Src Family Kinases, leading to signal attenuation downstream of BCR. In LYN-/- mice, Fyn showed enhanced activity as a consequence of impaired CSK recruitment. These mechanisms may explain the autoimmune phenotype characteristic of LYN-/- mice.

PI3K isoforms: The Type I Phosphoinositide 3-Kinases consist of PI3Kα, PI3Kβ, PI3Kδ, and PI3Kγ isoforms. These enzymes are dual lipid and protein kinases that catalyze the conversion of phosphatidylinositol-4,5-bisphosphate (PIP2) to phosphatidylinositol-3,4,5-trisphosphate (PIP3). PI3Ks are heterodimers, consisting of a p100 catalytic subunit and a p85 regulatory subunit. PI3Kα and PI3Kβ are expressed in all organs, whereas PI3Kδ and PI3Kγ are usually found in cells of hematopoietic lineage (14). PI3Kα, β and δ are activated after Receptor Tyrosine Kinase (RTK) stimulation, through binding to phosphorylated tyrosine motifs in the cytoplasmic domain of the receptor or through binding to similar motifs in adaptor proteins like GAB2. PI3Kγ is distinct from these other isoforms, and associates with G-Protein

Coupled Receptors (GPCR). PIP3 production by PI3K is critical for BCR signaling. Many downstream regulators such as PLCγ2, BLNK, BTK and Vav, contain Pleckstrin Homology (PH) domains which allow them to bind to PIP3 and localize to the plasma membrane.

PI3Kα and PI3Kβ are essential for the normal functioning of multiple organ systems. As a consequence, knockout of PI3Kα and PI3Kβ causes embryonic lethality. On the other hand, PI3Kδ and PI3Kγ ablation in mice is not associated with any significant effects on development and viability (15, 16). In these mice, aberrant phenotypes are manifested only upon challenge of the immune system. PI3Kγ deficiency is associated with diminished T-cell activation, and faulty recruitment of macrophages and neutrophils in response to inflammatory stimuli. On the other hand, PI3Kδ deficiency is associated with extensive defects in B-cell development. PI3Kδ-deficient mice display defective BCR signaling, compromised IL-4 mediated survival effects, and impaired responses to both TI and TD antigens.

SYK: Spleen Tyrosine Kinase (SYK) is a cytoplasmic tyrosine kinase which functions as a critical mediator of signal propagation downstream of the BCR. In fact, most of the effects of BCR ligation are facilitated by SYK. The tandem SH2 domains of SYK bind to phosphorylated ITAMs on CD79A and CD79B after BCR ligation (17). As a consequence, SYK knockout leads to perinatal lethality in mice, making it considerably difficult to study *in vivo* (18). Tyrosines-526/526 located in the activation loop are auto-phosphorylated by SYK, although LYN may initially contribute to this. Phosphorylation of SYK at Y323 negatively regulates its activity and recruits Cbl, leading to its ubiquitination and degradation.

BTK: Bruton's Tyrosine Kinase (BTK) is a cytoplasmic kinase that was identified as the product of the gene responsible for causing X-linked Agammaglobulinemia (XLA) in humans (19). Patients with this disorder suffer from an impaired humoral immune response caused by the lack of antibody-producing plasma cells. BTK consists of PH, Tec homology, SH3, SH2 and SH1 domains. Interestingly, mutations in BTK represent the highest number of mutations

found in a kinase gene. The phenotype associated with Xid (X-linked immunodeficiency) mice result from a disruptive R28C mutation in the phospholipid-binding PH domain of BTK, which prevents localization of the kinase to the inner leaflet of the plasma membrane. BTK is activated by LYN-mediated phosphorylation of Y551, which then promotes autophosphorylation at Y223 (19). BTK is inactivated by serine/threonine phosphorylation performed by AKT and PKCβ. AKT-induced phosphorylation recruits 14-3-3 proteins and leads to BTK degradation (20).

1.1.4 Positive and negative co-receptors of the BCR

CD19: CD19 is a transmembrane protein which functions as a positive co-receptor of the BCR. CD19 forms a complex with Complement Receptor-2 (CD21) and Tetraspan Membrane Protein TAPA-1 (CD81). This complex functions to lower the threshold for BCR activation in response to initial antigen binding (21). The CD19 cytoplasmic tail has nine conserved tyrosine residues. The tyrosine residues at positions 482 and 513 lie within YXXM SH2-binding motifs, which recruit the p85 subunit of PI3-Kinase. Therefore, tyrosine phosphorylation of CD19 is primarily responsible for PI3K activation. Accordingly, studies have showed that PTEN deletion in CD19-/- mice can rescue GC B-cell formation by allowing sustained PIP3 generation. CD19-mediated activation of LYN induces feedback inhibition of BCR signaling via increased phosphatase activity (SHP1). B-cells in CD19-deficient mice do not respond to TD (KLH), TI-1 (LPS), and TI-2 antigens, except for Ficoll towards which they demonstrate hyperresponsivity. CD19-/- mice show reduced serum Ig levels, and the isotypes IgG1 and IgG2a are the most affected (22). CD19 is required for initial B-cell activation in response to TD antigen, and generation of memory B-cells at a later stage in the germinal center.

CD22: Negative co-receptors play a key role in the down-regulation of BCR signaling. CD22 is an inhibitory co-receptor of the BCR that belongs to the Siglec family. It is a transmembrane

protein that consists of an extracellular domain that binds sialylated glycans, and a cytoplasmic domain that is involved in signaling (23). Binding to sialylated glycans allows discrimination between self and non-self, and promotes B-cell tolerance. Interestingly, CD22 is a strong cis-ligand for itself, and forms homooligomers. Binding to cis ligands reduces its availability for binding to the BCR. Disruption of CD22 homooligomers promotes its association with the BCR, and potently controls antigen-induced signaling. CD22 contains ITIMs in its cytoplasmic domain, which functions to recruit and activate phosphatases, thereby dampening BCR signaling. BCR ligation leads to rapid phosphorylation of CD22 on ITIMs by LYN kinase, and recruits SHP-1 phosphatase (12). SHP-1 then dephosphorylates the adaptor protein BLNK/SLP65 which bridges PLCγ2 to BTK, and promotes attenuation of calcium signaling.

CD72 and its ligand CD100/Sema4D: Similar to CD22, CD72 also functions as an inhibitory co-receptor that down-regulates BCR signaling. CD72 is a transmembrane protein belonging to the C-type lectin family, which also contains ITIMs in its cytoplasmic domain. CD72 is a low-affinity receptor for the semaphorin ligand CD100 (Sema4D), which also serves as a ligand for Plexin-B1 and regulates axon guidance in the central nervous system (24). In the absence of ligand stimulation, CD72 remains unphosphorylated and facilitates constitutive SHP1 phosphatase activity. However, upon binding to CD100, it becomes phosphorylated and SHP1 activity is switched off (25). This facilitates enhanced BCR signaling (Figure 3). CD100 is expressed by multiple cell types in the immune system, and also amplifies the effect of CD40 signaling in B-cells and Dendritic Cells during interactions with activated T-cells (26).

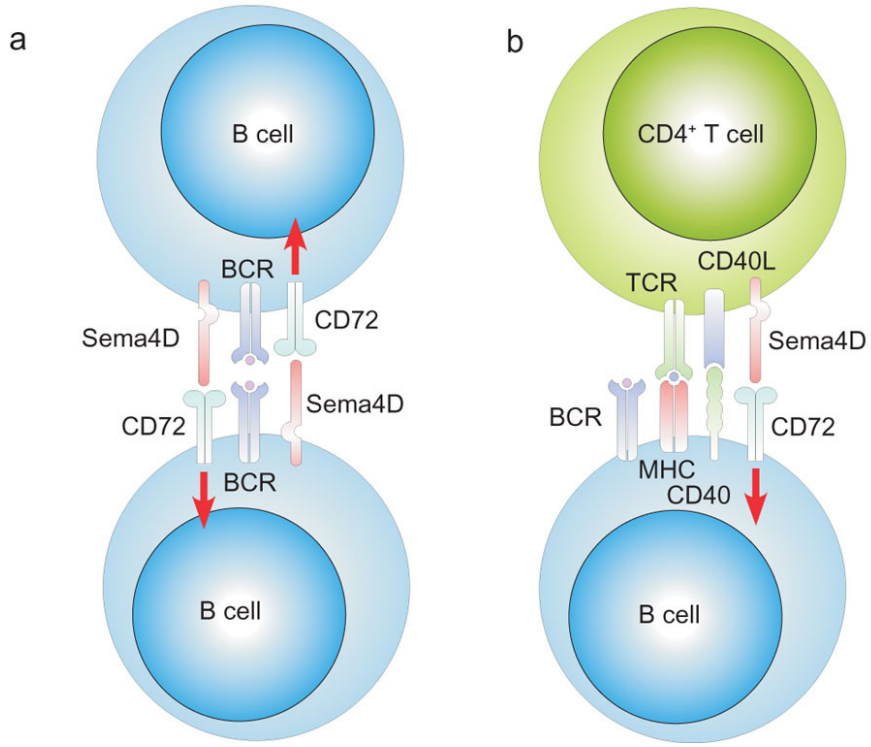

Figure 3. CD100/Sema4D is a ligand for the negative co-receptor CD72. **(a)** Homotypic interactions between activated B-cells expressing CD100/Sema4D enhances BCR signaling by engaging the negative co-receptor CD72 and 'switching off' its inhibitory function. **(b)** In a similar fashion, CD100/Sema4D expressed by CD4+ T-cells aid in B-cell activation and maturation by amplifying CD40 signaling. This image is published with permission from Nature Publishing Group, license number 4150320395172 (27).

1.2 Diffuse Large B-Cell Lymphoma

1.2.1 Subtypes of Diffuse Large B-Cell Lymphoma

Diffuse Large B-Cell Lymphoma can be classified into different subtypes based on the gene expression profile and immunohistochemistry: Germinal Center B-cell-like (GCB), Activated B-cell-like (ABC) and Primary Mediastinal B-cell Lymphoma (PMBL) (28). The GCB subtype of DLBCL expresses BCL6 and CD10, which is characteristic of centroblasts in the dark zone of the germinal center. This subtype is also predictive of better overall survival rates and favorable response to the standard-of-care chemoimmunotherapy. In comparison, the ABC-subtype of lymphoma is associated with poor prognosis (29). ABC-DLBCL expresses differentiation markers like IRF4/MUM1, which resemble centrocytes in the light zone of the germinal center (30). Over the last decade, new algorithms for more accurate immunohistochemical classification of DLBCL subtypes have been developed, and these methods continue to evolve over time (31, 32). Sequencing of DLBCL patient samples have revealed mutations in genes that play an important role in the normal germinal center (33). Some of these mutations target components of BCR and NFκB signaling (CD79A/B, CARD11, MYD88), epigenetic regulators involved in B-cell development (MLL2/3, CREBBP, EP300, EZH2), critical transcription factors and apoptosis regulators (MYC, TP53, BCL2, PRDM1).

1.2.2 Epigenetic deregulation in DLBCL

Combinations of posttranslational modifications on histone tails may govern transcriptional activation or repression at specific genes (34). These modifications include lysine and arginine methylation, lysine acetylation, and lysine ubiquitination, to name a few. When these marks are present at specific locations on a histone tail, they may signal either transcriptional activation or repression. For example, lysine acetylation affects the charge on a histone tail by reducing the positive charge on the lysine residue (35). This weakens interactions between

the negatively-charged DNA and the histone tail, and 'opens up the chromatin' to facilitate recruitment of transcription factors. On the other hand, modifications like lysine/arginine methylation do not have an impact on charge, but mediate their effects by creating binding sites for proteins called 'readers' (36, 37). These proteins can recognize specific modifications and assemble protein complexes to effect changes to the transcriptional status of a gene. Histone methyltransferases and acetyltransferases are examples of 'writers' that catalyze these various histone modifications (38). EZH2 is a histone methyltransferase that catalyzes Histone H3 Lysine-27 tri-methylation (H3K27me3) at enhancer and promoter regions (Figure 4a). This particular modification promotes transcriptional repression and 'switches off' gene expression. KMT2C/MLL3 and KMT2D/MLL2 are histone methyltransferases that catalyze Histone H3 Lysine-4 methylation (39). H3K4me1 is a modification that is enriched at enhancer regions, while H3K4me3 is typically found at promoter regions. EP300 and CREBBP are histone acetyltransferases that catalyze lysine acetylation on a variety of different histone tail residues. Interestingly, mutations in epigenetic 'writers' are rampant in different cancer types, including DLBCL.

EZH2 mutations are exclusively found in GCB-DLBCL tumors, whereas KMT2C/2D, EP300 and CREBBP mutations are found in both ABC and GCB subtypes (40). The most common alterations in EZH2 that occur in DLBCL are gain-of-function mutations that lead to enhanced H3K27me3 deposition at differentiation-associated genes. Loss-of-function mutations in KMT2D/2C, CREBBP and EP300 compromise their catalytic activities to block activation of differentiation-associated genes (41-44). Therefore, mutations in these epigenetic 'writers' co-occur in many DLBCL tumors, and act together to maintain B-cells in a stem-like state (Figure 4b) (45-47). Overall, epigenetic mutations in DLBCL shift the balance towards global gene repression (Figure 4c). However, this also creates many opportunities for therapeutic intervention. CREBBP and EP300 are commonly associated with acetylation at enhancer

regions, which is followed by recruitment of bromodomain-containing proteins. As a representative example, the Bromodomain and Extra-Terminal (BET) family of proteins are ‘readers’ of lysine acetylation that were first identified due to their heavy asymmetric loading at enhancer regions (48). In DLBCL, BRD4 is recruited to the super-enhancers of critical transcription factors such as POU2AF1, PAX5, IRF8 and BCL6, to name a few (49). BET bromodomain inhibitors like JQ1 and OTX015 demonstrate therapeutic efficacy against a wide range of different tumor types, including hematologic malignancies. Bromodomain inhibitors are effective against lymphoma, and lead to cell cycle arrest, senescence or apoptosis in DLBCL cell lines and tumor models (50-52).

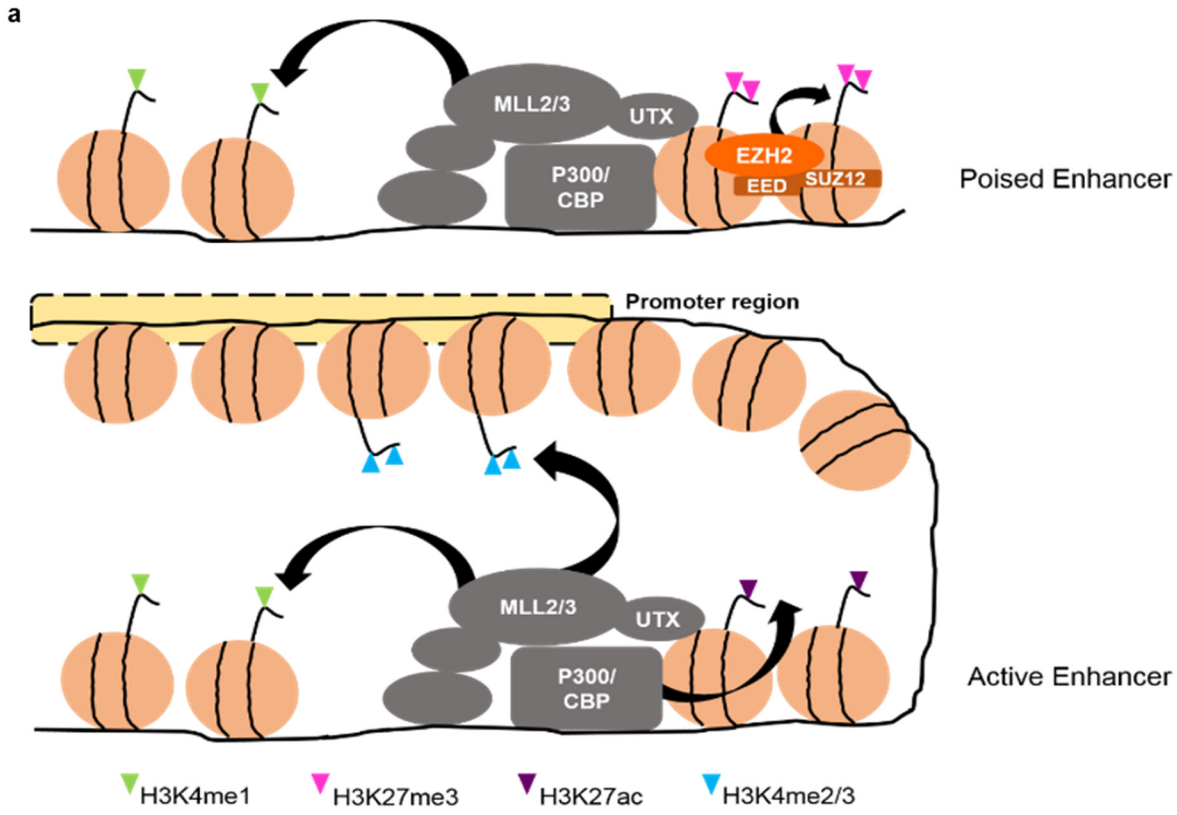
a
MLL2/3
UTX
P300/
CBP
EZH2
EED
SUZ12
Poised Enhancer
Promoter region
MLL2/3
UTX
P300/
CBP
Active Enhancer
H3K4me1
H3K27me3
H3K27ac
H3K4me2/3

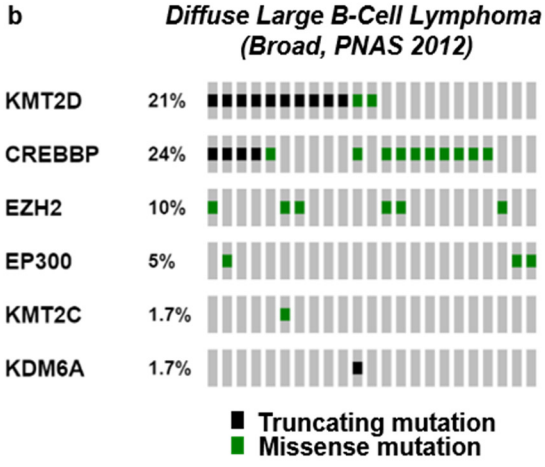
b
Diffuse Large B-Cell Lymphoma
(Broad, PNAS 2012)
KMT2D 21%
CREBBP 24%
EZH2 10%
EP300 5%
KMT2C 1.7%
KDM6A 1.7%
Truncating mutation
Missense mutation

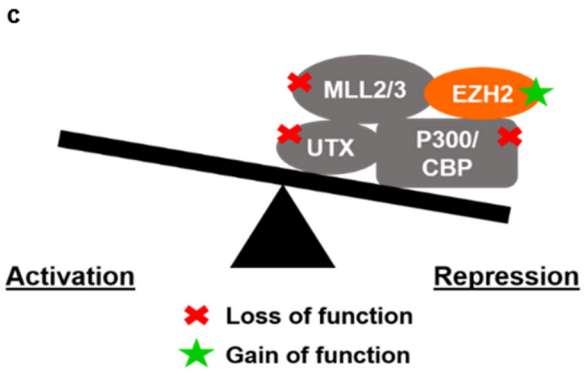
c
MLL2/3
EZH2
UTX
P300/
CBP
Activation
Repression
Loss of function
Gain of function

Figure 4. Epigenetic regulators are frequently mutated in diffuse large B-cell lymphoma. (a) The methyltransferases KMT2D/2C (also known as MLL2/3) catalyze H3K4me1 at enhancer regions and H3K4me3 at promoter regions. Enhancers containing both H3K4me1 and EZH2-catalyzed H3K27me3 maintain a 'poised' state. De-methylation of H3K27me3 by KDM6A (UTX) leads to enhancer activation, facilitates histone acetylation by EP300/CREBBP (p300/CBP) and promotes gene expression. **(b)** Without subtype classification, loss-of-function mutations in KMT2D (21%) and CREBBP (25%) are the most frequent, while EZH2 gain-of-function mutations occur in 10% of all DLBCL cases (cBioPortal). Mutations in different epigenetic enzymes co-occur in lymphoma patients (45-47). 25-30% of patients with the GCB subtype of DLBCL harbor EZH2 mutations. **(c)** In lymphoma, mutations targeting epigenetic enzymes 'switch off' transcriptional activators (KMT2D/CREBBP) and hyperactivate the transcriptional repressor EZH2, shifting the balance towards global gene repression.

1.2.3 Consequences of EZH2 mutation in GCB-DLBCL

In 2010, studies first reported the identification of EZH2 mutations in 25-30% of GCB-DLBCL cases (53). These mutations are localized to the catalytic SET domain of EZH2, and the three most commonly mutated sites are Y641, A677 and A687 (54-56). Due to their location, they were first believed to be loss-of-function mutations, but research later showed that these mutations conferred gain-of-function activity to EZH2. EZH2 is the catalytic core component of the Polycomb Repressive Complex 2 (PRC2), which methylates Histone H3 Lysine-27. EZH2 is capable of mono-, di- and tri-methylating H3K27, with tri-methylation generating a repressive modification that switches off gene expression, usually through recruitment of the Polycomb Repressive Complex 1 (PRC1) complex which performs Histone H2A Lysine-119 mono-ubiquitination (H2AK119ub) (57). While wildtype EZH2 is highly capable of catalyzing mono- and di-methylation of H3K27, mutations in the substrate-binding channel render the mutant EZH2 enzyme superior at catalyzing the di- to tri-methylation reaction. Together, the combination of wildtype and mutant EZH2 produce high global levels of H3K27me3, leading to widespread gene repression (58, 59). Accordingly, EZH2 mutations are found to be heterozygous in DLBCLs, with a wildtype allele necessary to maintain optimal H3K27me3 levels. Recent studies have showed that the EZH2 mutants A677G and A687V can catalyze all three steps of H3K27 methylation on their own, without the need for wildtype EZH2 (Figure 5a). For this reason, they have been dubbed ‘super-mutants’. Similarly, Y641F displays a limited capacity to catalyze all three methylation reactions, while all other Y641X (X=N/S/H/C) mutations cannot do this (Figure 5b). In the presence of wildtype EZH2, the Y641N/S mutants are comparable to A677G, A687V, and Y641F, but superior to Y641H/C at catalyzing H3K27me3.

Therefore, it is apparent that all EZH2 gain-of-function mutations are not identical, and each one may influence the level of dependency of lymphoma cells on EZH2 activity (Figure 5c).

For example, the cell line Pfeiffer harbors an A677G mutation, and displays remarkable hypersensitivity to EZH2 inhibitors, exceeding the response of all other EZH2-mutant cell lines. SUDHL-10 and WSU-DLCL2, which both harbor Y641F mutations, exhibit significant cytotoxic responses to the EZH2 inhibitor GSK126 (60). On the other hand, Y641X mutations in EZH2 are present in many lymphoma cell lines, but display a broad spectrum of sensitivity to EZH2 inhibitors. Cell lines RL and SUDHL-4 harbor Y641N and Y641S mutations respectively, but are resistant to EZH2 inhibition, while SUDHL-6 and DB both harbor Y641N mutations and demonstrate cytostatic responses to EZH2 inhibitors.

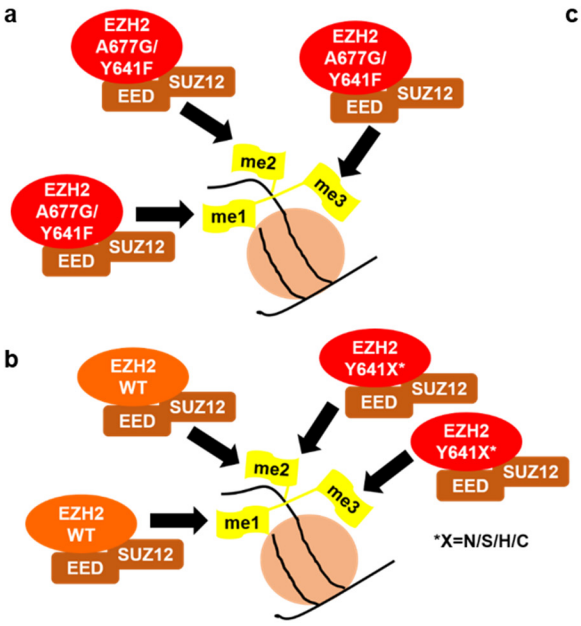

c

Cell line	*EZH2 status*	*EPZ-6438 sensitivity*
Pfeiffer	A677G	Sensitive
SUDHL-10	Y641F	Sensitive
DB	Y641N	Sensitive
SUDHL-6	Y641N	Sensitive
SUDHL-4	Y641S	Resistant
RL	Y641N	Resistant
HT	WT	Sensitive
OCI-Ly7	WT	Sensitive
SUDHL-5	WT	Resistant
SUDHL-7	WT	Resistant
OCI-Ly8	WT	Resistant
Toledo	WT	Resistant

Sensitive= EPZ-6438 11-day IC50 < 1uM
Resistant= EPZ-6438 11-day IC50 > 1uM

Figure 5. EZH2 mutations and differential sensitivity to EZH2 inhibitor treatment. (a) The EZH2 mutants A677G, A687V and Y641F can perform all three (-mono, -di, and –tri) methylation reactions at H3K27, without the requirement for wildtype-EZH2. **(b)** EZH2-Y641X (where X=N/S/H/C) cooperates with wildtype EZH2 to generate high levels of H3K27me3. Wildtype EZH2 catalyzes H3K27me0 to me1 with high efficiency, while EZH2-Y641X cannot perform this reaction. Both wildtype and EZH2-Y641X can transform H3K27me1 to me2 with reasonable efficiency. However, only EZH2-Y641X can generate high levels of H3K27me3 from me2. **(c)** Table of lymphoma cell lines along with information about EZH2 mutation status and sensitivity to the EZH2 inhibitor EPZ-6438 at 11 days of treatment. Within each category (wildtype and mutant), cell lines are listed in increasing order of EPZ-6438 IC50 values.

1.2.4 EZH2 inhibitors and ongoing clinical trials

EZH2 inhibitors have been developed by multiple pharmaceutical companies, including Epizyme, GlaxoSmithKline, and Constellation. All of these inhibitors function by competing with the co-factor S-adenosylmethionine for binding to the EZH2 enzyme, and are therefore termed SAM-competitive inhibitors. EPZ005687 was the first selective EZH2 inhibitor reported to show high efficacy in lymphoma cell lines with EZH2 mutations (61). This was followed by GSK126, UNC1999, EPZ-6438, CPI-1205, and ZLD10A (62-65). Currently, GSK126, EPZ-6438 and CPI-1205 are in different phases of clinical trial. Phase I clinical trials of EPZ-6438 in patients with relapsed and refractory DLBCL reported an impressive Objective Response Rate (ORR) of 60%. Interestingly, responses were recorded in both EZH2-wildtype and EZH2-mutant patients. Gene expression profiling of lymphoma cell lines after EZH2 inhibitor treatment did not reveal any significant overlap or distinct differences between genes de-repressed in sensitive and resistant cell lines (60, 63). Therefore, factors that determine favorable response to EZH2 inhibitors remain largely unknown. Notably, early results of Phase II EPZ-6438 clinical trials reported that the ORR was lower, and a majority of EZH2-wildtype patients did not respond to treatment. EZH2-mutant patients showed a 40% ORR, but all were partial responses and there were no complete responses. On the other hand, EZH2-wildtype patients showed a 14% ORR and exhibited a mix of partial and complete responses.

1.2.5 Targeted therapies for DLBCL subtypes

The GCB subtype of DLBCL responds favorably to the standard-of-care R-CHOP therapy (Rituximab, Cyclophosphamide, Doxorubicin, Vincristine, Prednisone) with an overall survival rate of 80% at 5 years post-treatment (29). Rituximab is an anti-CD20 antibody that mediates B-cell targeting by Natural Killer (NK) cells through antibody-dependent complement cytotoxicity (ADCC) (66). However, patients who relapse or suffer from refractory disease have few options. ABC-DLBCL is marked by activating mutations in BCR signaling elements

such as CD79A, MYD88 and CARD11. Chronic activation of the BCR signaling pathway is responsible for rapid proliferation and survival in the ABC-subtype of lymphoma (67). Therefore, targeting kinases in this pathway is a successful strategy for treatment. The BTK inhibitor ibrutinib has been largely successful in clinical trials, and represents a breakthrough therapy for patients with this subtype of lymphoma (68). Other treatment options for patients with ABC-DLBCL are SYK inhibitors (R406, PRT062607), PI3Kδ inhibitors (idelalisib), PKCβ inhibitors (enzastaurin), NFκB pathway inhibitors (bortezomib and lenalidomide), and BCL2 antagonists (venetoclax) (68-74). On the other hand, GCB-DLBCL is characterized by a basal level of antigen-independent BCR signaling, called tonic BCR signaling. In this type of signaling, the downstream effects of BCR activation are propagated through SYK and PI3K/AKT (9, 10). Interestingly, PTEN deletions have been identified in a significant percentage of GCB-DLBCL cases, and lead to increased AKT activation (75). SYK inhibitors offer a promising avenue for the treatment of GCB-DLBCL by blocking tonic BCR signaling. However, SYK inhibitors would not work in cases where PTEN is deleted. In these instances, direct targeting of PI3K isoforms or AKT would be more effective.

SYK inhibitors: The first reported orally bioavailable SYK inhibitor is Fostamatinib (R406), which shows significant off-target effects on other kinases such as FLT3, JAK1, JAK3 and LCK (76). Newer and more specific SYK inhibitors such as PRT062607 (Portola) and TAK-659 (Takeda) show promise in early stage clinical trials for Chronic Lymphocytic Leukemia (CLL), and appear to work well against DLBCL in preclinical experiments (77-80).

PI3K inhibitors: Idelalisib (CAL101, Gilead) is a potent and specific PI3Kδ inhibitor, which does not significantly affect PI3Kα and PI3Kβ isoforms. Idelalisib is approved for the treatment of CLL, indolent B-cell Non-Hodgkin's Lymphoma (B-NHL) and relapsed Small Lymphocytic Lymphoma (SLL). Duvelisib (IPI-145, Infinity) is a dual PI3Kδ/γ inhibitor, which has demonstrated activity against CLL and T-cell lymphomas. Copanlisib (BAY 80-6946, Bayer)

is a dual inhibitor of PI3Kα/δ that showed clinical activity in Mantle Cell Lymphoma (MCL) patients (81). One of the major drawbacks of PI3K inhibitors like idelalisib is the adverse toxicity observed in patients, especially when combined with other therapies (72).

BTK inhibitors: Ibrutinib (PCI-32765, Pharmacyclics) is a BTK inhibitor which also targets EGFR, ITK, TEC and SRC family kinases at higher doses. Ibrutinib is FDA-approved for the treatment of CLL, MCL, Marginal Zone Lymphoma (MZL) and Waldenstrom's Macroglobulinemia (WM) (82). Acalabrutinib (ACP-196) is a novel second-generation BTK inhibitor from Acerta Pharmaceuticals, which is more specific for BTK and expected to have less off-target toxicity. In clinical trials, acalabrutinib showed efficacy in CLL and lymphomas that are difficult to treat (83-86).

BCL2 antagonists: Another promising class of inhibitors for the treatment of GCB and ABC-DLBCL are BCL2 antagonists such as Venetoclax (ABT-199, AbbVie) (87). In the germinal center, GC B-cells in the dark zone are 'primed' for apoptosis and maintain very low levels of the anti-apoptotic protein BCL2. As a result, B-cells that acquire deleterious mutations during the SHM process will undergo apoptosis. Upon exit into the light zone, survival signals are delivered through BCR signaling, CD40L/CD40 engagement and BAFF/BAFF-R ligation (88). These signals increase the expression of MCL-1, which is critical for germinal center initiation and maintenance (89, 90). In DLBCL and FL, chromosomal translocations drive BCL2 overexpression and promote resistance to apoptosis. EZH2 mutations commonly co-occur with BCL2 chromosomal translocations, and an EZH2-mutant mouse model demonstrates lymphomagenesis when combined with BCL2 overexpression (91, 92). Therefore, combining EZH2 inhibitors with BCL2 antagonists may improve therapeutic efficacy in lymphoma (65).

1.3 Protein Arginine Methyltransferases in Cancer

1.3.1 Type I PRMTs and their substrates

Protein Arginine Methyltransferases are divided into two families, with Type I representing the largest family. Type I PRMTs are asymmetric arginine methyltransferases, consisting of PRMT1, 2, 3, 4, 6 and 8 (Figure 6a). PRMT5 and PRMT9 are symmetric arginine methyltransferases categorized as Type II, and PRMT7 is a mono-methyltransferase categorized as Type III. PRMT1 is the major arginine methyltransferase in the cell, contributing to 85% of the global arginine methylation (93, 94). PRMT1 is overexpressed in multiple cancer types, including breast, prostate, colon, ovarian and pancreatic cancers. PRMT1 and PRMT4/CARM1 are best known for their roles as transcriptional coactivators for nuclear receptors such as ERα (95). PRMT1-mediated asymmetric di-methylation of histone H4 at arginine-3 (H4R3me2a) sets off a sequence of events that culminates in transcriptional activation (96). One of the earliest studies on PRMT1 function showed that ordered activity of PRMT1, p300, and CARM1, was responsible for transcriptional activation by the p53 tumor suppressor (Figure 6b) (97). Other studies have also demonstrated that PRMT1 and CARM1 synergize to activate genes under different contexts (98). CARM1 methylates histone H3 at both arginine-17 and -26, although the former is its major substrate (99). Arginine methylation of histone H3 by CARM1 leads to the displacement of transcriptional repressors from chromatin (100). PRMT6 acts as a transcriptional repressor, and catalyzes histone H3R2 methylation, which blocks H3K4 methylation by MLL proteins (Figure 6c) (101). In addition to their activity towards histone substrates, PRMT1 and CARM1 display methyltransferase activity towards a variety of non-histone substrates. In breast cancer, CARM1 methylates the SWI/SNF chromatin remodeler BAF155 and this methylation promotes tumor cell migration and metastasis (102). Arginine methylation of the RNA polymerase II subunit MED12 by CARM1 improves sensitivity to chemotherapy drugs (103). Although CARM1 mainly functions

as a transcriptional coactivator, there are instances where it also promotes repression. Methylation of RUNX1 by CARM1 leads to the assembly of a multi-protein repressor complex that blocks myeloid differentiation of Hematopoietic Progenitor/Stem Cells (HPSCs) (104). Another example is CARM1-mediated methylation of the acetyltransferase CREBBP, which negatively modulates its transcriptional coactivator function by blocking its interaction with CREB (105). Therefore, in these contexts, CARM1 acts directly or indirectly to promote transcriptional repression. Similarly, there are a few cases where PRMT1 promotes repression of genes, such as HIF1 and HIF2 (106). PRMT1 is implicated in pro-oncogenic functions across many cancer types. In colon cancer, PRMT1 methylates EGFR and promotes resistance to the monoclonal antibody cetuximab (107). In pancreatic cancer, PRMT1 methylates GLI1 and increases activation of its target genes (108). In breast cancer, PRMT1 activates ZEB1 at the transcriptional level, and promotes the Epithelial-to-Mesenchymal Transition (EMT) (109). In glioblastoma, PRMT1 links 5-hydroxymethylcytosine to gene activation via H4R3 methylation activity (110). In acute myelogenous leukemia, PRMT1 supports the oncogenic function of MLL-fusion proteins in partnership with the histone H3K9 demethylase KDM4C (111). The importance of PRMT1 in the cell is exemplified by extensive substrate scavenging performed by other PRMTs when PRMT1 is knocked out in mouse embryonic fibroblasts (112). This shows that Asymmetric Dimethyl Arginine (ADMA) formation by PRMT1 serves as a placeholder to prevent accumulation of Monomethyl Arginine (MMA) and Symmetric Dimethylarginine (SDMA).

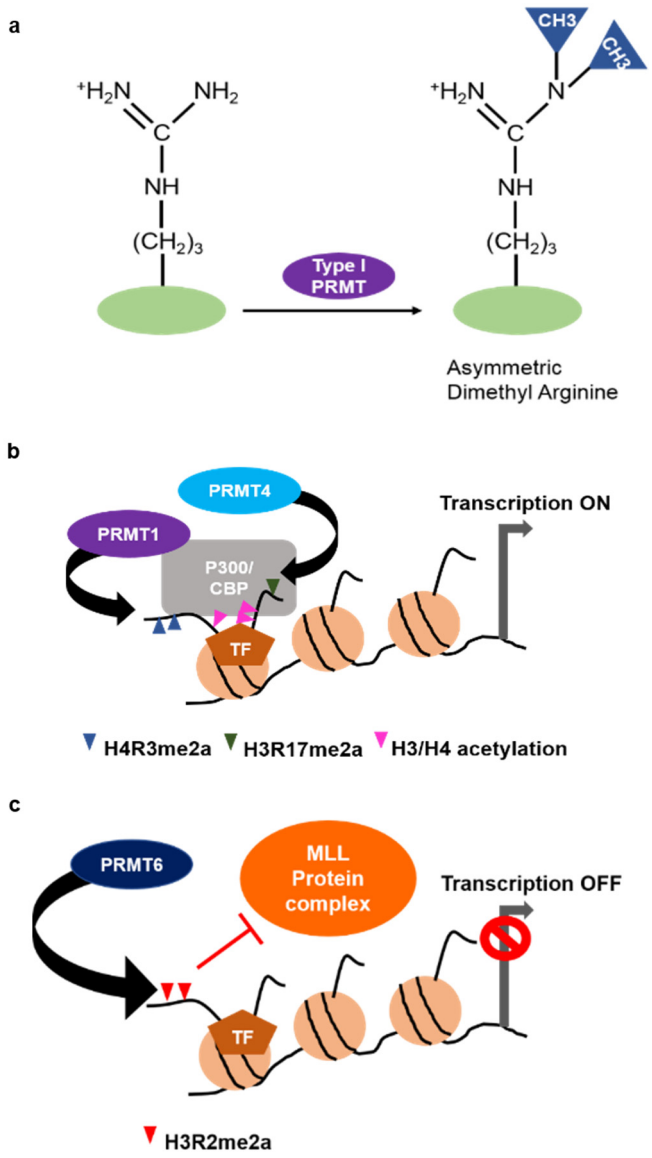

Figure 6. Type I PRMTs methylate histone tails on arginine residues to regulate gene expression. (a) Type I PRMTs can perform mono-methylation or asymmetric di-methylation at arginine residues. **(b)** PRMT1 and PRMT4/CARM1 catalyze asymmetric di-methylation at histone H4 arginine-3 (H4R3me2a) and histone H3 arginine-17 (H3R17me2a) respectively to activate gene expression. During this process, histone acetyltransferases such as p300/CBP may cooperate with PRMT1 and CARM1. **(c)** PRMT6 catalyzes asymmetric di-methylation of Histone H3 at Arginine-2 (H3R2me2a) to block Lysine-4 tri-methylation (H3K4me3) and gene activation by the MLL protein complex.

1.3.2 Structural attributes of PRMT1 and CARM1

PRMT1 and CARM1 possess a Rossman fold that is typical of methyltransferases from this family (113). The catalytic core of PRMTs consist of the cofactor-binding Rossman fold and a β-barrel. Many type I PRMTs, including PRMT1 and CARM1, are known to undergo homo-dimerization. The dimerization arm emerging from the β-barrel of one PRMT monomer makes contacts with the Rossman fold of the other PRMT monomer, with both of them arranged in head-to-tail orientation. The N-terminal section preceding the Rossman fold consists of multiple α-helices, which are involved in formation of the cofactor binding site and the dimerization interface (114). The structure of PRMT1 exemplifies the typical structural characteristics of Type I PRMTs. On the other hand, CARM1 possesses a unique N-terminal domain which adopts a PH-like superfold conformation (115). Historically, PH-domains have been associated with binding to phospholipids, such as BTK binding to PIP3. However, PH-domains are extremely diverse, and in fact only a minority of them bind to phospholipids. This domain regulates protein-protein interactions by binding to proline-rich regions, phosphorylated or unphosphorylated tyrosine residues (116). The latter two types of interactions are characteristic of Phosphotyrosine Binding Domains (PTBs) present in Insulin Receptor Substrate 1 (IRS1). In the case of CARM1, the N-terminal domain forms a homodimer with another CARM1 molecule, which would prevent its involvement in binding to other proteins. However, in instances where the dimer dissociates, the PH-like domain could play a role in promoting interactions with other proteins. In fact, it was reported very recently that the N-terminal domain of CARM1 plays a critical role in the recognition and methylation of its substrates (117). The central portion of CARM1 possesses methyltransferase activity, and the C-terminal domain is involved in its transactivation function. Interestingly, the C-terminal domain also contains an auto-methylation site (R551) that is reported to be extensively di-methylated *in vivo* (118). Mutation of this auto-methylation site does not affect

CARM1's catalytic activity, but abrogates its ability to activate transcription and pre-mRNA splicing.

1.3.3 Therapeutic potential of PRMT inhibitors in cancer treatment

In the last few years, small-molecule inhibitors targeting PRMTs have been developed. Although PRMT5 inhibitors are far ahead in pre-clinical development, there have been few selective inhibitors of the Type I PRMTs. The aryl pyrazole derivative compound EPZ020411 (Epizyme) is the first reported PRMT6 inhibitor, which also demonstrates off-target effects on PRMT1 and PRMT8 at higher concentrations (119). Based on the structure of EPZ020411, the Structural Genomics Consortium developed MS023, a pan-Type I PRMT inhibitor which affects PRMT1, 3, 4, 6, and 8 (120). MS049 inhibits PRMT4 and PRMT6, but does not affect PRMT1 activity (121). SGC707 is an allosteric inhibitor of PRMT3, which makes it highly specific (122). Structural similarities make it difficult to obtain inhibitors with high selectivity towards PRMT1 over the other type I PRMTs. AMI-1 was the first reported small-molecule inhibitor of PRMTs that demonstrated specificity towards arginine methyltransferases, unlike other published inhibitors that also targeted lysine methyltransferases (123). In recent times, an early phase PRMT1 inhibitor called AMI-408, which was derived from AMI-1, has been used successfully for *in vivo* studies in acute myeloid leukemia (111). Many new compounds are in preclinical development by pharmaceutical companies. Over the next few years, we can expect highly selective and specific inhibitors against PRMT1, CARM1, and PRMT6 to be available for clinical use.

Chapter 2:

MATERIALS AND METHODS

2.1 Cell Culture

Diffuse Large B-Cell Lymphoma cell lines SUDHL-6, SUDHL-4, RL, HT, DB, U-2932, SUDHL-5, SUDHL-7, HBL-1, SUDHL-10, Toledo and Pfeiffer were maintained in RPMI-1640 medium containing 10% heat-inactivated Fetal Bovine Serum and 1% Penicillin-Streptomycin. Knockout and mutant versions of SUDHL-6, DB, SUDHL-10, SUDHL-7, OCI-Ly7 and OCI-Ly8 were maintained in the same medium. All DLBCL cell lines were obtained from Dr. R.E. Davis. 293T and MCF7 cells were cultured in DMEM/F12 medium supplemented with 10% FBS, penicillin, streptomycin and glutamine.

2.2 Cell Growth Assays

Cell growth was measured using the CellTiter-Glo Viability Assay from Promega. Cells were seeded at a density of 20,000 cells/ml in 384-well plates and incubated with serial dilutions of inhibitors. After 4 days of treatment, the cells were split and fresh media containing inhibitor was added. At 8 days, the assay was completed by adding CTG assay buffer equal to the volume of media in each well, and luminescence was determined using a Synergy H4 Hybrid Reader.

2.3 Apoptosis Assays

After drug treatment, apoptosis was measured via flow cytometry. Live cells were incubated with CaspGLOW Active Caspase reagent (Biovision) for 1 hour, and FITC+ cells were quantified using a BD FACS Aria flow cytometer. Alternatively, cells were stained with 7-Aminoactinomycin-D and Annexin V (Biolegend). Single-stained and double-stained cells were examined to identify early apoptotic, late apoptotic and necrotic cells. FlowJo software was used to analyze data.

2.4 Cell Cycle Analysis

Cells were fixed with cold 70% ethanol for 2 hours and treated with RNase to eliminate RNA contamination. Propidium iodide (Biolegend) was added to stain the DNA, and cells were analyzed using a BD FACS Aria flow cytometer. Cell cycle staging was performed using FlowJo software.

2.5 Determination of IC50 and drug synergy

Data from CellTiter-Glo assays was graphed using GraphPad Prism software, and non-linear regression analysis was utilized to generate IC50 values. For drug synergy experiments, CompuSyn software Version 1.0 (ComboSyn) was used to compute Combination Index values using the Chou-Talalay method.

2.6 Generation of BCR-KO, CD19-KO, and CD79A-mutant cell lines

All knockout cell lines and CD79A-mutants were generated using the CRISPR/Cas9 system, by O Havranek and RE Davis. Chimeric plasmids from the Zhang laboratory were used for this technique: pX330-U6-Chimeric_BB-CBh-hSpCas9 (pX330; Addgene plasmid # 42230, coding for Cas9 as well as gRNA) and pSpCas9(BB)-2A-GFP (pX458; Addgene plasmid # 48138; coding for Cas9 linked by 2A peptide with GFP and for gRNA expression) (124, 125). The online CRISPR Design Tool from the Zhang laboratory was used to design target sequences (http://crispr.mit.edu/) (126). Target sequences were ligated as annealed oligos into BbsI-opened pX330, pX335, or pX458 plasmids according to the published protocol. After verification of gRNA sequences, transfections were performed with electroporation to deliver maxiprep DNA. For each electroporation, 12 µg of plasmid DNA was delivered (pX330 or pX458, with cloned gRNA sequence) per 120 µL of cell suspension (1 million cells per 100 µL) in electroporation buffer. Cells with successful knockout were detected by flow cytometry and sorted routinely to maintain pure populations.

Name	Target Sequence (5' to 3')	Plasmid	Location	Use
SUDHL6_HV_02	GAAGTGCAGATGGTGGAATCTGG	pX330	SUDHL-6 H-HVR V region	BCR KO in SUDHL-6
IGHG-C4	CGGTGAGGACGCTGACCACACGG	pX330	exon 3 of IGHG1, IGHG2, IGHG4; exon 6 of IGHG3	BCR KO in DB, SUDHL-7, SUDHL-10
IGHM-C4	AGATGAGCTTGGACTTGCGGGGG	pX330	exon 2 of IGHM	BCR KO in Ly8
CD19_01	TGGAATGTTTCGGACCTAGGTGG	pX330	exon 3 of CD19	CD19 KO

CD79A mutations were introduced in the last two exons (exon 4 and 5), which code for the ITAM domain. Double-strand breaks in both exons were generated using two pX330 plasmids as outlined in the table below. Homology arms upstream of the CRISPR/Cas9 target site in exon 4 and downstream of the target site in exon 5 were included in the Homologous Recombination template. This allowed efficient translation of the endogenous CD79A exon 4 while exon 5 was translated from the knocked-in sequence, which ended with a stop codon and a bGH polyA signal sequence. Using this method, three different versions of CD79A were generated: wildtype full-length CD79A with GFP fusion, full-length CD79A-GFP fusion with a Tyrosine to Phenylalanine mutation (Y188F), and full-length CD79A-GFP fusion with an Arginine to Lysine mutation (R204K). Both the pX330 plasmids (6 µg each) and the HR template plasmid (7 µg) were delivered through electroporation to 1.2 million cells re-suspended in 120 µL of R or T buffer.

Name	Target Sequence (5' to 3')	Plasmid	Location	Use
CD79A modifications				
CD79A_01	ACCCTTCACTCACTTCATAAAGG	pX330	End of CD79A exon 4	CD79A modification by KI
CD79A_02	GGACGACTGCTCCATGTATGAGG	pX330	Beginning of CD79A exon 5	CD79A modification by KI

2.7 PRMT1 siRNA transfection

Knockdown was achieved using PRMT1-specific siRNA (SASI_Hs01_00133430, SASI_Hs01_00133431 and SASI_Hs01_00133433) or universal negative control siRNA (Sigma) and an Amaxa Nucleofector II (Lonza). Electroporation was performed using program number O-017, according to the manufacturer's protocol.

2.8 Real-time Quantitative PCR

Total RNA was isolated from cell lines using the RNeasy Mini Kit (Qiagen). Reverse transcription was performed using Superscript III First-strand Synthesis System (Fisher). Real-time PCR was completed with iQ SYBR Green Supermix (Biorad) and a plate reader.

BCL2_F1: 5'-TGCACCTGACGCCCTTCAC-3'

BCL2_R1: 5'-CTCTCCACACACATGACCCC-3'

ACTB_F1: 5'-AGAGCTACGAGCTGCCTGAC-3'

ACTB_R1: 5'-AGCACTGTGTTGGCGTACAG-3'

PAX5_F1: 5'-GGGAGTGAGTTTTCCGGGAG-3'

PAX5_R1: 5'-ATAGTAGGGGGAGCCAAGCA-3'

POU2AF1_F1: 5'-TATGCCTCTCCGCCACTCAT-3'

POU2AF1_R1: 5'-GGGAAATAGGTGAGGGGTGC-3'

P_BCL2_F4 (ChIP): 5'-CCCTTGTTTTCATGGCGCAC-3'

P_BCL2_R4 (ChIP): 5'-GTGCGGACTTGGTGGTCG-3'

2.9 Chromatin Immunoprecipitation

ChIP assay was performed using the Millipore Magna ChIP A/G Kit. Sonication was done using a sonicator bath and 3 cycles of 10 pulses each was used to shear the chromatin. 10ug of H4R3me2a antibody or an equal amount of Rabbit IgG antibody was added. The control primer mix for GAPDH was obtained from the kit.

2.10 Protein Immunoprecipitation

Cell lysates were prepared in RIPA buffer. Anti-FLAG M2 affinity beads (Sigma A2220) were incubated with lysate for 4 hours at 4ºC. Beads were washed four times for fifteen minutes each and 3X-Flag peptide was used as elution buffer. After incubation for thirty minutes at room temperature, the eluate was collected and boiled at 95ºC with SDS-PAGE loading buffer added.

2.11 Imaging

SUDHL-6 and DB cells expressing CD79A-GFP were imaged over the course of 7 days of EPZ-6438 treatment using an Incucyte Zoom instrument at 20X magnification. For Duolink Proximity Ligation Assay, MCF7 cells were imaged using a Leica confocal microscope.

2.12 Mass Spectrometry

MCF7 breast cancer cells expressing myc-tagged EZH2 were cultured in 150mm dishes, collected and frozen as cell pellets. Pellets were thawed and lysed with RIPA buffer. Anti-c-Myc affinity beads were incubated with lysate overnight and washes were performed. Bound protein was eluted and concentrated using Trichloroacetic acid precipitation. Silver staining was performed to confirm successful pulldown. Trypsin digestion and mass spectrometry was carried out by Dr. Proma in Taiwan.

2.13 Western Blotting and Antibodies

Cell lysates were extracted with Sodium Dodecyl Sulfate(SDS)-Urea buffer. Samples were run on 10-15% SDS-PAGE gels, transferred to PVDF membrane and western blotting was performed using the following antibodies. BCL2 (BD Biosciences 551052), BCL2 (R&D Systems AF810), Bcl-XL (Cell Signaling 2764), MCL-1 (Cell Signaling 4572), GAPDH (), Actin (Sigma A2066), Tubulin (Millipore 05-829), Caspase-3 (Novus Biologicals MAB835), Asymmetric Dimethyl Arginine motif (Cell Signaling 13522S), Monomethyl Arginine motif (Cell Signaling 8015S), PRMT1 (Cell Signaling 2449), CARM1 (Cell Signaling 3379s), Phospho-BLNK Tyr96 (Cell Signaling 3601), Phospho-SYK Tyr525/526 (Cell Signaling 2710), Phospho-PLCγ2 Tyr759 (Cell Signaling 3874), Phospho-CD79A Tyr182 (Cell Signaling 5173), Phospho-SRC Family Tyr416 (Cell Signaling 6943), Phospho-BTK Tyr223 (Cell Signaling 5082), Phospho-AKT Ser473 (Cell Signaling 9271), Phospho-AKT Thr308 (Cell Signaling 2965), Total CD79A (Cell Signaling 3351), Phospho-CD19 Tyr531 (Cell Signaling 3571), Total CD19 (Bethyl A304-392A), Total SYK (Bethyl A300-559A), Total BTK (Novus MAB5807), Total AKT (Cell Signaling 9272), Total PLCγ2 (Novus MAB3716), Irf4 (Active Motif 61512), H4R3me2a (Active Motif 39705), H3R2me2a (Epigentek A-3714-050), H3K27me3 (Cell Signaling 9756), Total Histone H3 (Abcam AB1791), Total Histone H4 (Bethyl A300-646A), H3R17me2a (Active Motif 39710), H3K4me3 (Cell Signaling 9727), H3R26me2a (EMD Millipore 07-215), H3K36me2 (Active Motif 39256), H3K79me2 (Active Motif 39144), Pan-Acetyl H3 (Active Motif 39140), H3K27ac (Active Motif 39136).

2.14 In Vitro Methylation Assays

Methylation assays were performed using recombinant GST-PRMT1 (BPS Biosciences 51041) and recombinant FLAG-CARM1 (Active Motif 31347) purified from Sf9 cells. Recombinant PRC2 complex (His-EZH2/Flag-EED/His-SUZ12), His-GST-EZH2, and His-FLAG-SUZ12 were also expressed in insect cells (BPS Biosciences 51003, 50279, 50282).

Nucleosome methylation assays used recombinant FLAG-CARM1 purified from HEK293 cells (BPS Biosciences 51047) and recombinant polynucleosomes derived from E. coli (Active Motif 31468). The assays used either PRC2 buffer (10X: 0.5M Tris pH 9.0, 5mM MgCl2, 4mM DTT) or PRMT1 buffer (10X Phosphate Buffered Saline pH 7.4). Radioactive assays were performed using tritiated S-adenosylmethionine ([^{3}H]-SAM) as a cofactor.

Chapter 3:

RESULTS

3.1 Targeting BCR signaling to potentiate EZH2 inhibitor efficacy in DLBCL

3.1.1 EZH2 inhibitor treatment increases global tyrosine phosphorylation and activates B-Cell Receptor signaling in lymphoma cells

To determine whether there were any changes in intracellular kinase signaling after EZH2 inhibitor treatment, we assessed tyrosine phosphorylation patterns in three cell lines with variable sensitivity to the EZH2 inhibitor EPZ-6438. All three cell lines display tonic B-Cell Receptor (BCR) signaling, which is necessary for SYK kinase-induced PI3K/AKT activation. H3K27 tri-methylation was effectively depleted after EZH2 inhibitor treatment (Figure 7a). Interestingly, two cell lines that were moderately sensitive (SUDHL-6) and resistant (SUDHL-4) to EPZ-6438, showed a marked up-regulation in global tyrosine phosphorylation levels, while the hypersensitive cell line (SUDHL-10) showed an increase at lower doses but a negligible change at higher doses of the EZH2 inhibitor. High levels of global tyrosine phosphorylation in SUDHL-4 came from phosphorylation of key components of the BCR signaling pathway, such as SRC, SYK, CD79A, CD19, BLNK and PLCγ2 (Figure 7b). Interestingly, total CD79A levels also increased after EPZ-6438 treatment. Upon analysis of ChIP-Seq and gene expression data from a published study of the EZH2 inhibitor GSK126, we discovered that CD79A and SRC family kinases (SRC/HCK/LCK) are targets repressed by EZH2 in lymphoma cells (Figure 7c) (60). Although the lowest concentration of EPZ-6438 was adequate to de-repress CD79A and increase its total protein level, phosphorylation of CD79A increased with higher concentrations of the inhibitor and correlated with SYK phosphorylation at Y525/526. BTK auto-phosphorylation at Y223 changed marginally. However, increased phosphorylation of its substrate PLCγ2 is an indicator of enhanced BTK activity in the context of SYK-induced BLNK phosphorylation. The involvement of different kinases and adaptor proteins in the BCR signaling pathway are shown for reference (Figure 7d). Intriguingly, tonic BCR signaling involves only SYK-mediated AKT activation, and does

not involve BTK or PLCγ2. BTK activation upon EZH2 inhibitor treatment is indicative of an antigen-type BCR response, signifying a transformation of these cells to a centrocyte-like phenotype with active BCR.

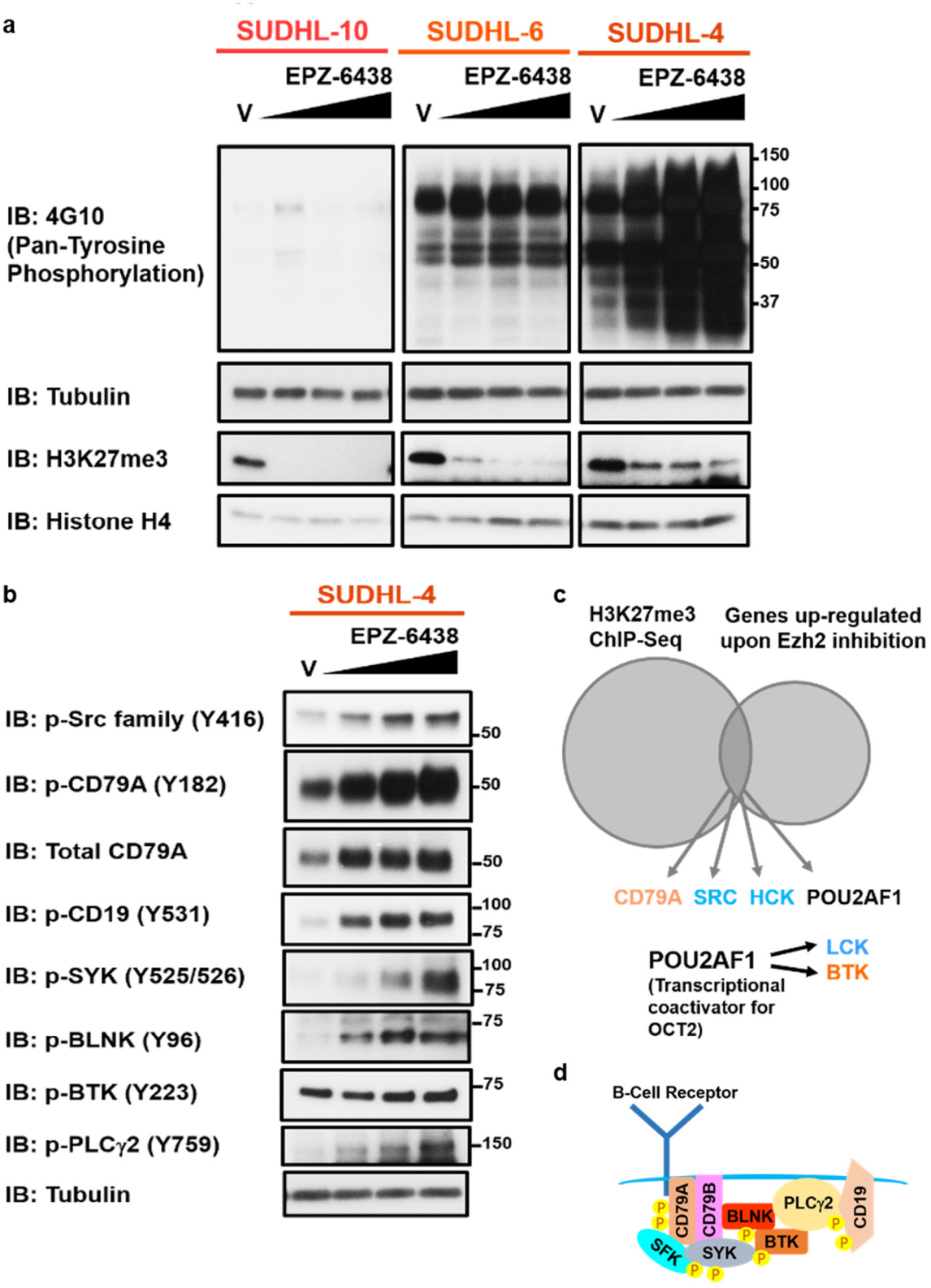
a
SUDHL-10
SUDHL-6
SUDHL-4
EPZ-6438
V
IB: 4G10
(Pan-Tyrosine
Phosphorylation)
150
100
75
50
37
IB: Tubulin
IB: H3K27me3
IB: Histone H4
b
SUDHL-4
EPZ-6438
V
IB: p-Src family (Y416)
IB: p-CD79A (Y182)
IB: Total CD79A
IB: p-CD19 (Y531)
IB: p-SYK (Y525/526)
IB: p-BLNK (Y96)
IB: p-BTK (Y223)
IB: p-PLCγ2 (Y759)
IB: Tubulin
50
100
75
150
c
H3K27me3
ChIP-Seq
Genes up-regulated
upon Ezh2 inhibition
CD79A SRC HCK POU2AF1
POU2AF1
(Transcriptional
coactivator for
OCT2)
LCK
BTK
d
B-Cell Receptor
CD79A
CD79B
BLNK
PLCγ2
CD19
SFK
SYK
BTK
P

Figure 7. EZH2 inhibitor treatment enhances global tyrosine phosphorylation and BCR signaling. (a) Lymphoma cell lines SUDHL-10, SUDHL-6 and SUDHL-4 were treated with 0.25, 0.5 and 1uM doses of EPZ-6438 for 6 days and changes in tyrosine phosphorylation were assessed using a pan-tyrosine phosphorylation (4G10) antibody. H3K27me3 was depleted in all three cell lines after EZH2 inhibitor treatment. **(b)** Before and after EPZ-6438 treatment, SUDHL-4 cell lysates were analyzed for phosphorylation of key components of the BCR signaling pathway, including the SRC Family of Kinases (SFK), CD79A, CD19, SYK, BLNK, BTK and PLCγ2. **(c)** ChIP-Seq and gene expression data from a study of the EZH2 inhibitor GSK126 was analyzed to identify BCR signaling pathway components that may be EZH2 targets in lymphoma cells (60). Results are represented as a Venn diagram. **(d)** Simplified model of kinases and adaptor proteins in the BCR pathway.

3.1.2 Genetic Manipulation of BCR and CD19 augments EZH2 inhibitor efficacy

To study the importance of BCR signaling after EZH2 inhibition, we analyzed EPZ-6438 sensitivity of EZH2-mutant lymphoma cells engineered to delete the Hypervariable Region of the B-Cell Receptor (BCR-KO) using CRISPR/Cas9 technology (cell lines established by O Havranek and RE Davis). The moderately sensitive cell line SUDHL-6 was rendered hypersensitive to EPZ-6438 after BCR knockout, yielding a 44-fold shift in its IC50 value, from 2.169uM to 0.049uM, at 7 days of treatment (Figure 8a). As a positive co-receptor of the BCR, CD19 lowers the threshold for BCR signaling, and acts as a molecular scaffold for multiple downstream regulators, most notably playing a role in PI3K activation. Therefore, we used SUDHL-6 cells with CD19 co-receptor knockout (CD19-KO) to assess whether CD19 was critical for sustaining BCR signaling in the absence of EZH2 activity. CD19-KO cells displayed a remarkable 271-fold shift in their IC50 value for EPZ-6438, from 2.169uM to 0.008uM, supporting the observation that BCR signaling becomes essential after inhibitor treatment. The sensitivity of CD19-KO cells to the inhibitor was still 6-fold higher than BCR-KO cells, suggesting that BCR-independent functions of CD19 may come into play and add to the role of this positive co-receptor post-EZH2 inhibition. Tonic BCR signaling is propagated by SYK, and primarily activates AKT to mediate cell survival. However, cells with PTEN-knockout do not depend on the BCR-SYK pathway to activate AKT. Accordingly, in the EZH2-wildtype cell line OCI-LY7, BCR-knockout renders it highly sensitive to EPZ-6438 treatment (0.025uM vs. 0.441uM for BCR-KO vs. BCR-WT), but PTEN-knockout increases the EZH2 inhibitor IC50 value to 0.095uM when combined with BCR-knockout (Figure 8b). On the other hand, the cell line DB, which is sensitive to EPZ-6438 and demonstrates little to no tonic BCR signaling, was only marginally affected by BCR-knockout (0.339uM vs 0.680uM for BCR-KO vs. BCR-WT), with a 2-fold shift in IC50 (Figure 8c). SUDHL-10 cells are PTEN-deficient with low BCR surface density, and are therefore not as dependent on tonic signaling as SUDHL-6 cells.

Interestingly, even though SUDHL-10 cells are already hypersensitive to EPZ-6438, they show a further shift in IC50 (3-fold) after BCR-knockout, from 0.377nM to 0.110nM. SUDHL-7 and OCI-Ly8 cells, which are both EZH2-wildtype, displayed negligible changes in their IC50 values for EPZ-6438 after BCR-knockout, and remained completely resistant to the inhibitor (Figure 8d). EPZ-6438 IC50 values for all the cell lines discussed above are displayed for comparison in Figure 8e. Together, these results support the hypothesis that signaling through the B-Cell Receptor, regardless of tonic or antigen type, sustains cell growth and survival in the aftermath of EZH2 inhibition in a subset of lymphoma cell lines. However, EZH2 dependency may be a key factor in determining whether targeting BCR signaling can enhance response to the EZH2 inhibitor, since EZH2-wildtype cell lines originally lacking sensitivity to the inhibitor do not show any marked changes in sensitivity after BCR-knockout.

3.1.3 Deficient tonic BCR signaling improves EZH2 inhibitor sensitivity

Next, to assess the contribution of tonic BCR signaling specifically to the sensitizing effect of BCR-knockout in lymphoma cells, we used a GFP-fusion knock-in mutant of CD79A (Y188F) which blocks only tonic BCR signaling, but has no effect on active BCR signaling. CD79A becomes tyrosine phosphorylated at tyrosine residues in its ITAM domains upon BCR activation, enabling binding and activation of signaling mediators such as SYK kinase. In congruence with our observations in BCR-KO cells, the CD79A-Y188F mutant had no effects on EZH2 inhibitor sensitivity of the cell line DB, which demonstrates low levels of tonic signaling (Figure 8f). In SUDHL-6 cells, the Y188F mutant displayed a 7.6-fold shift in the IC50 value for EPZ-6438 (0.144uM vs 1.098uM for CD79A-Y188F vs CD79A-WT). Differences between SUDHL-6 CD79A-WT and CD79A-Y188F cells after 8 days of EPZ-6438 treatment can be clearly observed through GFP imaging (Figure 8g). These results indicate that tonic BCR signaling via SYK and AKT at least partly contributes to the BCR-mediated response to

EZH2 inhibitor therapy. However, this phenomenon may be further reinforced by antigen-type BCR signaling, and provide a compensatory mechanism for cell growth and survival in the absence of EZH2 activity.

EZH2-mutant ***EZH2-wildtype***

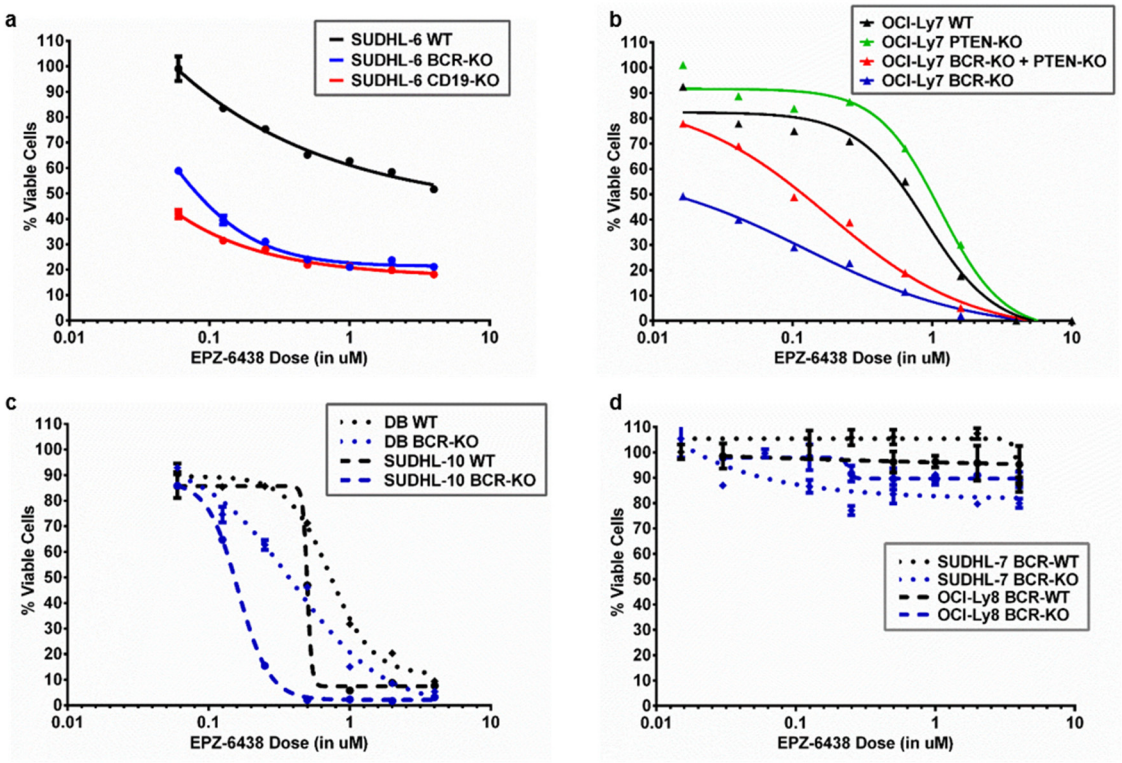

e

Cell Line	Manipulation	EPZ-6438 IC50 (in uM)	Shift in IC50
SUDHL-6	WT	2.169	1.0
	BCR-KO	0.049	44.3
	CD19-KO	0.008	271.1
OCI-Ly7	WT	0.441	1.0
	BCR-KO	0.025	17.6
	PTEN-KO	0.770	0.6
	BCR+PTEN-KO	0.095	4.6
*SUDHL-10	WT	0.377	1.0
	BCR-KO	0.112	3.4
DB	WT	0.680	1.0
	BCR-KO	0.339	2.0
SUDHL-7	WT	>10	1.0
	BCR-KO	>10	1.0
OCI-Ly8	WT	>10	1.0
	BCR-KO	>10	1.0

*PTEN-deficient

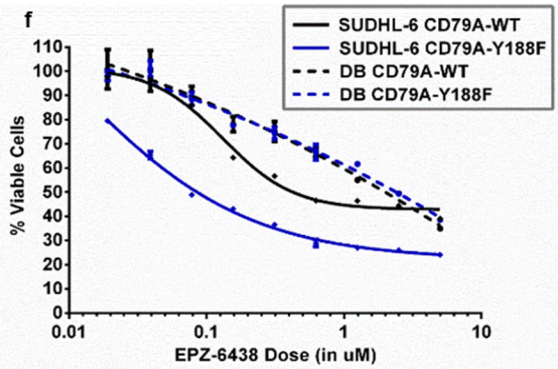

Cell Line	Manipulation	EPZ-6438 IC50 (in uM)	Shift in IC50
SUDHL-6	CD79A-WT	1.098	1.0
	CD79A-Y188F	0.144	7.6
DB	CD79A-WT	1.488	1.0
	CD79A-Y188F	1.600	0.9

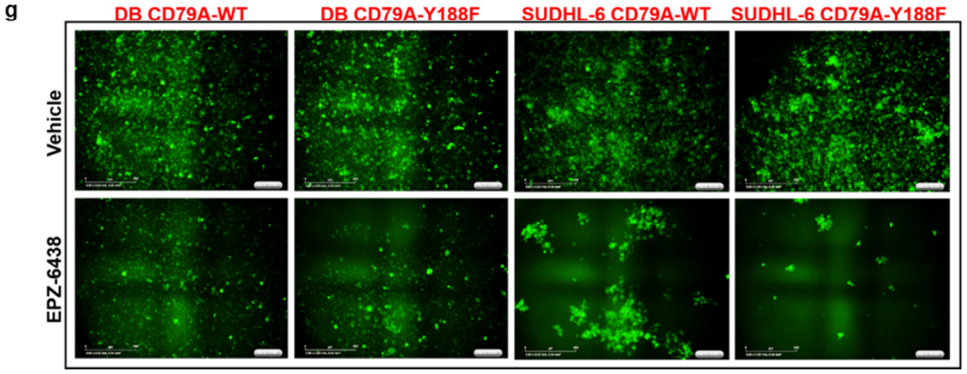

Figure 8. Genetic manipulation of components of the BCR signaling pathway potentiates sensitivity of lymphoma cells to the EZH2 inhibitor EPZ-6438. (a) EZH2-mutant SUDHL-6 WT, BCR-KO and CD19-KO cells were treated with EPZ-6438 for 7 days and cell growth was measured using CellTiter-Glo viability assay. **(b)** Sensitivity to EPZ-6438 treatment was determined in EZH2-wildtype OCI-Ly7 cells with PTEN-KO, BCR-KO or combined BCR and PTEN-KO (data generated by O Havranek and RE Davis). **(c)** EZH2-mutant SUDHL-10 and DB cells with BCR-WT or BCR-KO were assessed for changes in proliferation after 7 days of EPZ-6438 treatment using CellTiter-Glo viability assay. **(d)** EZH2-wildtype SUDHL-7 and OCI-Ly8 cells with wildtype-BCR or BCR-KO were treated with EPZ-6438 for 7 days and analyzed using a similar method. **(e)** EPZ-6438 IC50 values for all cell lines described above are shown in tabular format. IC50 values were determined using Compusyn software. Shifts in IC50 value ≥ 2.0 are highlighted in red. **(f)** SUDHL-6 and DB cells expressing wildtype-CD79A or the Y188F mutant of CD79A were assessed for changes in cell proliferation after 7 days of EPZ-6438 treatment using CellTiter-Glo viability assay. IC50 values are displayed in tabular format and a shift in IC50 value ≥ 2.0 is highlighted in red. **(g)** GFP fused to CD79A facilitated imaging of SUDHL-6 and DB CD79A-WT and CD79A-Y188F cells using an Incucyte Zoom instrument at 20X magnification after 8 days of Vehicle or EPZ-6438 treatment.

3.1.4 EZH2 inhibitor-treated lymphoma cells exhibit an activated B-cell phenotype

The threshold for BCR signaling is tightly controlled by co-receptors and their associated phosphatases. To assess if changes in BCR signaling were occurring as a result of imbalances in co-receptor expression, we analyzed cell surface expression of positive (CD19) and negative (CD22, CD72) co-receptors of the BCR, and the ligand for CD72 (CD100) in SUDHL-6 cells after EPZ-6438 treatment. We treated BCR-knockout and CD19-knockout cells alongside wildtype cells to be able to make a better comparison (Figure 9a). After 7 days of EZH2 inhibitor treatment, SUDHL-6 cells displayed increased CD19 and increased CD100 expression (Figure 9b). There were no changes in CD72 (not shown) and IgM cell surface expression. Although the mean surface expression of CD22 marginally decreased after EPZ-6438 treatment, there was a CD22-low population in the untreated condition that disappeared upon EZH2 inhibitor treatment. This was also seen in BCR-KO cells, but not in CD19-KO cells where the decrease in CD22 expression was more distinct than in the other two cell types. Interestingly, CD100 uniformly increased in all three types of SUDHL-6 cells after EPZ-6438 treatment. Overall, these observed changes in co-receptor expression suggest that altered BCR signaling thresholds may at least partly contribute to aberrant activation of the BCR pathway after EZH2 inhibitor treatment. CD100 is a ligand belonging to the semaphorin family, which acts by switching off inhibitory signaling of the negative co-receptor CD72 and leading to SHP1 dissociation. CD72-CD100 ligation through B-cell:T-cell interactions are commonly associated with B-cell activation, and CD100 is sometimes expressed on the cell surface of activated B-cells themselves. SUDHL-6 cells pre-treated with EPZ-6438 demonstrate a robust proliferative response when stimulated with B-cell activating ligands such as CD40L and BAFF (Figure 9c). While EPZ-6438 treatment reduces SUDHL-6 cell growth by 30-40%, addition of CD40L or BAFF potently negates growth suppression by the EZH2 inhibitor. A similar phenomenon is observed in SUDHL-4 cells pre-treated with the EZH2 inhibitor. Since SUDHL-

4 cells are resistant to the EZH2 inhibitor, there is a net increase in cell growth when EPZ-6438 pre-treated cells are stimulated with CD40L. These results indicate that EZH2 inhibition promotes B-cell activation, and that the anti-proliferative effects of EPZ-6438 can be antagonized by microenvironmental stimuli supporting centrocyte survival and growth.

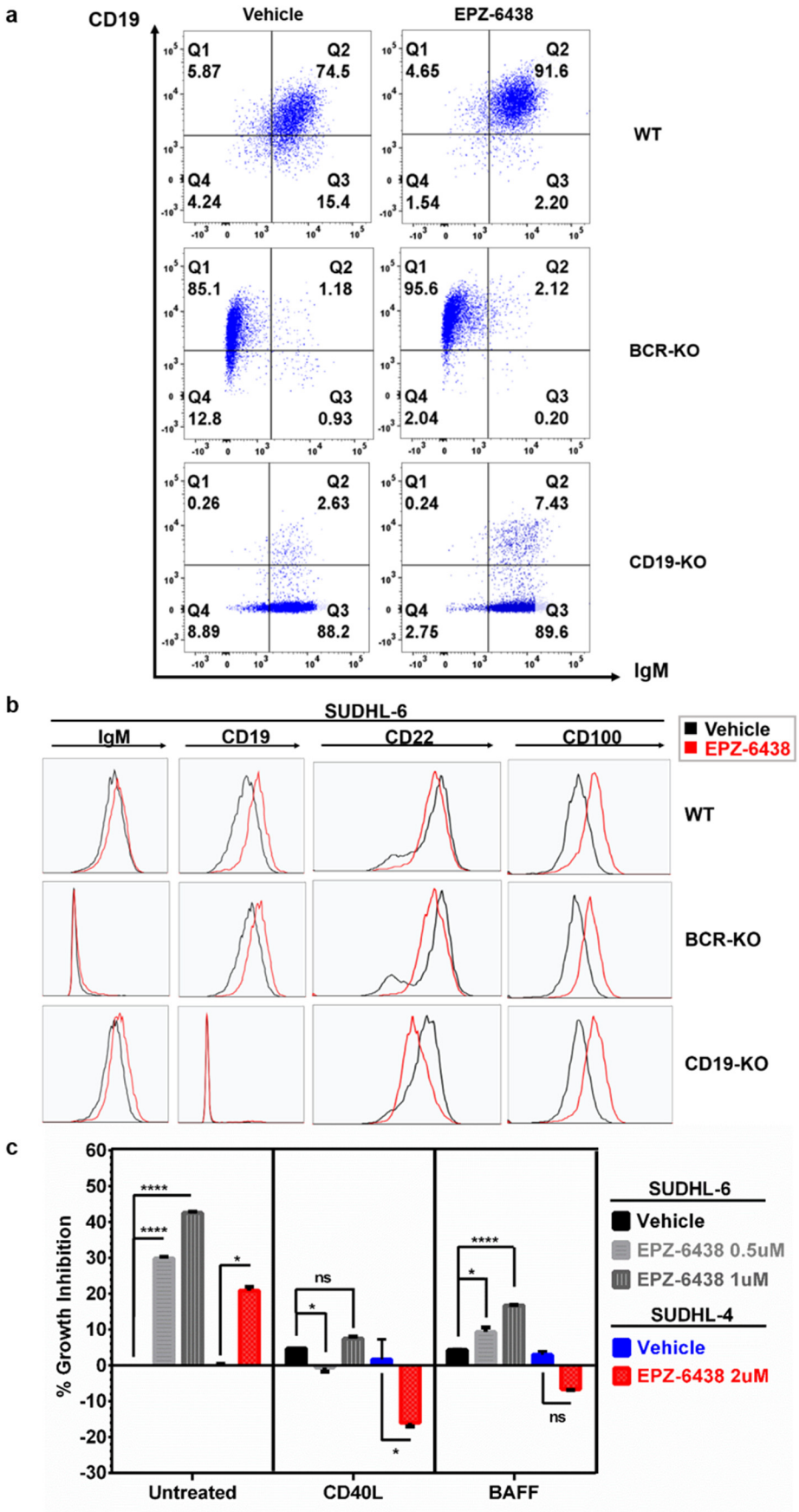
a
CD19
Vehicle
EPZ-6438
Q1 5.87
Q2 74.5
Q4 4.24
Q3 15.4
Q1 4.65
Q2 91.6
Q4 1.54
Q3 2.20
WT
Q1 85.1
Q2 1.18
Q4 12.8
Q3 0.93
Q1 95.6
Q2 2.12
Q4 2.04
Q3 0.20
BCR-KO
Q1 0.26
Q2 2.63
Q4 8.89
Q3 88.2
Q1 0.24
Q2 7.43
Q4 2.75
Q3 89.6
CD19-KO
IgM
b
SUDHL-6
IgM
CD19
CD22
CD100
Vehicle
EPZ-6438
WT
BCR-KO
CD19-KO
c
% Growth Inhibition
60
50
40
30
20
10
0
-10
-20
-30
****
****
*
ns
*
*
****
*
ns
Untreated
CD40L
BAFF
SUDHL-6
Vehicle
EPZ-6438 0.5uM
EPZ-6438 1uM
SUDHL-4
Vehicle
EPZ-6438 2uM

Figure 9. EZH2-mutant lymphoma cells show an Activated B-cell-like phenotype after EZH2 inhibition. (a) Flow cytometry was used to analyze CD19 and IgM cell surface expression after 7 days of EPZ-6438 treatment in SUDHL-6 cells with intact CD19 and IgM (WT), with IgM knockout (BCR-KO), or with CD19 knockout (CD19-KO). **(b)** CD19 and IgM cell surface expression are represented as histograms to visualize changes in the mean expression of these markers. In the same populations, cell surface expression of the negative co-receptor CD22 and the activating ligand CD100 (for the negative co-receptor CD72) was determined using flow cytometry. **(c)** Parental SUDHL-6 cells were pre-treated with vehicle or EPZ-6438 for 4 days and then inhibitor treatment was combined with CD40L or BAFF stimulation for another 3 days. Cell proliferation was assessed using CellTiter-Glo viability assay. Statistical significance was determined by 2-way ANOVA ($p>0.05$=ns, $p<0.05$*, $p<0.0001$****).

3.1.5 BCR-knockout cells demonstrate sustained CD19 signaling and PI3Kδ/BTK dependency

We studied the effects of BCR-knockout on SUDHL-6 cells to determine which signaling pathways were most affected by the absence of a functional BCR (Figure 10a). As expected, loss of tonic BCR signaling via SYK led to the depletion of both CD79A phosphorylation (Tyr-182) and AKT phosphorylation (Ser-473). However, CD19 phosphorylation was notably higher in SUDHL-6 BCR-KO cells, and BTK displayed increased phosphorylation at a tyrosine residue (Tyr-551) targeted by LYN/SYK kinases. Accordingly, the BTK substrate PLCγ2 was increasingly phosphorylated in BCR-KO cells despite the absence of BCR signaling and lack of SYK activation. Interestingly, EZH2 inhibitor treatment in BCR-KO cells led to a reversal of PLCγ2 phosphorylation levels to that of control BCR-WT cells. This suggests that SUDHL-6 BCR-KO cells maintain increased PLCγ2 phosphorylation through a mechanism that may depend on intact EZH2 activity. Combined with the loss of AKT activity, the inability of SUDHL-6 BCR-KO cells to activate signaling downstream of BTK may be one of the reasons for their increased susceptibility to EZH2 inhibition. To assess the importance of BTK activation in these cells, we tested the effect of kinase inhibitors targeting PI3Kδ and BTK in BCR-WT and BCR-KO cells (Figure 10b). SUDHL-6 BCR-KO cells were extremely sensitive to PI3Kδ and BTK inhibition even at low doses, while their wildtype counterparts were resistant to the PI3Kδ inhibitor, and showed BTK inhibitor sensitivity only at high doses with possible off-target toxicity.

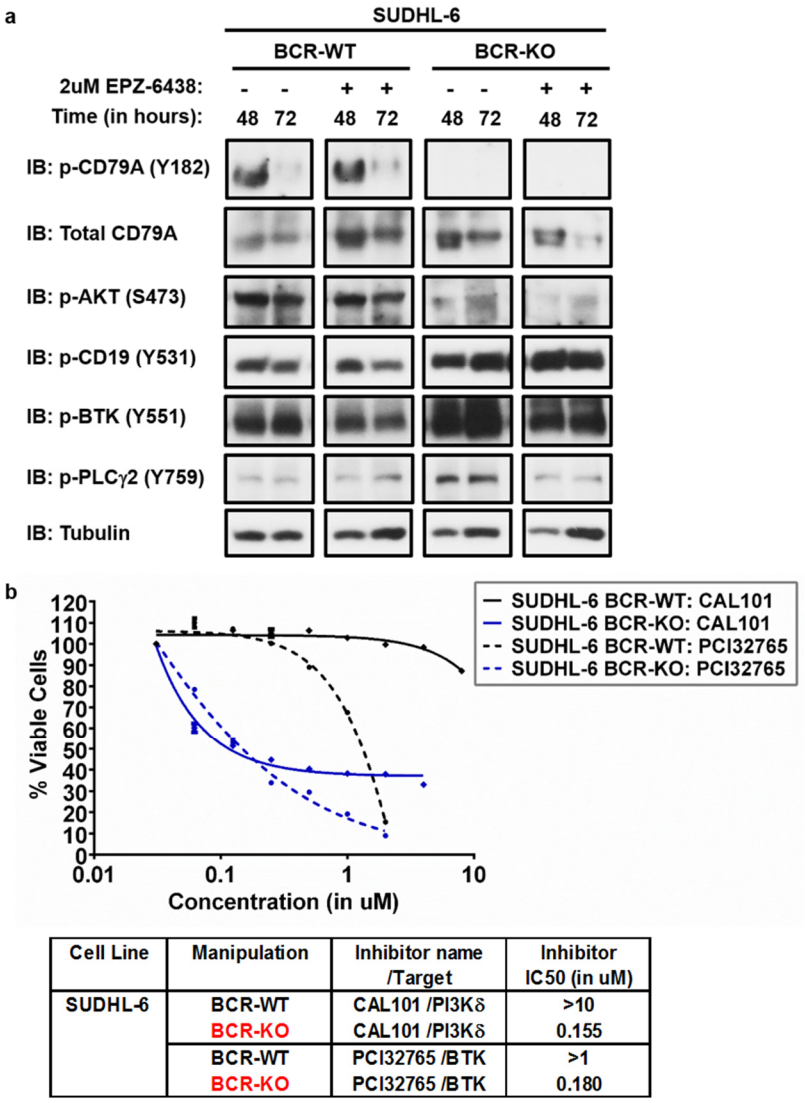

Cell Line	Manipulation	Inhibitor name /Target	Inhibitor IC50 (in uM)
SUDHL-6	BCR-WT	CAL101 /PI3Kδ	>10
	BCR-KO	CAL101 /PI3Kδ	0.155
	BCR-WT	PCI32765 /BTK	>1
	BCR-KO	PCI32765 /BTK	0.180

Figure 10. BCR-knockout cells display impaired CD79A signaling but maintain CD19 signaling. (a) SUDHL-6 BCR-WT and BCR-KO cells were treated with EPZ-6438 at 2uM for 48 hours and 72 hours. Cell lysates were collected and BCR signaling pathway components were analyzed for their phosphorylation status. **(b)** SUDHL-6 BCR-WT and BCR-KO cells were treated with varying doses of PI3Kδ inhibitor (CAL101) or BTK inhibitor (PCI32765) for 4 days and cell proliferation was measured using CellTiter-Glo viability assay. IC50 values for each inhibitor were determined using Compusyn software and displayed in table format.

3.1.6 Inhibitors of kinases downstream of BCR and CD19 show potent synergy in combination with EPZ-6438

We used kinase inhibitors targeting three nodes of BCR signaling to assess rational combination therapies with the EZH2 inhibitor: the SYK inhibitor P505-15, the PI3Kδ inhibitor CAL101, and the BTK inhibitor PCI32765. SYK and PI3Kδ inhibition would block both tonic and active BCR signaling, while BTK inhibition would selectively target active BCR signaling. SUDHL-6 and SUDHL-4, which display high levels of tonic BCR signaling, were both sensitive to combinations of EPZ-6438 and all three kinase inhibitors (SYK/PI3Kδ/BTK). The SYK inhibitor is effective as a single agent in these two cell lines that rely on tonic BCR signaling, but even more effective when combined with the EZH2 inhibitor (Figure 11a). GCB-DLBCL cell lines are only sparingly sensitive to PI3Kδ inhibition as a single agent, but become highly sensitive to CAL101 when combined with EPZ-6438 treatment (Figure 11b). The remarkable efficacy of PCI32765 in combination studies with EPZ-6438 suggests that BTK becomes highly relevant in the absence of EZH2 activity, while GCB-DLBCL cell lines generally do not respond to this inhibitor as a single agent (Figure 11c). The EZH2-wildtype cell line HT is moderately sensitive to EPZ-6438 due to a loss-of-function mutation in the H3K27 demethylase KDM6A/UTX. Interestingly, it also lacks PTEN protein, leading to a high level of AKT activation. In this cell line, inhibitor combination studies showed significant synergy with the PI3Kδ inhibitor and the BTK inhibitor. The EZH2-wildtype cell line SUDHL-5 was sensitive to PI3Kδ inhibition in combination with EPZ-6438, despite being resistant to EZH2 inhibition as a single agent. In conclusion, we have showed that the EZH2 inhibitor synergizes with multiple inhibitors of kinases downstream of BCR signaling. Figure 11d is a model of 'targetable' dependencies that could arise from EZH2 inhibitor treatment. Inhibitors targeting kinases in the BCR signaling pathway are in different stages of clinical trial for DLBCL, and therefore combinations with the EZH2 inhibitor represent an achievable clinical possibility.

a

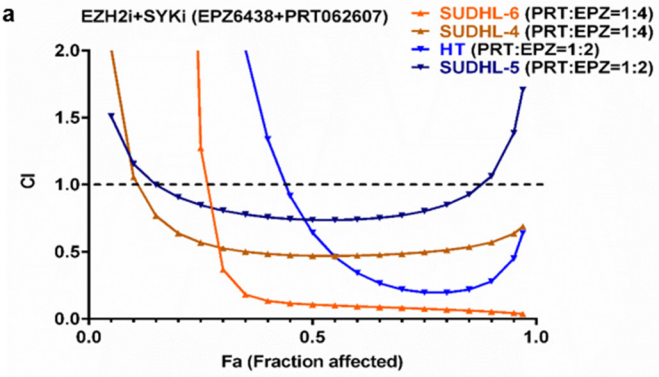

Combination	Cell line	Ratio	CI
PRT062607+EPZ6438 (SYKi+EZH2i)	SUDHL-6	1:1	0.2370
		1:2	0.1116
		1:4	0.1063
	SUDHL-4	1:2	0.5543
		1:4	0.4698
	HT	1:2	0.6423
		1:4	0.6352
	SUDHL-5	1:2	0.7375
		1:4	0.9657

b

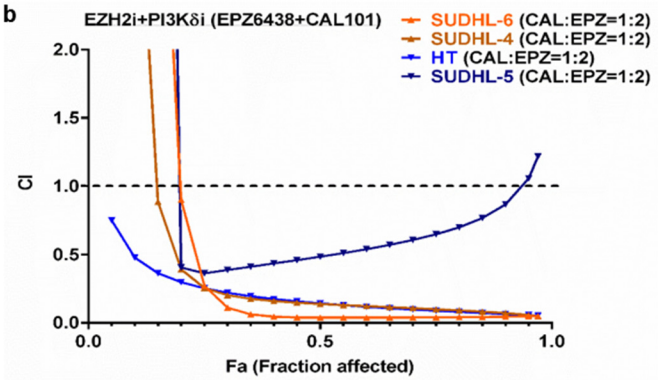

Combination	Cell line	Ratio	CI
CAL101+EPZ6438 (PI3Kδi+EZH2i)	SUDHL-6	1:1	0.1112
		1:2	0.0372
		1:4	0.0902
	SUDHL-4	1:2	0.1382
		1:4	0.2314
	HT	1:2	0.1421
		1:4	0.3581
	SUDHL-5	1:2	0.4841
		1:4	0.7183

c

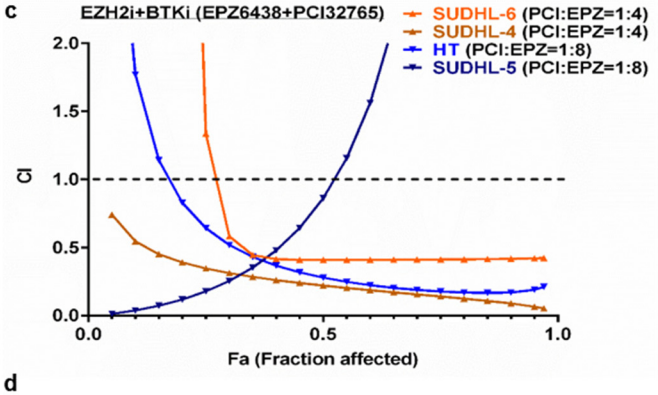

Combination	Cell line	Ratio	CI
PCI32765+EPZ6438 (BTKi+EZH2i)	SUDHL-6	1:1	0.2491
		1:4	0.4083
		1:8	0.3091
	SUDHL-4	1:4	0.2208
		1:8	0.2765
	HT	1:4	0.2697
		1:8	0.2792
	SUDHL-5	1:4	0.6896
		1:8	0.8626

CI<0.1	Very highly synergistic
CI 0.1-0.3	Highly synergistic
CI 0.3-0.9	Synergistic
CI 0.9-1.1	Additive

d

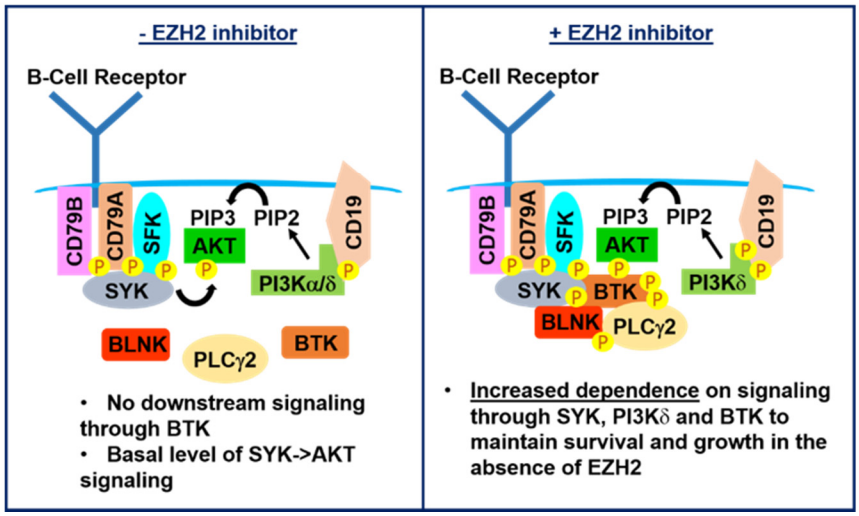

Figure 11. The EZH2 inhibitor EPZ-6438 synergizes with SYK, PI3Kδ and BTK inhibitors in lymphoma cell lines. (a) Combinations of the SYK inhibitor PRT062607 and EPZ-6438 were analyzed at multiple constant ratios (1:1, 1:2, 1:4) in SUDHL-6, SUDHL-4, HT and SUDHL-5. Cells were pre-treated with the EZH2 inhibitor for 3 days, followed by 4 days of combined treatment with SYK and EZH2 inhibitors. Cell proliferation was measured using CellTiter-Glo viability assay, and combination indices were generated by Chou-Talalay analysis using Compusyn software. **(b)** A similar method was used for combinations of EPZ-6438 and the PI3Kδ inhibitor CAL101. **(c)** For combinations of the EZH2 inhibitor with the BTK inhibitor, ratios of 1:1, 1:4 and 1:8 were used for PCI32765 and EPZ-6438 respectively. **Right,** combination indices derived from different cell lines and inhibitors are provided in table format next to each panel. Dark red to yellow coloring marks CI values ranging from very highly synergistic (CI<0.1) to additive (CI between 0.9-1.1) at different doses of the inhibitors. **(d)** A model illustrating targetable dependencies that may arise from EZH2 inhibitor treatment in lymphoma cells. When EZH2 activity is intact, GCB-DLBCL cells display tonic BCR signaling via PI3K/AKT, and are sensitive only to SYK inhibitors. However, lymphoma cells treated with the EZH2 inhibitor display both tonic and antigen-type BCR signaling, which makes them dependent on SYK, PI3Kδ, and BTK for survival and growth.

3.2 Type I PRMTs are novel and effective epigenetic targets in DLBCL

3.2.1 Prolonged EZH2 inhibitor treatment increases global asymmetric di-methylation of histone H4 at arginine-3

Suppression of EZH2 activity in lymphoma cells is expected to lead to global de-repression of its target genes and 'rewiring' of the epigenetic circuitry. Therefore, we examined global changes in histone modifications after prolonged EZH2 inhibitor treatment to assess if there were any epigenetic changes tightly associated with H3K27me3 depletion. 12 days of EPZ-6438 treatment in SUDHL-6 and DB cells did not produce significant changes in most of the histone modifications that we profiled (Figure 12a). SUDHL-6 cells showed a significant increase in H3K36me2 levels, which is associated with MMSET activity. Interestingly, H3K4me3 levels were depleted and H4R3me2a levels were greatly enhanced after prolonged EPZ-6438 treatment. We analyzed H4R3me2a levels in multiple lymphoma cell lines after short-term EZH2 inhibitor treatment, and found that 5/6 cell lines showed a greater than 1.5-fold enhancement in this modification (Figure 12b). DB cells did not display a change in H4R3me2a at 4 days of treatment, but showed a distinct increase in this modification after longer durations of treatment. There was no correlation between EZH2 mutation status, sensitivity to the EZH2 inhibitor, and fold-change in H4R3me2a levels. We wanted to determine whether the increase in H4R3me2a was indicative of a favorable response to the EZH2 inhibitor, or whether it was involved in protecting lymphoma cells against the effects of EZH2 inhibition. PRMT1 is the major arginine methyltransferase known to catalyze the H4R3me2a modification. PRMT1-specific inhibitors are not available, but a Type I inhibitor called MS023 can effectively deplete H4R3me2a in different cell types (120). Therefore, we used MS023 in combination with EPZ-6438 to assess whether Type I PRMT inhibition can enhance the growth-suppressive effect of EZH2 inhibition or perhaps block these suppressive effects. When combined, EPZ-6438 and MS023 significantly increased apoptotic cell death in

DB and SUDHL-5 cells, while neither of them induced apoptosis as a single agent (Figure 12c). Co-treatment with EPZ-6438 and MS023 synergistically controlled cell growth in four lymphoma cell lines: DB, SUDHL-5, HT and RL (Figure 12d). Interestingly, RL and SUDHL-5 are EZH2-mutant and EZH2-wildtype respectively, but both are resistant to EPZ-6438 treatment. In SUDHL-6 cells, the Type I PRMT inhibitor MS023 as a single agent was far more effective than the combination treatment, and astonishingly superior to the EZH2 inhibitor alone. Similarly, the lymphoma cell line RL was also highly sensitive to MS023 as a single agent. These observations prompted us to investigate whether Type I PRMT inhibition as a single agent may have therapeutic potential in the treatment of DLBCL. To understand the mechanism behind MS023 and EPZ-6438 synergy, we first had to study the role of Type I PRMTs in DLBCL.

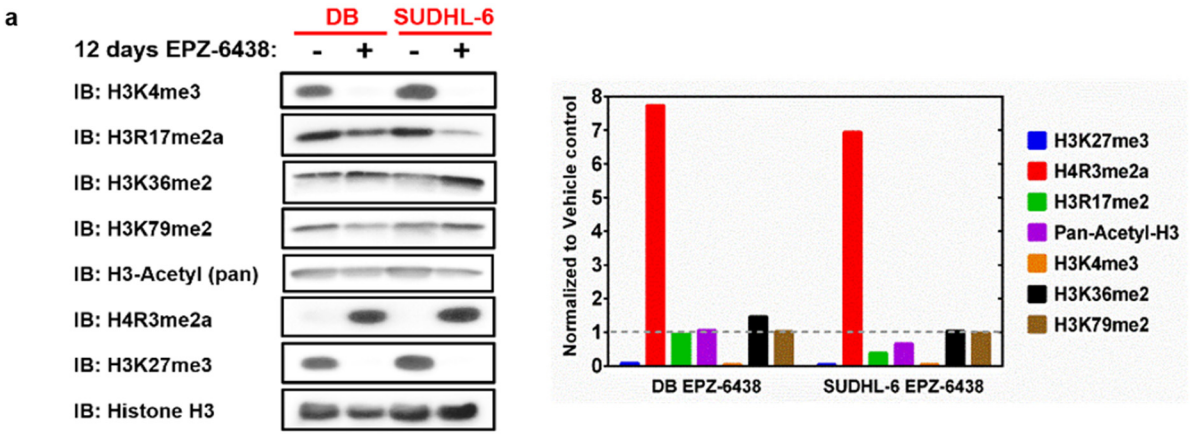

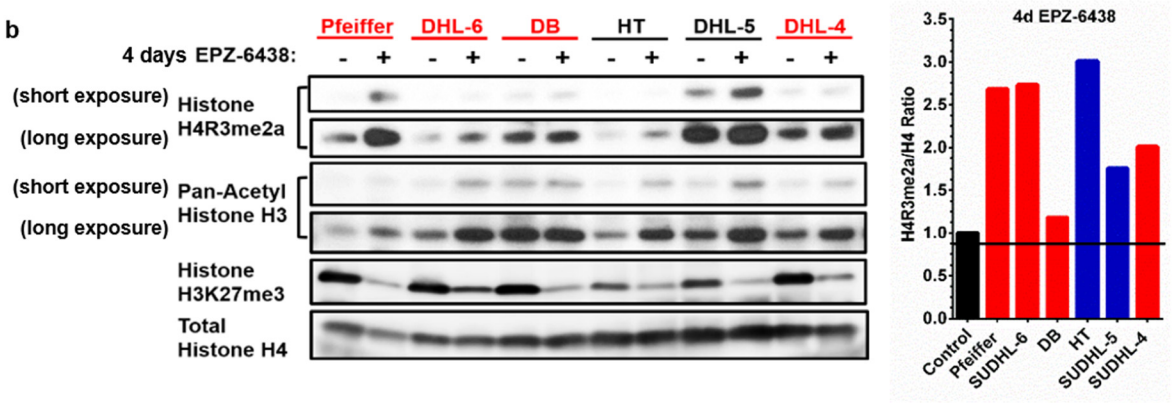

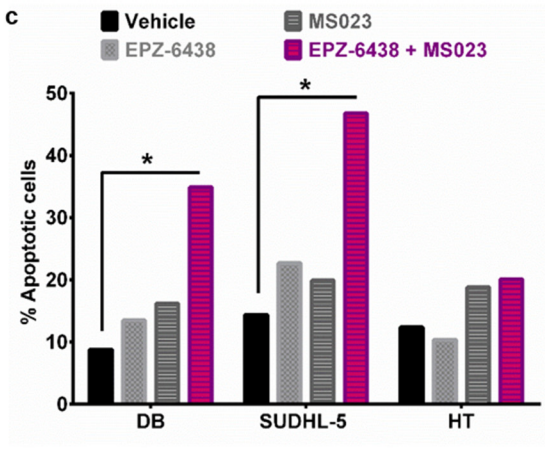

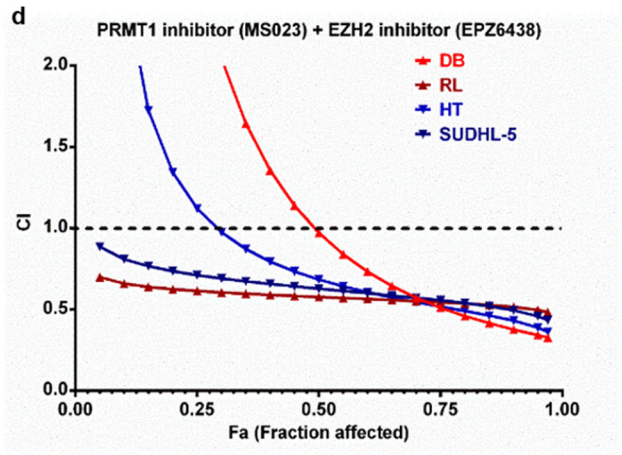

Combination Index at:

Combination	Cell line	ED50	ED75	ED90	ED95
MS023+EPZ6438	RL	0.57721	0.54493	0.51565	0.49698
	SUDHL-5	0.62818	0.55686	0.49547	0.45851
	HT	0.68458	0.5182	0.43138	0.38892
	DB	0.97217	0.5116	0.37719	0.34209

Figure 12. EZH2 inhibitor treatment increases global Histone H4 Arginine-3 asymmetric di-methylation and synergizes with the Type I PRMT inhibitor MS023 in lymphoma cells. **(a)** SUDHL-6 and DB cells were treated with EPZ-6438 for 12 days. Cell lysates were analyzed for changes in multiple histone modifications including H3K4me3, H3R17me2a, H3K36me2, H3K79me2, H3-acetyl (pan), H4R3me2a, and H3K27me3. Fold-change in histone marks are represented as a graph. **(b)** Pfeiffer, SUDHL-6, DB, SUDHL-5, HT and SUDHL-4 cells were treated with EPZ-6438 for 4 days. H4R3me2a, pan-acetyl histone H3, H3K27me3 and total histone H4 levels were assessed. Fold-change is represented in graphical format. EZH2-mutant cell lines are colored in red and EZH2-wildtype cell lines are colored in blue. **(c)** DB, SUDHL-5 and HT cells were co-treated with 1uM MS023 and 2uM EPZ-6438 for 8 days and the percentage of apoptotic cells was measured using Active Caspase-FITC staining coupled with flow cytometry. Statistical significance was calculated using 2-way ANOVA ($p<0.05$*) **(d)** DB, SUDHL-5, SUDHL-4, HT, and RL cell lines were co-treated with MS023 and EPZ-6438 for 8 days at a constant ratio of 1:2. Cell growth was measured using CellTiter-Glo viability assay, and combination indices were generated by Chou-Talalay analysis using Compusyn software. Combination indices are displayed in tabular format. Synergistic values (CI<0.9) are highlighted in red, and additive values (CI 0.9-1.1) are highlighted in white.

3.2.2. Type I PRMT inhibition suppresses cell growth and viability in a subset of DLBCL cell lines

In a panel of DLBCL cell lines, Type I PRMT inhibition using MS023 led to a significant reduction in the number of viable cells after 7 days of treatment (Figure 13a). The cell lines RL, Toledo, SUDHL-6, SUDHL-4, SUDHL-7 and DB were highly sensitive to MS023, with IC50 values less than 1uM. Considering that many of these cell lines are EZH2-mutant, it is interesting to note that RL, SUDHL-6 and SUDHL-4 have much lower IC50 values for MS023 in comparison to EPZ-6438. The ABC-DLBCL cell lines U-2932 and HBL-1, and the EZH2-wildtype cell lines SUDHL-5 and HT, were less sensitive to the Type I PRMT inhibitor with IC50 values greater than 1uM. Next, we performed cell cycle analysis for RL, SUDHL-4 and DB after 7 days of MS023 treatment (Figure 13b). DB and SUDHL-4 displayed G1-phase cell cycle arrest, while RL displayed a less marked difference. We also quantified the percentage of apoptotic cells after 7 days of MS023 treatment in RL, SUDHL-6 and DB cells (Figure 13c). For RL and SUDHL-6, there was a distinct increase in the percentage of apoptotic cells by active caspase staining. On the other hand, DB showed negligible changes in apoptosis after inhibitor treatment. Using COSMIC Cell Lines project and cBioPortal, we looked for mutations in epigenetic regulators among the DLBCL cell lines used in our study (Figure 13d) (46, 47, 127). Cell lines that were highly sensitive to MS023 harbored mutations in multiple epigenetic enzymes such as KMT2D/2C, EZH2, CREBBP and EP300.

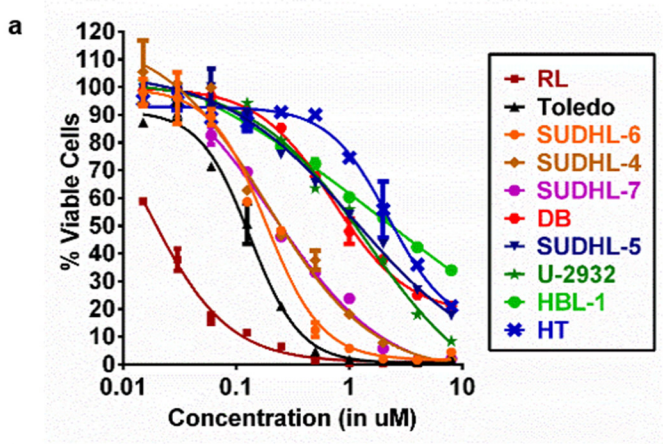

Subtype	Cell Line	MS023 IC50 (in uM)
GCB	RL	0.016
GCB	Toledo	0.133
GCB	SUDHL-6	0.185
GCB	SUDHL-4	0.186
GCB	SUDHL-7	0.215
GCB	DB	0.716
GCB	SUDHL-5	1.117
ABC	U-2932	1.465
ABC	HBL-1	2.071
GCB	HT	2.245

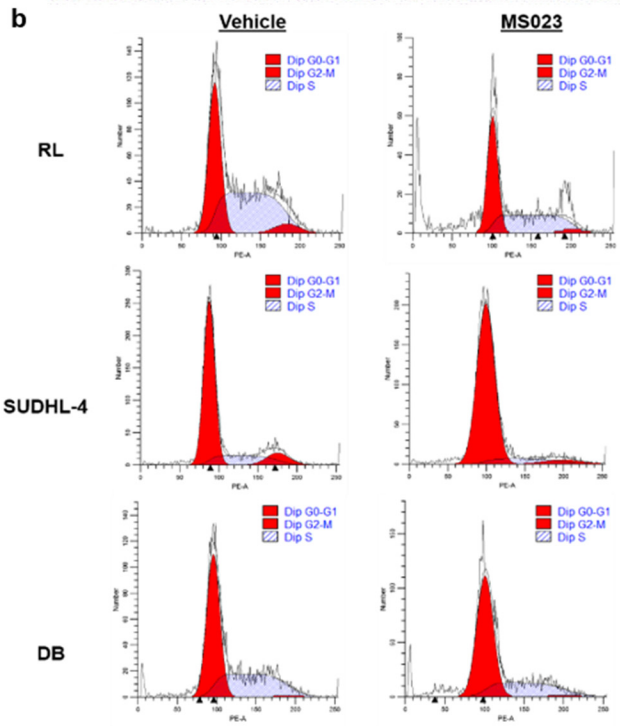

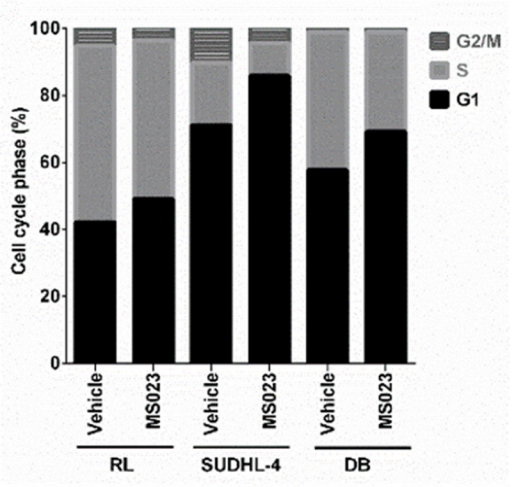

Cell line	Treatment	G1 (%)	S (%)	G2/M (%)
RL	Vehicle	42.1	52.7	5.2
	MS023	49.1	47.4	3.6
SUDHL-4	Vehicle	71.1	18.6	10.3
	MS023	85.8	9.8	4.5
DB	Vehicle	57.7	41.2	1.1
	MS023	69.1	29.9	1

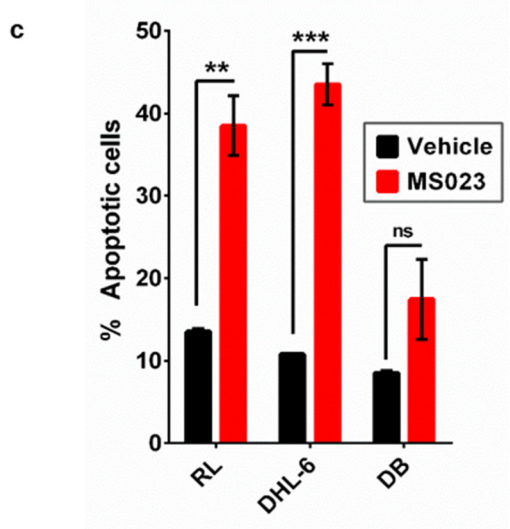

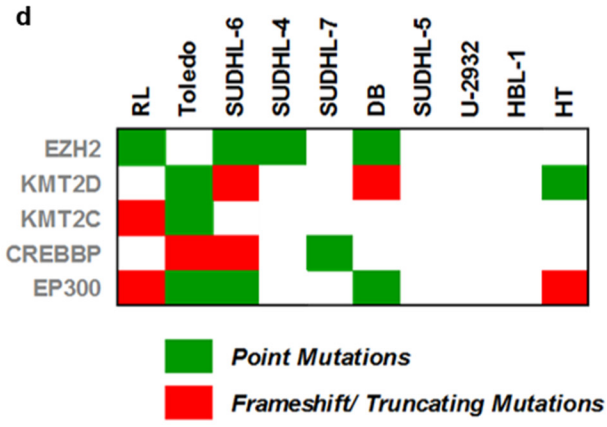

Figure 13. The Type I PRMT inhibitor MS023 induces cell cycle arrest and apoptosis in a panel of lymphoma cell lines. (a) DLBCL cell lines were treated with varying doses of MS023 for 7 days and cell growth was measured using CellTiter-Glo viability assay. IC50 values were calculated from MS023 dose-response curves using nonlinear regression analysis in GraphPad Prism, and these values are represented in table format to the right of the graph. **(b)** Propidium iodide staining and flow cytometry was used to determine cell cycle staging in RL, SUDHL-4 and DB cells after MS023 treatment for 7 days. Data analyzed using ModFit LT 5.0 software is displayed in both graphical and tabular format. **(c)** After 8 days of MS023 treatment, the percentage of apoptotic cells in RL, SUDHL-6 and DB was quantified using Active Caspase-FITC staining and flow cytometry. Statistical significance was assessed using 2-way ANOVA and the Bonferroni method ($p<0.01$** and $p<0.001$***). **(d)** Using data from COSMIC Cell Lines project and cBioPortal, the lymphoma cell lines utilized in our study were examined for alterations in the most frequently mutated epigenetic enzymes (46, 47, 127).

3.2.3 MS023 treatment reduces BCL2 levels to induce apoptosis in sensitive lymphoma cells

Many DLBCL cell lines harbor genomic amplification of the BCL2 locus or a t(14;18) chromosomal translocation leading to BCL2 overexpression (Figure 14a). To identify mechanisms contributing to apoptosis in cell lines sensitive to MS023, we screened for changes in key apoptosis mediators. This revealed a distinct reduction in the level of anti-apoptotic BCL2 protein after MS023 treatment in all cell lines tested (Figure 14b). Interestingly, the cell lines that underwent cell death upon Type I PRMT inhibition were previously reported to be BCL2-dependent cell lines with high sensitivity to the BCL2 antagonist ABT-199 (Venetoclax) (87). Protein levels of PRMT1, CARM1 and PRMT6 did not show any significant correlations with BCL2 levels across different cell lines. After 72 hours of MS023 treatment, BCL-XL levels did not change appreciably. In DB and HT cells, MCL-1 protein levels increased after PRMT inhibition, presumably as a compensatory mechanism after BCL2 loss. Interestingly, DB and HT are both reported to be MCL-1-dependent cell lines, even though DB has high BCL2 levels arising from a t(14;18) chromosomal translocation (128). While asymmetric arginine methylation was predictably depleted at a global level after MS023 treatment, changes in histone methylation marks unique to different PRMTs gave us a hint about the primary target of the inhibitor that leads to BCL2 loss. PRMT1 activity was significantly suppressed by the inhibitor, as seen from near complete depletion of H4R3me2a levels. However, CARM1/PRMT4 and PRMT6 inhibition was insufficient and variable across different cell lines, as evidenced by residual levels of H3R17me2a and H3R2me2a respectively. This observation prompted us to question whether PRMT1 was the primary effector of BCL2 down-regulation and apoptosis in lymphoma cell lines.

3.2.4 PRMT1 regulates BCL2 in DLBCL cell lines

Using inhibitors specific to different Type I PRMTs, we analyzed changes in BCL2 protein levels in the cell line HT (Figure 14c). None of the inhibitors which targeted PRMT3, PRMT4/6 or PRMT6 alone were able to modulate BCL2 levels. A global increase in Mono-Methyl Arginine (MMA) is indicative of effective PRMT1 inhibition (112). BCL2 levels were only reduced by the two inhibitors that could target PRMT1: MS023 and IACS-013355. In RL cells, at higher concentrations of the PRMT6 inhibitor EPZ020411, we could observe a decrease in the BCL2 level (Figure 14d). This correlated with an increase in global MMA, which is in agreement with published reports that EPZ020411 has off-target effects on PRMT1 and PRMT8 at higher concentrations of the inhibitor. Therefore, we hypothesized that the change in BCL2 was a result of PRMT1 inhibition. Using siRNA specific to PRMT1, we knocked down PRMT1 expression in two BCL2-dependent DLBCL cell lines RL and Toledo, and examined changes in cell viability and BCL2 protein levels. PRMT1 knockdown reduced cell viability by 40% and 60% in RL and Toledo cells respectively (Figure 14e). PRMT1 knockdown in RL cells led to a decrease in BCL2 levels and completely depleted histone H4R3 asymmetric di-methylation (Figure 14f). From these observations, we concluded that MS023 mediated its effects on BCL2 by targeting PRMT1 activity.

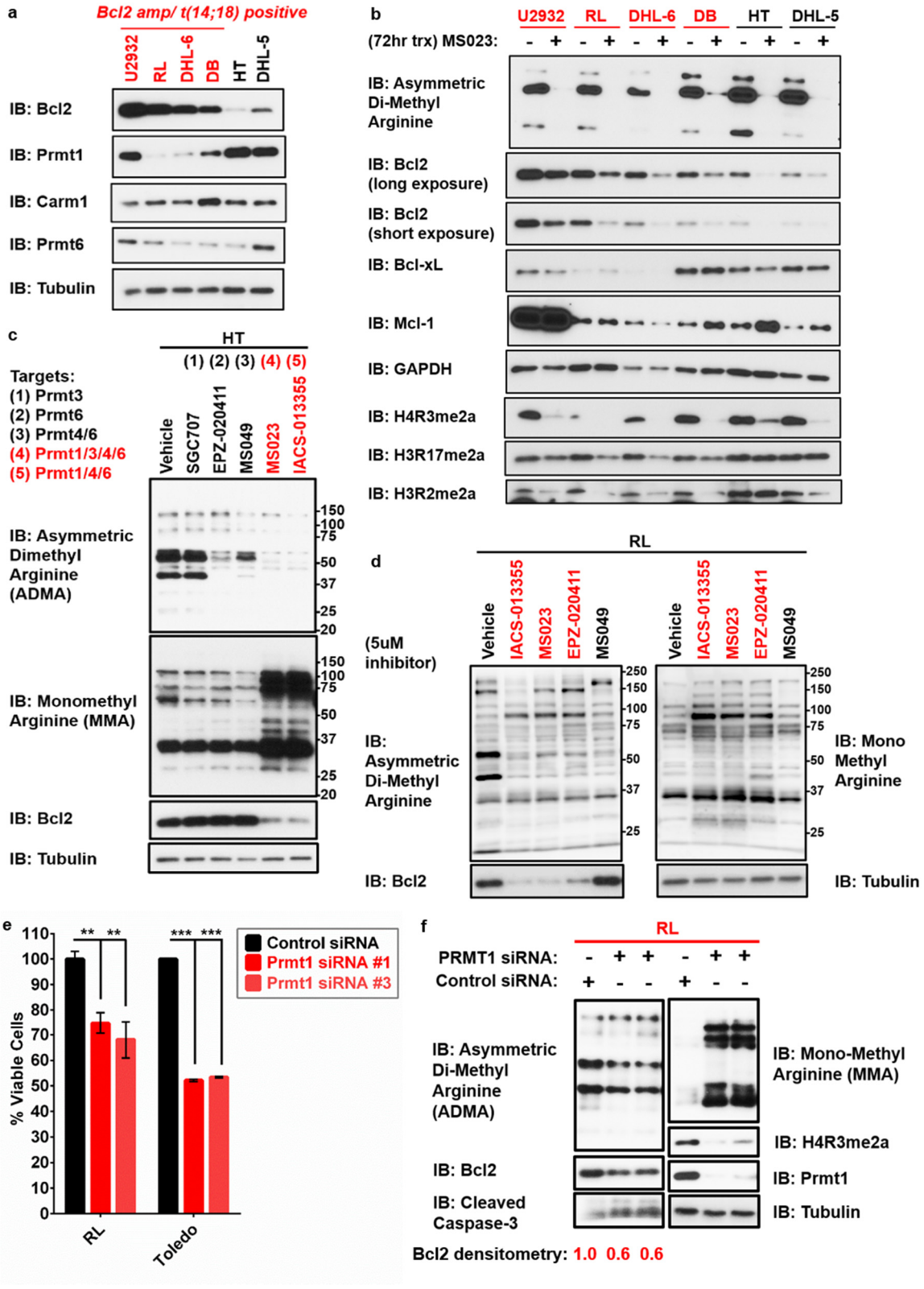
a
Bcl2 amp/ t(14;18) positive
U2932
RL
DHL-6
DB
HT
DHL-5
IB: Bcl2
IB: Prmt1
IB: Carm1
IB: Prmt6
IB: Tubulin
b
U2932 RL DHL-6 DB HT DHL-5
(72hr trx) MS023: - + - + - + - + - + - +
IB: Asymmetric Di-Methyl Arginine
IB: Bcl2 (long exposure)
IB: Bcl2 (short exposure)
IB: Bcl-xL
IB: Mcl-1
IB: GAPDH
IB: H4R3me2a
IB: H3R17me2a
IB: H3R2me2a
c
HT
(1) (2) (3) (4) (5)
Targets:
(1) Prmt3
(2) Prmt6
(3) Prmt4/6
(4) Prmt1/3/4/6
(5) Prmt1/4/6
Vehicle
SGC707
EPZ-020411
MS049
MS023
IACS-013355
IB: Asymmetric Dimethyl Arginine (ADMA)
IB: Monomethyl Arginine (MMA)
IB: Bcl2
IB: Tubulin
150
100
75
50
37
25
20
d
RL
(5uM inhibitor)
Vehicle
IACS-013355
MS023
EPZ-020411
MS049
IB: Asymmetric Di-Methyl Arginine
IB: Mono Methyl Arginine
IB: Bcl2
IB: Tubulin
250
150
100
75
50
37
25
e
Control siRNA
Prmt1 siRNA #1
Prmt1 siRNA #3
% Viable Cells
110
100
90
80
70
60
50
40
30
20
10
0
** **
*** ***
RL
Toledo
f
RL
PRMT1 siRNA: - + + - + +
Control siRNA: + - - + - -
IB: Asymmetric Di-Methyl Arginine (ADMA)
IB: Mono-Methyl Arginine (MMA)
IB: H4R3me2a
IB: Bcl2
IB: Prmt1
IB: Cleaved Caspase-3
IB: Tubulin
Bcl2 densitometry: 1.0 0.6 0.6

Figure 14. MS023 decreases levels of anti-apoptotic BCL2 protein in DLBCL cell lines through efficient PRMT1 inhibition. (a) Lysates from multiple lymphoma cell lines were blotted for protein levels of BCL2, PRMT1, CARM1 and PRMT6. Cell lines were grouped according to BCL2 amplification and translocation status. **(b)** DLBCL cell lines were treated with MS023 for 72 hours and cell lysates were blotted for apoptosis regulators like BCL2, BCL-XL and MCL-1. Histone arginine methylation marks associated with PRMT1, CARM1 and PRMT6 activity were also assessed**. (c)** HT cells were treated with inhibitors specific to different PRMTs at 2uM concentration for 96 hours. Lysates were collected and blotted for asymmetric arginine di-methylation, mono-methylation and BCL2. **(d)** RL cells were treated with different PRMT inhibitors at 5uM concentration for 96 hours and assayed for changes in arginine methylation and BCL2. **(e)** PRMT1 was knocked down using two different siRNA in BCL2-dependent RL and Toledo cell lines. Changes in cell viability after 4 days of siRNA treatment were determined using the CellTiter-Glo viability assay. Statistical significance was assessed using 2-way ANOVA ($p<0.01$** and $p<0.001$***). **(f)** Lysates were collected from RL cells treated with PRMT1 siRNA for 96 hours. Western blotting was performed to examine changes in the protein level of BCL2, the histone modification H4R3me2a, and caspase-3 cleavage.

3.2.5 Type I PRMT inhibition modulates BCL2 at the transcriptional level

In RL cells, ectopically expressed BCL2 was unaffected by MS023 treatment, indicating that BCL2 regulation may occur at the transcriptional level and involve the native promoter of BCL2 (Figure 15a). Additionally, ectopic BCL2 expression partially protected RL cells from apoptosis induced by PRMT inhibitor treatment, as indicated by reduced caspase-3 cleavage. Using qRT-PCR, we showed that BCL2 mRNA was reduced by 50% upon MS023 treatment in RL and SUDHL-6 cells (Figure 15b). Next, we performed Chromatin Immunoprecipitation (ChIP) in RL cells to assess H4R3me2a deposition in the promoter region of BCL2 (Figure 15c). Compared to the IgG control, there was an 8-fold enrichment of H4R3me2a in the BCL2 promoter region. This result supports the idea that the PRMT1 inhibitor MS023 down-regulates BCL2 by blocking its transcriptional activation (Figure 15d). In this way, MS023 promotes mitochondrial apoptosis in lymphoma cells.

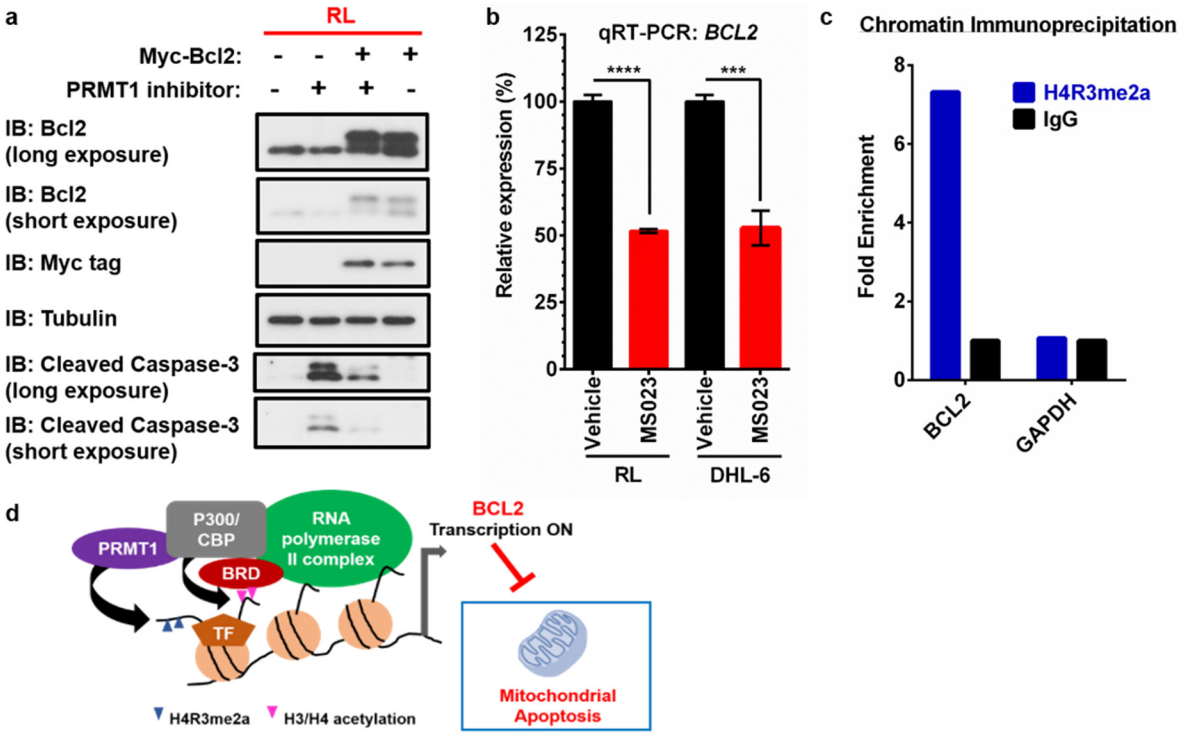

Figure 15. MS023 regulates BCL2 at the transcriptional level. (a) Ectopic expression of BCL2 in RL cells was followed by inhibitor treatment for 72 hours. Lysates were collected and blotted for BCL2, myc-tag and caspase-3 cleavage. **(b)** RL cells were treated with MS023 for 72 hours, RNA was extracted and analyzed by qRT-PCR using primers against BCL2 and GAPDH (control). Statistical significance was determined using a two-tailed unpaired t-test ($p<0.0001$**** and $p<0.001$***). **(c)** RL cells were fixed with formaldehyde, sonicated and subjected to chromatin immunoprecipitation using antibodies against H4R3me2a and isotype control (IgG). Primers against BCL2 and GAPDH promoter regions were used to amplify DNA fragments, followed by qPCR. **(d)** A model illustrating the role of PRMT1 in regulating mitochondrial apoptosis in lymphoma cells. PRMT1 activates anti-apoptotic BCL2 at the transcriptional level and protects against cell death.

3.2.6 PRMT1 is overexpressed in DLBCL tumors and correlates with poor prognosis

Using gene expression data from Oncomine, we analyzed PRMT1 expression in normal B-cells and DLBCL patient tumors from two independent cohorts (Figure 16a) (129-131). The mean expression of PRMT1 was 1.95-fold and 1.93-fold higher in tumor cells compared to their normal counterparts, and the difference was statistically significant ($p<0.0001$****) for both cohorts. Next, we determined whether PRMT1 expression levels may relate to overall survival in patients with DLBCL (Figure 16b-d). With the help of three different datasets extracted from Oncomine, we first established the optimal cutoff for each dataset using KaplanScan (132-134). Then, we plotted Kaplan-Meier curves using the individual cutoff values, with patients assigned to 'High' or 'Low' expression categories based on expression values above or below the cutoff respectively. In all datasets that were examined, high PRMT1 expression correlated with poor overall survival in patients, and the p-values were statistically significant. These results support the idea that PRMT1 may play an important role in DLBCL and contribute to disease aggressiveness.

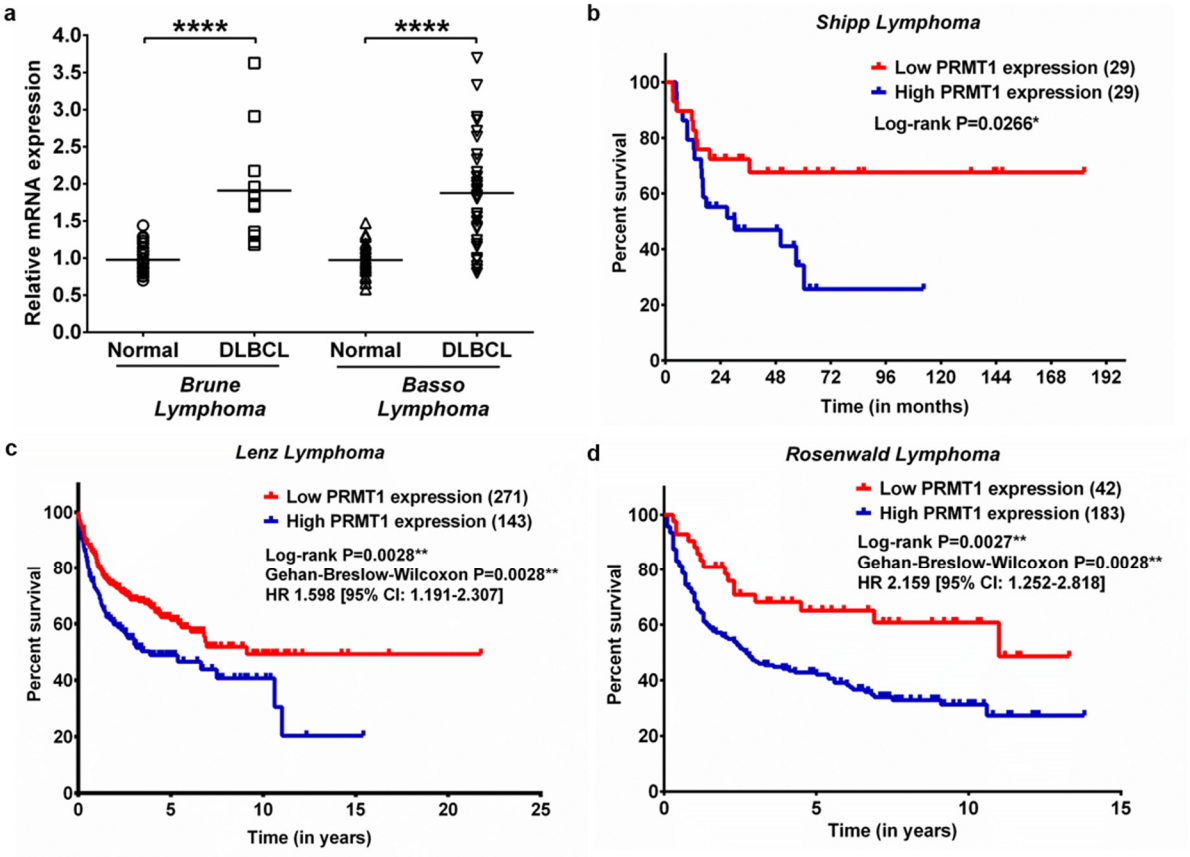
a
****
****
Relative mRNA expression
4.0
3.5
3.0
2.5
2.0
1.5
1.0
0.5
0.0
Normal
DLBCL
Normal
DLBCL
Brune Lymphoma
Basso Lymphoma
b
Shipp Lymphoma
Low PRMT1 expression (29)
High PRMT1 expression (29)
Log-rank P=0.0266*
Percent survival
Time (in months)
c
Lenz Lymphoma
Low PRMT1 expression (271)
High PRMT1 expression (143)
Log-rank P=0.0028**
Gehan-Breslow-Wilcoxon P=0.0028**
HR 1.598 [95% CI: 1.191-2.307]
Percent survival
Time (in years)
d
Rosenwald Lymphoma
Low PRMT1 expression (42)
High PRMT1 expression (183)
Log-rank P=0.0027**
Gehan-Breslow-Wilcoxon P=0.0028**
HR 2.159 [95% CI: 1.252-2.818]
Percent survival
Time (in years)

Figure 16. PRMT1 is overexpressed in DLBCL tumors and correlates with poor overall patient survival. (a) Using two different datasets from Oncomine, 'Brune Lymphoma' and 'Basso Lymphoma', PRMT1 expression in normal B-cells and lymphoma cells from patients was analyzed and statistical significance was determined using a two-tailed t-test ($p<0.0001$****). **(b)** Using the dataset 'Shipp Lymphoma' to analyze overall patient survival, PRMT1 expression cutoffs were calculated with the help of the software KaplanScan and patients were divided into low PRMT1-expressing and high PRMT1-expressing categories. Statistical differences in overall patient survival between the two categories were determined by the Log-rank method ($p<0.05$*). **(c)** A similar method was used to analyze overall patient survival in 'Lenz Lymphoma' and statistical differences were determined by both Log-rank method ($p<0.01$**) and Gehan-Breslow-Wilcoxon method ($p<0.01$**). **(d)** For 'Rosenwald Lymphoma', a similar method was used for overall patient survival, and statistical analysis was performed by Log-rank method ($p<0.01$**) and Gehan-Breslow-Wilcoxon method ($p<0.01$**).

3.2.7 Arginine methylation of CD79A does not play a role in the lymphoma cell response to EPZ-6438 and MS023

In normal B-cells, PRMT1 was previously reported to methylate CD79A at R204, leading to altered downstream B-Cell Receptor signaling through SYK and AKT. Since we observed synergy between EPZ-6438 and MS023 in multiple lymphoma cell lines, and we have showed that BCR signaling blockade sensitizes cells to the EZH2 inhibitor, we analyzed whether arginine methylation of CD79A might contribute to this phenomenon. Using SUDHL-6 and DB cells expressing an arginine methylation-resistant mutant of CD79A (R204K), we assayed for EPZ-6438 sensitivity of mutant cells compared to wildtype-CD79A expressing cells (Figure 17a). There was no significant change in the EZH2 inhibitor sensitivity of both SUDHL-6 and DB cells expressing the R204K mutant. Additionally, we examined whether MS023 exerted any of its anti-proliferative or apoptotic effects by modulating BCR signaling. We achieved this by assessing the MS023 dose-response of BCR-WT and BCR-KO cells (Figure 17b). Again, BCR-knockout did not significantly affect MS023 sensitivity in both SUDHL-6 and DB cells. From these results, we can conclude that arginine methylation of CD79A is not likely to play an important role in lymphoma cells.

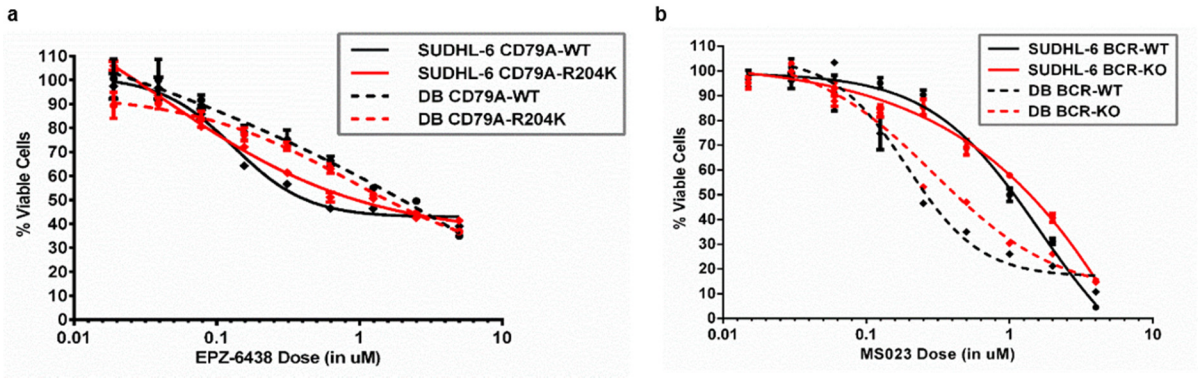

Figure 17. Arginine methylation of CD79A is not an important mediator of the response to MS023 and EPZ-6438 in lymphoma cells. (a) SUDHL-6 and DB cells expressing CD79A with an R204K mutation were assessed for their response to 7 days of EPZ-6438 treatment, and compared to cells expressing wildtype-CD79A. **(b)** SUDHL-6 and DB cells with BCR-knockout were exposed to varying doses of MS023 for 7 days and cell proliferation was analyzed with CellTiter-Glo viability assay.

3.3 Physical and functional interactions between EZH2, PRMT1, and CARM1

3.3.1 Mass Spectrometry reveals novel EZH2-interacting proteins in cancer cells

To identify novel EZH2 interacting proteins, we immunoprecipitated myc-tagged EZH2 from MCF7 breast cancer cells and performed mass spectrometric analysis. This yielded a comprehensive list of potential interacting partners. When ranked according to the signal ratio of EZH2 immunoprecipitate compared to the isotype control immunoprecipitate, the top hits were core and accessory components of the PRC2 complex: SUZ12, AEBP2, JARID2, and PHF1. Other PRC2 components such as PHF19, EED, RBBP7 and RBBP4 were ranked lower in the list due to background signal in the control sample. For the other hits, we categorized proteins based on their functions, and focused mainly on enzymes (kinases, phosphatases, methyltransferases, ubiquitin ligases, deubiquitinases) for further study. Interestingly, the arginine methyltransferases PRMT1 and CARM1 were identified as EZH2 interacting proteins. Although they were not highly ranked, this may be a result of weak or transient interactions between EZH2 and PRMT1/CARM1.

Rank	Uniprot	Protein Name	Gene Name	Avg-EZH2	Avg-Control	EZH2/C	Unique #	Coverage [%]
1	Q15022	Polycomb protein SUZ12	SUZ12	22107000	0	∞	20	46
2	Q6ZN18	Zinc finger protein AEBP2	AEBP2	8363500	0	∞	11	34
3	Q92833	Protein Jumonji	JARID2	6648100	0	∞	14	18
4	P49761	Dual specificity protein kinase CLK3	CLK3	5056300	0	∞	9	18
5	O95340	Bifunctional 3'-phosphoadenosine 5'-phosphosulfate synthase 2	PAPSS2	2538800	0	∞	8	17
6	Q06830	Peroxiredoxin-1	PRDX1	2437350	0	∞	4	28
7	P62937	Peptidyl-prolyl cis-trans isomerase A	PPIA	2230050	0	∞	2	18
8	O43189	PHD finger protein 1	PHF1	1933750	0	∞	5	20
9	Q8N5D0	WD and tetratricopeptide repeats protein 1	WDTC1	1871200	0	∞	10	19
10	O15042	U2 snRNP-associated SURP motif-containing protein	U2SURP	1604950	0	∞	5	6
11	Q9P1Y6	PHD and RING finger domain-containing protein 1	PHRF1	1558200	0	∞	4	4
12	P24666	Low molecular weight phosphotyrosine protein phosphatase	ACP1	1461950	0	∞	3	25
13	P24468	COUP transcription factor 2	NR2F2	1351100	0	∞	3	8
14	O00241	Signal-regulatory protein beta-1 [CD172b]	SIRPB1	1265950	0	∞	2	7
15	O00361	P40	ORF1	1167700	0	∞	4	17
16	P35241	Radixin	RDX	1046600	0	∞	5	13
17	O95782	AP-2 complex subunit alpha-1	AP2A1	1010330	0	∞	9	13
18	P62995	Transformer-2 protein homolog beta	TRA2B	1001420	0	∞	4	16
19	Q00577	Transcriptional activator protein Pur-alpha	PURA	894195	0	∞	2	15
20	Q9NRA8	Eukaryotic translation initiation factor 4E transporter	EIF4ENIF1	715250	0	∞	5	11
21	Q6AI08	HEAT repeat-containing protein 6	HEATR6	708815	0	∞	4	5
22	Q5T6S3	PHD finger protein 19	PHF19	708210	0	∞	5	11
23	P10155	60 kDa SS-A/Ro ribonucleoprotein	TROVE2	696520	0	∞	2	8
24	Q7Z404	Transmembrane channel-like protein 4	TMC4	665960	0	∞	2	4
25	Q13427	Peptidyl-prolyl cis-trans isomerase G	PPIG	661715	0	∞	2	3
26	P62857	40S ribosomal protein S28	RPS28	639735	0	∞	3	52
27	Q9NYL9	Tropomodulin-3	TMOD3	614640	0	∞	3	13
28	P63092	Guanine nucleotide-binding protein G(s) subunit alpha isoforms short	GNAS	578465	0	∞	3	6
29	P09382	Galectin-1	LGALS1	573680	0	∞	2	22
30	O60313	Dynamin-like 120 kDa protein, mitochondrial	OPA1	531700	0	∞	4	6
31	P00558	Phosphoglycerate kinase 1	PGK1	469445	0	∞	2	8
32	Q92616	Translational activator GCN1	GCN1L1	426625	0	∞	3	2
33	O00311	Cell division cycle 7-related protein kinase	CDC7	412365	0	∞	2	3
34	Q9UK61	Protein FAM208A	FAM208A	408355	0	∞	6	6
35	Q9P2M7	Cingulin	CGN	371255	0	∞	4	5
36	P16989	Y-box-binding protein 3	YBX3	357890	0	∞	3	25
37	O15231	Zinc finger protein 185	ZNF185	342750	0	∞	2	7
38	Q96A33	Coiled-coil domain-containing protein 47	CCDC47	327470	0	∞	2	5
39	Q99569	Plakophilin-4	PKP4	256935	0	∞	2	2
40	Q8NHV4	Protein NEDD1	NEDD1	254810	0	∞	2	6
41	P51659	Peroxisomal multifunctional enzyme type 2	HSD17B4	250935	0	∞	3	6
42	P35606	Coatomer subunit beta'	COPB2	226825	0	∞	3	3
43	Q7Z5K2	Wings apart-like protein homolog	WAPAL	222535	0	∞	3	5
44	Q9NZC9	SWI/SNF-related matrix-associated actin-dependent regulator of chromatin subfamily A-like protein 1	SMARCAL1	217405	0	∞	3	3
45	P56192	Methionine--tRNA ligase, cytoplasmic	MARS	213295	0	∞	2	4

Rank	Uniprot	Protein Name	Gene Name	Avg-EZH2	Avg-Control	EZH2/C	Unique #	Coverage [%]
46	Q8NDV7	Trinucleotide repeat-containing gene 6A protein	TNRC6A	192034.5	0	∞	2	3
47	Q96G46	tRNA-dihydrouridine(47) synthase [NAD(P)(+)]-like	DUS3L	167495	0	∞	2	5
48	P28290	Sperm-specific antigen 2	SSFA2	158608	0	∞	2	2
49	Q14573	Inositol 1,4,5-trisphosphate receptor type 3	ITPR3	153010	0	∞	2	1
50	Q9NTI5	Sister chromatid cohesion protein PDS5 homolog B	PDS5B	136915	0	∞	3	3
51	Q9NYU2	UDP-glucose:glycoprotein glucosyltransferase 1	UGGT1	92704	0	∞	2	2
52	Q15910	Histone-lysine N-methyltransferase EZH2	EZH2	76772000	77995	**984**	26	55
53	O75530	Polycomb protein EED	EED	73774000	259190	**285**	26	64
54	Q14764	Major vault protein	MVP	7554750	54645	**138**	21	34
55	O75165	DnaJ homolog subfamily C member 13	DNAJC13	6742600	61855	**109**	33	21
56	O60216	Double-strand-break repair protein rad21 homolog	RAD21	8470650	221760	**38**	17	43
57	Q9NYF8	Bcl-2-associated transcription factor 1	BCLAF1	4.31E+08	12555000	**34**	3	40
58	P06396	Actin-depolymerizing factor Gelsolin	GSN	8189200	243920	**34**	14	32
59	Q08380	Basement membrane autoantigen p105	LGALS3BP	38215000	1288450	**30**	17	39
60	Q92624	Amyloid beta precursor protein-binding protein	APPBP2	18453000	627700	**29**	15	33
61	Q6ZRI8	Rho GTPase-activating protein 36	ARHGAP36	7101500	252025	**28**	10	28
62	Q9Y2W1	Thyroid hormone receptor-associated protein 3	THRAP3	4.57E+08	16447500	**28**	44	37
63	Q8NEY8	Gastric cancer antigen Ga50	PPHLN1	3290850	119050	**28**	3	7
64	Q99590	CTD-associated SR protein 11	SFRS2IP	16787500	676305	**25**	22	24
65	P51116	Fragile X mental retardation syndrome-related protein 2	FXR2	8576450	355200	**24**	13	38
66	Q6ZRV2	Protein FAM83H	FAM83H	4952300	244780	**20**	11	16
67	P84090	Enhancer of rudimentary homolog	ERH	7206800	425170	**17**	6	55
68	Q2I5I4	Four and a half LIM-domain protein 2	FHL2	31677500	1903150	**17**	15	49
69	Q13303	K(+) channel subunit beta-2	KCNA2B	1.8E+08	11098500	**16**	1	66
70	P07339	Cathepsin D	CPSD	1287400	84950	**15**	2	7
71	P04406	Glyceraldehyde-3-phosphate dehydrogenase	GAPDH	1.08E+08	7303850	**15**	17	71
72	F5H012	Tripartite motif-containing protein 21	TRIM21	29155500	2099750	**14**	19	39
73	Q9H329	Erythrocyte membrane protein band 4.1 like 4B variant	EPB41L4B	18629000	1356900	**14**	13	35
74	Q9UQE7	Structural maintenance of chromosomes 3	SMC3	8056350	587685	**14**	22	23
75	Q15149	Plectin-1	PLEC1	2.57E+08	19045000	**13**	190	48
76	Q16576	Histone-binding protein RBBP7	RBAP46	3491900	276030	**13**	4	20
77	Q9Y3Y2	Chromatin target of PRMT1	CHTOP	29053500	2751000	**11**	5	26
78	P27694	Replication factor A protein 1	REPA1	1.65E+08	15682000	**11**	45	78
79	Q14683	Structural maintenance of chromosomes protein 1A	SMC1A	8659450	850275	**10**	31	32
80	Q5VTI5	Pleckstrin homology domain containing, family A member 6	PLEKHA6	661990	65210	**10**	6	10
81	Q5VWN6	Uncharacterized protein C10orf18	C10orf18	6323050	645940	**10**	15	8
82	Q13573	Nuclear receptor coactivator NCoA-62	SNW1	4997700	514150	**10**	2	5
83	P35244	Replication factor A protein 3	REPA3	9704350	1026710	**9**	3	38
84	P15927	Replication factor A protein 2	REPA2	21976000	2498450	**9**	11	64
85	Q14498	RNA-binding motif protein 39	RBM39	9100500	1051300	**9**	13	35
86	P19387	DNA-directed RNA polymerase II subunit C	POLR2C	1570700	181585	**9**	7	43
87	Q09028	Histone-binding protein RBBP4	RBAP48	6901850	799245	**9**	3	14
88	Q15654	Thyroid receptor-interacting protein 6	TRIP6	8276500	1011630	**8**	9	27
89	Q99873	Protein arginine N-methyltransferase 1	PRMT1	45628500	5930500	**8**	23	60
90	Q5JSZ5	HLA-B-associated transcript 2-like 1	BAT2L	24698000	4085600	**6**	38	29

Rank	Uniprot	Protein Name	Gene Name	Avg-EZH2	Avg-Control	EZH2/C	Unique #	Coverage [%]
91	P26196	ATP-dependent RNA helicase p54	DDX6	84645000	14177500	**6**	28	72
92	P50851	CDC4-like protein	CDC4L	754855	126715	**6**	6	3
93	Q96QE5	UPF0629 protein C17orf42	C17orf42	1638300	285115	**6**	6	22
94	Q9BY49	Peroxisomal trans-2-enoyl-CoA reductase	PECR	38369000	6706950	**6**	15	56
95	P24928	DNA-directed RNA polymerase II subunit A	POLR2A	13390500	2346250	**6**	31	22
96	P55884	Eukaryotic translation initiation factor 3 subunit B	EIF3B	4120900	732855	**6**	12	20
97	P30876	DNA-directed RNA polymerase II subunit B	POLR2B	6283450	1123950	**6**	25	30
98	P51114	Fragile X mental retardation syndrome-related protein 1	FXR1	36917000	6942150	**5**	7	48
99	P04792	Heat shock 27 kDa protein	HSP27	32687000	6233400	**5**	8	66
100	Q70EL4	Ubiquitin-specific-processing protease 43	USP43	1179650	225920	**5**	7	12
101	Q9BYD3	39S ribosomal protein L4, mitochondrial	MRPL4	20029500	4172800	**5**	10	47
102	Q9Y6J9	TAF6-like RNA polymerase II p300/CBP-associated factor-associated factor 65 kDa subunit 6L	TAF6L	2838050	608065	**5**	6	18
103	Q06787	Fragile X mental retardation 1 protein	FMR1	33417500	7262000	**5**	1	56
104	O60573	Eukaryotic translation initiation factor 4E type 2	EIF4E2	2955600	643405	**5**	5	26
105	Q9UH62	ARM protein lost in epithelial cancers on chromosome X 3	ALEX3	13639000	2992100	**5**	12	44
106	Q14966	Zinc finger protein 638	ZNF638	6515050	1545100	**4**	21	14
107	Q13045	Protein flightless-1 homolog	FLII	1053675	259020	**4**	10	11
108	Q15437	Protein transport protein Sec23B	SEC23B	310420	77580	**4**	1	3
109	Q86V97	Kelch repeat and BTB domain-containing protein 6	KBTBD6	16016500	4095600	**4**	14	57
110	Q9NWH9	Modulator of estrogen-induced transcription	MET	2058350	533500	**4**	8	10
111	Q8N539	Fibrinogen C domain-containing protein 1	FIBCD1	12338000	3208850	**4**	9	36
112	Q96QR8	Transcriptional activator protein Pur-beta	PURB	1635050	428165	**4**	4	30
113	Q86X55	Histone-arginine methyltransferase CARM1	PRMT4	8786350	2317000	**4**	7	16
114	Q96NB2	Sideroflexin-2	SFXN2	3915200	1035250	**4**	5	19
115	P07384	Calcium-activated neutral proteinase 1	CANPL1	2830850	750855	**4**	12	22
116	Q59G16	BRG1-associated factor 170	BAF170	179825	48666.5	**4**	2	4
117	P40429	60S ribosomal protein L13a	RPL13A	1711650	473410	**4**	3	18
118	P00338	L-lactate dehydrogenase	LDHA	1904850	529835	**4**	5	15
119	P50542	Peroxin-5	PEX5	3989900	1118100	**4**	15	42
120	P68104	Elongation factor 1-alpha 1	EEF1A	1.34E+08	37727000	**4**	15	46
121	Q8N4Q0	Zinc-binding alcohol dehydrogenase domain-containing protein 2	ZADH2	24600500	6989150	**4**	12	38

Table 1. EZH2-associated proteins in MCF7 cells identified through Mass Spectrometry. Myc-tagged EZH2 was immunoprecipitated from MCF7 breast cancer cells and interacting proteins were identified by mass spectrometry. This table lists only proteins that are more than 4-fold enriched compared to the isotype control. Proteins are ranked based on the signal ratio of EZH2 immunoprecipitate compared to control immunoprecipitate (EZH2/C). Core and accessory components of the PRC2 complex are highlighted in yellow.

3.3.2 PRMT1 and CARM1 methylate components of the PRC2 complex *in vitro*

Since EZH2, PRMT1 and CARM1 are methyltransferases, we wanted to know if they could modify each other at the post-translational level. We performed *in vitro* methylation assays using the core PRC2 complex (EZH2/SUZ12/EED) and either PRMT1 or CARM1, in the presence of tritiated S-Adenosylmethionine (SAM) (Figure 18a). We also used two different buffers (PRC2 and PRMT1), to maintain optimal enzymatic activity of the PRC2 complex and PRMT1 respectively as their names suggest, while both buffers work well for CARM1. The strongest methylation signal came from a protein at 90kDa, in the reaction containing PRC2 and CARM1. This protein could be either EZH2 or SUZ12, since both proteins have similar molecular weights. There was also a weaker methylation signal in the PRMT1/PRC2 reaction at the same molecular weight. Finally, there was a weak signal at the molecular weight corresponding to EED in both PRC2/PRMT1 and PRC2/CARM1 reactions, but only when PRMT1 buffer was used. From these observations, we can conclude that EZH2 cannot methylate PRMT1 or CARM1. However, it appears that PRMT1 and CARM1 can methylate PRC2 complex components *in vitro*.

To identify if the methylation signal at 90kDa came from SUZ12 or EZH2, we performed individual methylation reactions using recombinant SUZ12 and EZH2 protein (Figure 18b,c). PRMT1 was able to methylate SUZ12 alone, but not EZH2. CARM1 was unable to methylate EZH2 or SUZ12 alone, but could strongly methylate one or both of them as part of an intact PRC2 complex. Next, we used an antibody that recognizes asymmetric di-methylarginine motifs (ADMA) to detect methylation by PRMT1/CARM1 in immunoprecipitated PRC2 complexes after *in vitro* methylation reactions (Figure 18d). We performed the methylation reaction, immunoprecipitated PRC2 complex proteins, and performed stringent washes to remove the associated PRMT1/CARM1. PRMT1 easily disengaged from the PRC2 complex, but CARM1 remained strongly bound, leading to the presence of a strong CARM1 auto-

methylation signal in the eluate. Interestingly, the post-immunoprecipitation washes showed no presence of methylated CARM1, indicating that 100% of auto-methylated CARM1 associated with the PRC2 complex. Methylation of EZH2/SUZ12 by CARM1 could be detected by the ADMA antibody. Interestingly, methylation of EED by PRMT1 was recognized by this ADMA antibody, but SUZ12 methylation was not recognizable.

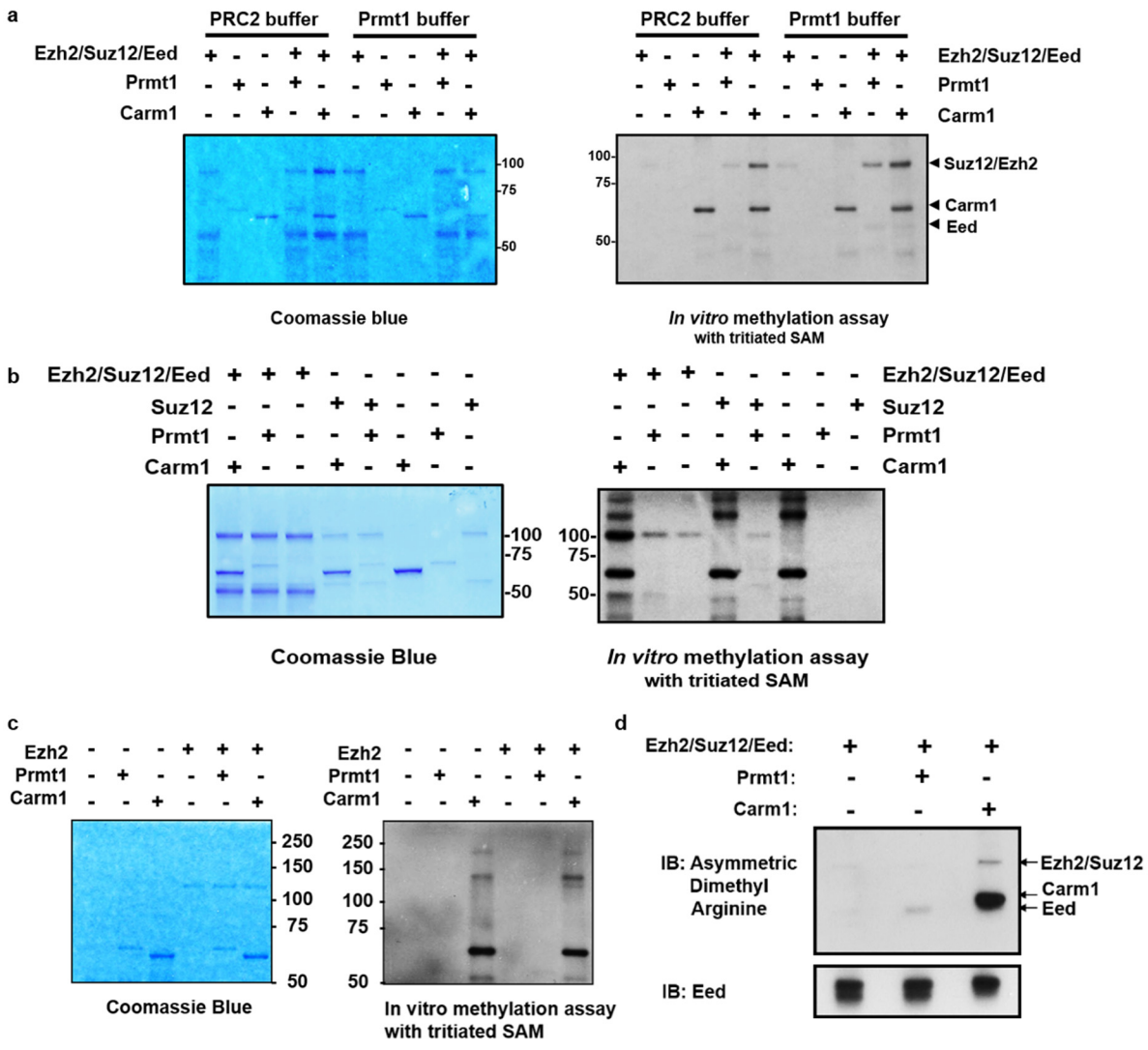
a
PRC2 buffer
Prmt1 buffer
Ezh2/Suz12/Eed
Prmt1
Carm1
100
75
50
Coomassie blue
Suz12/Ezh2
Carm1
Eed
In vitro methylation assay
with tritiated SAM
b
Suz12
Coomassie Blue
c
Ezh2
250
150
d
Ezh2/Suz12/Eed:
Prmt1:
Carm1:
IB: Asymmetric
Dimethyl
Arginine
IB: Eed
Ezh2/Suz12
In vitro methylation assay
with tritiated SAM

Figure 18. PRMT1 and CARM1 can methylate PRC2 complex members *in vitro*. (a) Methylation reactions were performed with recombinant EZH2/SUZ12/EED, combined with either PRMT1 or CARM1, and tritiated SAM. Two different buffers were used to facilitate optimal enzymatic activity of all components. **(b)** SUZ12 alone was used as a substrate for PRMT1 and CARM1 and similar methylation reactions were performed. Reactions performed under similar conditions with the PRC2 complex are included as a reference. **(c)** EZH2 alone was utilized as a substrate for PRMT1 and CARM1. **(d)** *In vitro* methylation was performed with PRC2 complex and PRMT1/CARM1. His-tagged EZH2 and SUZ12 were immunoprecipitated using Talon resin and PRMT1/CARM1 was washed away. The eluate was analyzed for asymmetric arginine di-methylation with an antibody that can recognize ADMA motifs.

3.3.3 PRMT1 and CARM1 co-immunoprecipitate with the PRC2 complex *in vivo*

We used Duolink Proximity Ligation assays to assess co-localization of EZH2 with PRMT1 and CARM1. EZH2 and PRMT1 showed significant co-localization in MCF7 breast cancer cells (Figure 19a). However, we were not able to detect CARM1/EZH2 co-localization using this assay. This might be a technical issue arising from antibody-epitope recognition. When we co-transfected HA-PRMT1 and the PRC2 component Flag-EED into 293T cells, we found that the interaction between PRMT1 and EED was detectable but weak (Figure 19b). This suggests that they may form part of a larger complex or that their interaction may not be strong enough to be maintained during conventional immunoprecipitation procedures. Interestingly, an enzyme-dead mutant of PRMT1 (E171Q) also interacted with EED to the same extent as the wildtype enzyme. Interactions between endogenous CARM1 and Flag-tagged EED were detectable in 293T cells, without the need for CARM1 overexpression (Figure 19c). In the context of PRMT1 overexpression, EED associated with an arginine-methylated protein that migrated at the same molecular weight as CARM1 and showed a similar expression pattern.

3.3.4 Nucleosome methylation by PRC2/CARM1 and PRC2/PRMT1 complexes

Using nucleosome methylation assays, we found that PRMT1 did not markedly affect histone H3K27 methylation by the PRC2 complex *in vitro* (Figure 19d). Surprisingly, the PRC2 complex promoted histone H4R3 asymmetric di-methylation by PRMT1. This phenomenon did not require the histone H4-binding accessory PRC2 component RbAp48. The core PRC2 complex consisting of EZH2, SUZ12, and EED was adequate for facilitating H4R3 methylation by PRMT1.

CARM1 strongly methylates Histone H3R17 and weakly methylates Histone H3R26 *in vitro*. Both of these modifications are involved in transcriptional activation. H3R26 methylation by CARM1 is predicted to block H3K27 methylation by PRC2, although this has not been

conclusively shown in literature. H3R17 methylation is also expected to block PRC2 activity, in a manner similar to other active marks like H3K4me3 and H3K36me2. Addition of PRC2 to a CARM1-containing nucleosome methylation reaction reduced both H3R17me2a and H3R26me2a signals, but dramatically increased the H3K27 tri-methylation signal (Figure 19e). Surprisingly, PRC2 and CARM1 together yielded a much higher H3K27me3 signal than PRC2 alone. This was unexpected, because CARM1 has never been shown to influence H3K27 methylation, especially in a positive way. Addition of PRMT1 to a CARM1-containing reaction increased arginine di-methylation of CARM1. This methylation activity may come from PRMT1-mediated methylation of CARM1 or from CARM1 auto-methylation. The latter is more likely since the reaction was performed in PRC2 buffer, and we have previously showed that this buffer is not optimal for PRMT1 activity. Another interesting observation from this experiment was that recognition of CARM1 by an antibody that binds to an epitope surrounding the amino acid arginine-49, was reduced by PRMT1 addition.

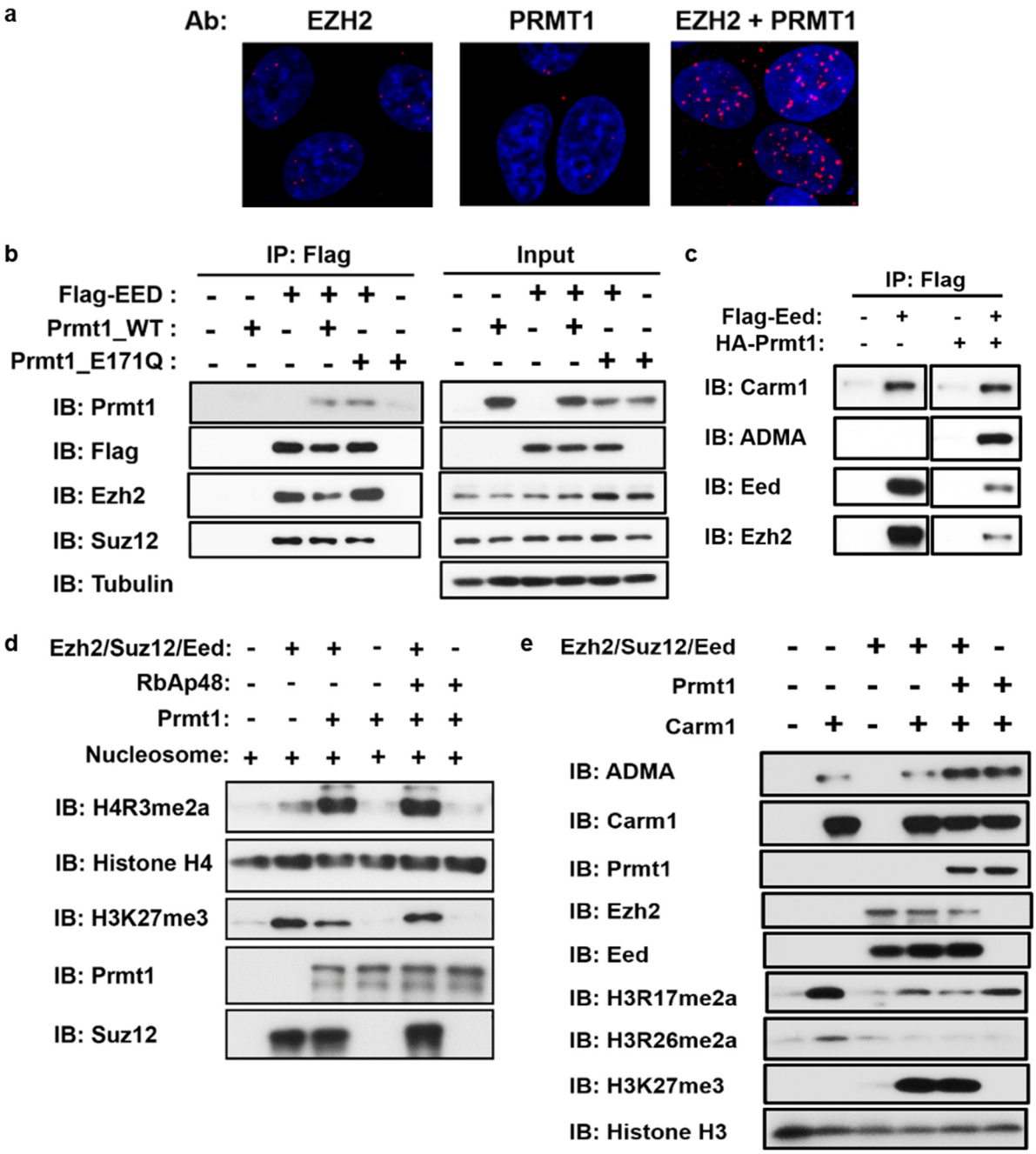
a
Ab:
EZH2
PRMT1
EZH2 + PRMT1
b
IP: Flag
Input
Flag-EED :
Prmt1_WT :
Prmt1_E171Q :
IB: Prmt1
IB: Flag
IB: Ezh2
IB: Suz12
IB: Tubulin
c
IP: Flag
Flag-Eed:
HA-Prmt1:
IB: Carm1
IB: ADMA
IB: Eed
IB: Ezh2
d
Ezh2/Suz12/Eed:
RbAp48:
Prmt1:
Nucleosome:
IB: H4R3me2a
IB: Histone H4
IB: H3K27me3
IB: Prmt1
IB: Suz12
e
Ezh2/Suz12/Eed
Prmt1
Carm1
IB: ADMA
IB: Carm1
IB: Prmt1
IB: Ezh2
IB: Eed
IB: H3R17me2a
IB: H3R26me2a
IB: H3K27me3
IB: Histone H3

Figure 19. Interactions between PRC2, PRMT1, and CARM1 may influence their enzymatic activities. (a) In MCF7 cells, Duolink Proximity Ligation assay was performed to detect interactions between PRMT1 and EZH2. **(b)** In 293T cells, Flag-tagged EED was co-transfected with wildtype or enzyme-dead (E171Q) HA-tagged PRMT1, and EED was immunoprecipitated with Flag-M2 beads. The eluate was blotted for PRMT1, Flag-tag, EZH2 and SUZ12. **(c)** Flag-tagged EED was immunoprecipitated from 293T cells co-expressing HA-PRMT1, and the eluate was blotted for ADMA and CARM1. An ADMA signal corresponding to the molecular weight of CARM1 was detected. **(d)** Nucleosome methylation reactions were performed with PRMT1, the core PRC2 complex, and PRC2 complex combined with RbAp48. Histone H4R3me2a and H3K27me3 levels were determined. **(e)** Nucleosome methylation reactions were performed with recombinant PRC2 complex, CARM1, and PRMT1/CARM1 together. Reaction samples were assayed for ADMA and histone H3 modifications catalyzed by CARM1 and EZH2.

Chapter 4:

DISCUSSION

4.1 Targeting kinases downstream of BCR to improve the therapeutic response to EZH2 inhibitors

SUDHL-6 BCR-knockout and CD19-knockout cells demonstrated remarkable hypersensitivity to EZH2 inhibition with EPZ-6438. This big shift in IC50 suggests that BCR/CD19 signaling may provide a compensatory mechanism that supports cell survival after EZH2 ablation. Based on this observation, we combined EPZ-6438 with inhibitors of kinases downstream of BCR, specifically targeting SYK, BTK and PI3Kδ. Although BTK was not expected to play a role in tonic BCR signaling, PCI32765 was able to sensitize lymphoma cells to EPZ-6438 treatment. PI3Kα is adequate to maintain tonic BCR signaling, and therefore PI3Kδ inhibition was not expected to have much of an effect either. Surprisingly, inhibitors targeting all three kinases (SYK, PI3Kδ and BTK) greatly synergized with EPZ-6438 in SUDHL-6, SUDHL-4 and HT cells. In the case of the PI3Kδ inhibitor CAL101, this was especially striking, because single-agent treatment yielded insignificant effects on the growth of GCB-DLBCL cell lines when used at low doses. The BTK inhibitor PCI32765 is known to have off-target effects at higher concentrations, and this can be seen clearly when it is used as a single-agent. However, when combined with EPZ-6438, its IC50 value dropped to a range that correlates with on-target efficacy in ABC-DLBCL cells. The SYK inhibitor PRT062607 has considerable anti-proliferative effects as a single-agent, and these effects are greatly potentiated by EPZ-6438 addition. These results support a critical role for the BCR signaling pathway after EZH2 inhibitor therapy. The contribution of BTK to this phenomenon suggests combined involvement of tonic and antigen-type BCR signaling. However, there is no antigen available to promote BCR ligation in these cells, and neither do they harbor mutations in BCR signaling elements. Therefore, the possible origin of antigen-type BCR signaling in these cells represents an interesting question. An imbalance in negative and positive co-receptors may greatly lower the threshold for BCR activation and allow enhanced downstream signaling. To

investigate this hypothesis, we analyzed cell surface expression of CD19, CD22, CD72, and its ligand CD100. CD100 was the only marker that consistently increased in lymphoma cells after EPZ-6438 treatment. Increased CD100 expression may decrease SHP-1 activity in these cells by switching 'off' inhibitory co-receptor signaling by CD72. This could lead to amplified and sustained BCR signaling in EPZ-6438-treated lymphoma cells. It would be interesting to determine whether CD100 knockdown could sensitize lymphoma cells to the EZH2 inhibitor and partially block BCR signaling. Another possible reason for altered tyrosine kinase signaling is co-opting of the BCR by another receptor which can be activated by secreted ligands in the media. EZH2 is a well-known repressor of cytokine genes, and therefore, EPZ-6438 treatment may induce these cells to release cytokines and activate cytokine receptors (135).

SUDHL-6 cells without functional BCR and CD19 are viable, but display a slightly slower growth rate. To understand how these cells can survive in the absence of tonic BCR signaling, we tested multiple kinase inhibitors and found that BCR-KO cells were highly sensitive to both BTK and PI3Kδ inhibition. Upon dissection of downstream signaling pathways, we noticed that CD19 phosphorylation was greatly increased in BCR-KO cells. This suggests that CD19 activation can occur independently of the BCR. This is not surprising, because CD19 has previously been implicated in PI3K/AKT activation that occurs independently of BCR/CD79A signaling (136). BTK is phosphorylated at Y551 to a greater extent in BCR-KO cells, and phosphorylation of its substrate PLCγ2 is observed. Y551 phosphorylation performed by either SYK or LYN kinase, is not necessarily indicative of BTK activation, and phosphorylation of its substrate is a more reliable indicator of its activity. Therefore, in this case, PLCγ2 phosphorylation in BCR-KO cells signifies BTK activation through a BCR-independent mechanism, and PI3Kδ activation downstream of CD19 may be responsible for this phenomenon. However, the depletion of AKT phosphorylation in BCR-KO cells confirms that

AKT is dependent on tonic BCR signaling and SYK activation, and cannot be maintained by BCR-independent CD19 signaling. Considering that both AKT and BTK require PIP3 generation by PI3K to become activated, it is interesting to consider why AKT activity is dependent on BCR and SYK, but BTK activity is not.

Tonic BCR signaling can occur through either PI3Kα or PI3Kδ, while active BCR signaling is uniquely reliant on PI3Kδ (11). Considering the increased dependence on PI3Kδ in BCR-KO cells, it is possible that the involvement of specific PI3K isoforms may influence the extent of BTK activation. Interestingly, AKT negatively regulates BTK signaling by phosphorylating it at two sites, promoting its sequestration by the 14-3-3 family of proteins, and consequently leading to its degradation. There is a possibility that enhanced BTK stability in the absence of AKT contributes to its increased activity. There are still many questions that remain unanswered. BLNK phosphorylation by SYK is required to bring BTK and PLCγ2 together, and it is not clear how this occurs in BCR-KO cells without SYK activity. The mechanism behind EZH2 inhibitor sensitivity of BCR-KO and CD19-KO cells warrants further investigation. EZH2 inhibitor treatment reduces BTK phosphorylation at Y551 and depletes PLCγ2 phosphorylation in BCR-KO cells. This suggests that the compensatory mechanisms sustaining SUDHL-6 cells in the absence of BCR and CD19 function are inadequate for maintaining cell survival and growth upon EZH2 ablation.

To summarize, our study demonstrates striking synergy between EZH2 inhibitors and kinase inhibitors targeting SYK, PI3Kδ, and BTK. Although the mechanism requires more detailed examination, our discovery has significant clinical implications for patients with GCB-DLBCL.

4.2 PRMT1 plays an important role in DLBCL before and after EZH2 inhibitor therapy

At the histone level, EZH2 inhibitor treatment wipes out H3K27 tri-methylation and induces de-repression of EZH2 target genes. Many of these genes are related to B-cell differentiation (IRF4, BLIMP1), cell-cycle progression (CDNK1A, CDKN2A), and apoptosis (BCL2) (5). EZH2 inhibition checks the uncontrolled growth of lymphoma cells by pushing them along a path to terminal differentiation. Increased histone acetylation at early time points (4 days) after inhibitor treatment is an indicator of EZH2 target gene re-activation. Histone acetylation is often preceded by histone methylation mediated by a variety of lysine and arginine methyltransferases. After 12 days of EPZ-6438 treatment, there was a slight increase in H3K36me2 upon H3K27me3 depletion, which correlates with reports of the antagonistic nature of these two marks. The existence of H3K36 methylation impedes H3K27 methylation by PRC2 *in cis* (137). Therefore, it is possible that the converse is also true.

The relationship between H3K27 methylation and histone arginine methylation is not well-studied, even though hints from *in vitro* studies suggest that CARM1-mediated H3R26 methylation may block H3K27 methylation. *In vivo*, H3R26me2a is a low abundance mark which is not detectable in lymphoma cells (unpublished data). In our experiments, we found that EZH2 inhibition led to a substantial increase in Histone H4 Arginine-3 asymmetric di-methylation across multiple cell lines, regardless of EZH2 mutation status. H4R3me2a is a mark of transcriptional activation, prompting us to question whether increased PRMT activity is a positive mediator of EZH2 inhibitor sensitivity. PRMTs have previously been linked to both promotion and blockade of cell differentiation. In neuronal cells, PRMT1 and PRMT8 regulate retinoic acid-induced differentiation (138). In hematopoietic stem cells, PRMT4/CARM1 methylates Runx1 to block their differentiation into myeloid progenitors (104).

We questioned whether Type I PRMT-mediated H4R3 di-methylation was instrumental in promoting terminal differentiation after EZH2 inhibitor treatment. Surprisingly, we found that

while Type I PRMT inhibition blocked the expression of differentiation-related genes like IRF4 in SUDHL-6 and Pfeiffer cells (unpublished data), it improved sensitivity to EZH2 inhibitor treatment in other cell lines like RL, DB, HT and SUDHL-5. In SUDHL-6 cells, PRMT inhibitor treatment displayed potent growth-suppressive effects as a single-agent, and EZH2 inhibitor addition did not produce additivity or synergy. To better understand the effects of PRMT inhibition, we tested the pan-Type I PRMT inhibitor MS023 as a single-agent in DLBCL cell lines. MS023 treatment prompted cell death in BCL2-dependent lymphoma cell lines, such as SUDHL-6, RL and Toledo. Apoptosis induction was minimal in cell lines known to be MCL1-dependent (HT, SUDHL-4, SUDHL-5) or dependent on neither MCL1 nor BCL2 (DB) (128). However, MS023 still induced anti-proliferative effects in these cell lines, and promoted cell-cycle arrest in DB and SUDHL-4. Using siRNA to dissect the contribution of different PRMTs, we showed that BCL2 down-regulation by MS023 was mediated by PRMT1.

PRMT1 has distinct functions in the cytoplasm and in the nucleus. Cytoplasmic functions of PRMT1 in B-cells are not well-studied. However, PRMT1 can methylate CD79A associated with the pre-BCR at Arginine-204 and deregulate signaling via SYK and PI3K/AKT. In our experiments, we did not observe any changes in EZH2 inhibitor sensitivity of SUDHL-6 and DB cells expressing CD79A with an R204K mutation, making it resistant to PRMT1-mediated arginine methylation. Additionally, we did not observe any shifts in the IC50 for MS023 in both SUDHL-6 and DB cells lacking the BCR, suggesting that MS023 does not mediate its apoptotic or growth-suppressive effects through altered BCR signaling. Therefore, we can conclude that CD79A arginine methylation by PRMT1 does not play a role in the response to EZH2 inhibitor treatment and is not involved in mediating the therapeutic effects of MS023.

Despite the potent effects of MS023 on BCL2 and apoptosis induction as a single-agent, we found that the cell lines responding well to combination therapy with MS023 and EPZ-6438 were not BCL2-dependent. Favorable responses to the combination also did not correlate

with the fold-increase in H4R3me2a after EZH2 inhibitor treatment. For example, DB and SUDHL-5 showed minimal changes in H4R3me2a at 8 days after EPZ-6438 treatment, but showed maximal synergy with MS023 treatment. Therefore, mechanisms contributing to inhibitor synergy remain under investigation.

Our study shows that PRMT1 is a promising target for the treatment of GCB-DLBCL, and adds to the list of epigenetics-based therapies in lymphoma, including EZH2, BET bromodomain, and HDAC inhibitors. DLBCL is characterized by mutations in multiple epigenetic regulators such as EZH2, KMT2D/2C, CREBBP and EP300, with a distinct shift in favor of global transcriptional repression. Co-occurrence of epigenetic mutations may create transcriptional vulnerabilities in lymphoma cells. CREBBP/EP300 mutations co-occur with inactivating mutations in KMT2D in 40% of DLBCL cases. Additionally, one functional allele of CREBBP/EP300 is always maintained, and concurrent inactivation of both histone acetyltransferases is rarely observed in the same tumor (43). Based on these observations, it has been suggested that CREBBP-mutant lymphoma cells may be 'addicted' to EP300 histone acetyltransferase activity. This hypothesis could be easily tested using newly available CREBBP/EP300 inhibitors (139). In our study, we have showed that Type I PRMT inhibitors potently suppress lymphoma cell growth and viability. Like KMT2D, CREBBP and EP300, PRMT1 also plays an important role in transcriptional activation via H4R3me2a deposition. It is possible that PRMT1 and KMT2D/CREBBP/EP300 have common target genes, and perhaps PRMT1 activity represents an additional vulnerability for lymphoma cells with mutations in these epigenetic regulators. Further examination is required to determine if there is any relationship between mutations in KMT2D/CREBBP/EP300 and PRMT1 inhibitor sensitivity. To summarize, our study demonstrates an important role for PRMT1 in DLBCL, and provides a novel epigenetic target for the treatment of this cancer type.

4.3 Interactions of PRC2 with PRMT1 and CARM1 may influence histone H4R3 and H3K27 methylation

When we first identified PRMT1 and CARM1 as potential binding partners of EZH2 in MCF7 breast cancer cells, we wanted to investigate if they could methylate each other. Initial experiments using EZH2 alone with PRMT1/CARM1 yielded negative results. However, when we used the critical core components of the PRC2 complex (EZH2/SUZ12/EED), we observed methylation of a protein at 90kDa by both PRMT1 and CARM1. Due to similar molecular weights, this created multiple possibilities: that either EZH2, or SUZ12, or both of these proteins can be methylated by PRMT1 and CARM1. Next, we used SUZ12 alone as a substrate and observed that it could be methylated by PRMT1. It is very interesting that neither EZH2 nor SUZ12 can be methylated as solo substrates by CARM1, although the signal at 90kDa is very strong when the PRC2 complex is used as a substrate. This may occur because complex formation changes the structural conformation of the substrate to expose the relevant arginine residues for methylation by CARM1. Previously, we have noticed that when individual components of the PRC2 complex are expressed separately, purified from insect cells and then mixed together in a reaction, the resulting complex is not as effective at catalyzing H3K27me3, compared to a complex that is derived from simultaneous expression of all three components (unpublished data).

An antibody recognizing the asymmetric dimethylarginine motif was able to recognize methylation of EZH2/SUZ12 by CARM1 when the PRC2 complex was immunoprecipitated after performing *in vitro* methylation reactions. This antibody could not recognize SUZ12 methylation by PRMT1, but interestingly, it detected a weakly methylated protein at 50kDa. Considering the high purity of the recombinant proteins used, there is a significant possibility that this signal corresponds to EED methylation. Next, we performed nucleosome methylation assays to assess whether the interactions of PRMT1/CARM1 with PRC2 might differentially

modulate their catalytic activities towards histone substrates. Remarkably, we noticed that the PRC2 complex enhanced histone H4R3 methylation by PRMT1. This activity did not require the presence of the accessory PRC2 component RbAp48 which binds to Histone H4. Since PRMT1 cannot directly bind to DNA, we suspect that the PRC2 complex may act as a 'bridge', by improving its access to histone H4 to perform methylation. PRMT1 did not significantly affect H3K27 methylation activity of the PRC2 complex.

Unexpectedly, CARM1 enhanced H3K27 tri-methylation by the PRC2 complex. This result was astonishing, because CARM1 methylates histone H3 at arginine-26 *in vitro*, which is supposed to block H3K27 tri-methylation. In our experiment, both H3R17 and R26 methylation by CARM1 was reduced in the presence of the PRC2 complex, and H3K27me3 was the predominant histone modification observed. Addition of PRMT1 to a reaction containing CARM1 and PRC2 did not affect H3K27me3, but increased the arginine di-methylation signal on CARM1. If PRMT1 increases auto-methylation of CARM1, it is possible that a site different from the well-documented R550 site may be undergoing methylation. Interestingly, PhosphositePlus indicates that amino acid R49 may undergo arginine methylation (140). The CARM1 antibody used in our studies recognizes an epitope surrounding R49. Therefore, if PRMT1 promotes CARM1 auto-methylation at R49, it might affect the antibody's ability to recognize the epitope. Since we used the same antibody to perform the Duolink Proximity Ligation Assay, it may well explain why there was no detectable interaction between EZH2 and CARM1. Accordingly, EED immunoprecipitated from cells with PRMT1 overexpression were found to associate with an arginine-methylated protein that migrated at the same molecular weight as CARM1. Additional experiments have to be performed to confirm that CARM1 can be methylated at arginine-49. Since R49 is in the N-terminal domain of CARM1 that assumes a PH-like superfold, it might play an important function in substrate recognition.

It is unclear how PRMT1 might regulate CARM1 methylation activity, and the significance of increased H3K27 tri-methylation by PRC2 in the presence of CARM1 is also not clear. We suspect that this enhancement of PRC2 methylation activity by CARM1 may not be involved in transcriptional repression, but play a role in alternative mRNA splicing. H3K27me3 has recently been linked to alternative splicing, and PRMTs have extensively been associated with regulation of mRNA splicing (141). It is important to note that the recombinant CARM1 used for *in vitro* methylation assays with PRC2 was extracted from insect cells and highly pure, but the CARM1 used in nucleosome methylation assays was derived from HEK293 cells and relatively less pure. Therefore, we remain cautious about contaminating proteins that may be mediating H3K27me3 enhancement in these assays. Further studies are required to confirm that this phenomenon genuinely arises from CARM1 activity.

BIBLIOGRAPHY

1. Vinuesa, C. G., and P. P. Chang. 2013. Innate B cell helpers reveal novel types of antibody responses. *Nature immunology* 14: 119-126.
2. Kurosaki, T., K. Kometani, and W. Ise. 2015. Memory B cells. *Nature reviews. Immunology* 15: 149-159.
3. Ma, C. S., E. K. Deenick, M. Batten, and S. G. Tangye. 2012. The origins, function, and regulation of T follicular helper cells. *The Journal of experimental medicine* 209: 1241-1253.
4. De Silva, N. S., and U. Klein. 2015. Dynamics of B cells in germinal centres. *Nature reviews. Immunology* 15: 137-148.
5. Caganova, M., C. Carrisi, G. Varano, F. Mainoldi, F. Zanardi, P. L. Germain, L. George, F. Alberghini, L. Ferrarini, A. K. Talukder, M. Ponzoni, G. Testa, T. Nojima, C. Doglioni, D. Kitamura, K. M. Toellner, I. H. Su, and S. Casola. 2013. Germinal center dysregulation by histone methyltransferase EZH2 promotes lymphomagenesis. *The Journal of clinical investigation* 123: 5009-5022.
6. Basso, K., and R. Dalla-Favera. 2015. Germinal centres and B cell lymphomagenesis. *Nature reviews. Immunology* 15: 172-184.
7. Zhang, Y., L. Garcia-Ibanez, and K. M. Toellner. 2016. Regulation of germinal center B-cell differentiation. *Immunological reviews* 270: 8-19.
8. Stavnezer, J., and C. E. Schrader. 2014. IgH chain class switch recombination: mechanism and regulation. *Journal of immunology* 193: 5370-5378.
9. Rickert, R. C. 2013. New insights into pre-BCR and BCR signalling with relevance to B cell malignancies. *Nature reviews. Immunology* 13: 578-591.
10. Young, R. M., and L. M. Staudt. 2013. Targeting pathological B cell receptor signalling in lymphoid malignancies. *Nature reviews. Drug discovery* 12: 229-243.

11. Ramadani, F., D. J. Bolland, F. Garcon, J. L. Emery, B. Vanhaesebroeck, A. E. Corcoran, and K. Okkenhaug. 2010. The PI3K isoforms p110alpha and p110delta are essential for pre-B cell receptor signaling and B cell development. *Science signaling* 3: ra60.

12. Gross, A. J., J. R. Lyandres, A. K. Panigrahi, E. T. Prak, and A. L. DeFranco. 2009. Developmental acquisition of the Lyn-CD22-SHP-1 inhibitory pathway promotes B cell tolerance. *Journal of immunology* 182: 5382-5392.

13. Xu, Y., N. D. Huntington, K. W. Harder, H. Nandurkar, M. L. Hibbs, and D. M. Tarlinton. 2012. Phosphatidylinositol-3 kinase activity in B cells is negatively regulated by Lyn tyrosine kinase. *Immunology and cell biology* 90: 903-911.

14. Okkenhaug, K. 2013. Signaling by the phosphoinositide 3-kinase family in immune cells. *Annual review of immunology* 31: 675-704.

15. Okkenhaug, K. 2013. Rules of engagement: distinct functions for the four class I PI3K catalytic isoforms in immunity. *Annals of the New York Academy of Sciences* 1280: 24-26.

16. Jou, S. T., N. Carpino, Y. Takahashi, R. Piekorz, J. R. Chao, N. Carpino, D. Wang, and J. N. Ihle. 2002. Essential, nonredundant role for the phosphoinositide 3-kinase p110delta in signaling by the B-cell receptor complex. *Molecular and cellular biology* 22: 8580-8591.

17. Geahlen, R. L. 2009. Syk and pTyr'd: Signaling through the B cell antigen receptor. *Biochimica et biophysica acta* 1793: 1115-1127.

18. Cheng, A. M., B. Rowley, W. Pao, A. Hayday, J. B. Bolen, and T. Pawson. 1995. Syk tyrosine kinase required for mouse viability and B-cell development. *Nature* 378: 303-306.

19. Smith, C. I. 2017. From identification of the BTK kinase to effective management of leukemia. *Oncogene* 36: 2045-2053.

20. Mohammad, D. K., B. F. Nore, A. Hussain, M. O. Gustafsson, A. J. Mohamed, and C. I. Smith. 2013. Dual phosphorylation of Btk by Akt/protein kinase b provides docking for 14-3-3zeta, regulates shuttling, and attenuates both tonic and induced signaling in B cells. *Molecular and cellular biology* 33: 3214-3226.

21. Barrington, R. A., T. J. Schneider, L. A. Pitcher, T. R. Mempel, M. Ma, N. S. Barteneva, and M. C. Carroll. 2009. Uncoupling CD21 and CD19 of the B-cell coreceptor. *Proc Natl Acad Sci U S A* 106: 14490-14495.

22. Sato, S., D. A. Steeber, and T. F. Tedder. 1995. The CD19 signal transduction molecule is a response regulator of B-lymphocyte differentiation. *Proc Natl Acad Sci U S A* 92: 11558-11562.

23. Muller, J., and L. Nitschke. 2014. The role of CD22 and Siglec-G in B-cell tolerance and autoimmune disease. *Nature reviews. Rheumatology* 10: 422-428.

24. Zhang, Y., B. Liu, Y. Ma, and B. Jin. 2013. Sema 4D/CD100-plexin B is a multifunctional counter-receptor. *Cellular & molecular immunology* 10: 97-98.

25. Kumanogoh, A., T. Shikina, C. Watanabe, N. Takegahara, K. Suzuki, M. Yamamoto, H. Takamatsu, D. V. Prasad, M. Mizui, T. Toyofuku, M. Tamura, D. Watanabe, J. R. Parnes, and H. Kikutani. 2005. Requirement for CD100-CD72 interactions in fine-tuning of B-cell antigen receptor signaling and homeostatic maintenance of the B-cell compartment. *International immunology* 17: 1277-1282.

26. Kumanogoh, A., K. Suzuki, E. Ch'ng, C. Watanabe, S. Marukawa, N. Takegahara, I. Ishida, T. Sato, S. Habu, K. Yoshida, W. Shi, and H. Kikutani. 2002. Requirement for the lymphocyte semaphorin, CD100, in the induction of antigen-specific T cells and the maturation of dendritic cells. *Journal of immunology* 169: 1175-1181.

27. Suzuki, K., A. Kumanogoh, and H. Kikutani. 2008. Semaphorins and their receptors in immune cell interactions. *Nature immunology* 9: 17-23.

28. Lenz, G., G. W. Wright, N. C. Emre, H. Kohlhammer, S. S. Dave, R. E. Davis, S. Carty, L. T. Lam, A. L. Shaffer, W. Xiao, J. Powell, A. Rosenwald, G. Ott, H. K. Muller-Hermelink, R. D. Gascoyne, J. M. Connors, E. Campo, E. S. Jaffe, J. Delabie, E. B. Smeland, L. M. Rimsza, R. I. Fisher, D. D. Weisenburger, W. C. Chan, and L. M. Staudt. 2008. Molecular subtypes of diffuse large B-cell lymphoma arise by distinct genetic pathways. *Proc Natl Acad Sci U S A* 105: 13520-13525.

29. Roschewski, M., L. M. Staudt, and W. H. Wilson. 2014. Diffuse large B-cell lymphoma-treatment approaches in the molecular era. *Nature reviews. Clinical oncology* 11: 12-23.

30. Hans, C. P., D. D. Weisenburger, T. C. Greiner, R. D. Gascoyne, J. Delabie, G. Ott, H. K. Muller-Hermelink, E. Campo, R. M. Braziel, E. S. Jaffe, Z. Pan, P. Farinha, L. M. Smith, B. Falini, A. H. Banham, A. Rosenwald, L. M. Staudt, J. M. Connors, J. O. Armitage, and W. C. Chan. 2004. Confirmation of the molecular classification of diffuse large B-cell lymphoma by immunohistochemistry using a tissue microarray. *Blood* 103: 275-282.

31. Choi, W. W., D. D. Weisenburger, T. C. Greiner, M. A. Piris, A. H. Banham, J. Delabie, R. M. Braziel, H. Geng, J. Iqbal, G. Lenz, J. M. Vose, C. P. Hans, K. Fu, L. M. Smith, M. Li, Z. Liu, R. D. Gascoyne, A. Rosenwald, G. Ott, L. M. Rimsza, E. Campo, E. S. Jaffe, D. L. Jaye, L. M. Staudt, and W. C. Chan. 2009. A new immunostain algorithm classifies diffuse large B-cell lymphoma into molecular subtypes with high accuracy. *Clin Cancer Res* 15: 5494-5502.

32. Menon, M. P., S. Pittaluga, and E. S. Jaffe. 2012. The histological and biological spectrum of diffuse large B-cell lymphoma in the World Health Organization classification. *Cancer journal* 18: 411-420.

33. Pasqualucci, L., V. Trifonov, G. Fabbri, J. Ma, D. Rossi, A. Chiarenza, V. A. Wells, A. Grunn, M. Messina, O. Elliot, J. Chan, G. Bhagat, A. Chadburn, G. Gaidano, C. G.

Mullighan, R. Rabadan, and R. Dalla-Favera. 2011. Analysis of the coding genome of diffuse large B-cell lymphoma. *Nature genetics* 43: 830-837.

34. Chi, P., C. D. Allis, and G. G. Wang. 2010. Covalent histone modifications--miswritten, misinterpreted and mis-erased in human cancers. *Nat Rev Cancer* 10: 457-469.

35. Bannister, A. J., and T. Kouzarides. 2011. Regulation of chromatin by histone modifications. *Cell research* 21: 381-395.

36. Hyun, K., J. Jeon, K. Park, and J. Kim. 2017. Writing, erasing and reading histone lysine methylations. *Experimental & molecular medicine* 49: e324.

37. Gayatri, S., and M. T. Bedford. 2014. Readers of histone methylarginine marks. *Biochimica et biophysica acta* 1839: 702-710.

38. Allis, C. D., and T. Jenuwein. 2016. The molecular hallmarks of epigenetic control. *Nature reviews. Genetics* 17: 487-500.

39. Fullgrabe, J., E. Kavanagh, and B. Joseph. 2011. Histone onco-modifications. *Oncogene* 30: 3391-3403.

40. Pasqualucci, L., and R. Dalla-Favera. 2015. The genetic landscape of diffuse large B-cell lymphoma. *Seminars in hematology* 52: 67-76.

41. Zhang, J., D. Dominguez-Sola, S. Hussein, J. E. Lee, A. B. Holmes, M. Bansal, S. Vlasevska, T. Mo, H. Tang, K. Basso, K. Ge, R. Dalla-Favera, and L. Pasqualucci. 2015. Disruption of KMT2D perturbs germinal center B cell development and promotes lymphomagenesis. *Nature medicine* 21: 1190-1198.

42. Pasqualucci, L., D. Dominguez-Sola, A. Chiarenza, G. Fabbri, A. Grunn, V. Trifonov, L. H. Kasper, S. Lerach, H. Tang, J. Ma, D. Rossi, A. Chadburn, V. V. Murty, C. G. Mullighan, G. Gaidano, R. Rabadan, P. K. Brindle, and R. Dalla-Favera. 2011. Inactivating mutations of acetyltransferase genes in B-cell lymphoma. *Nature* 471: 189-195.

43. Zhang, J., S. Vlasevska, V. A. Wells, S. Nataraj, A. B. Holmes, R. Duval, S. N. Meyer, T. Mo, K. Basso, P. K. Brindle, S. Hussein, R. Dalla-Favera, and L. Pasqualucci. 2017. The CREBBP Acetyltransferase Is a Haploinsufficient Tumor Suppressor in B-cell Lymphoma. *Cancer discovery* 7: 322-337.

44. Ortega-Molina, A., I. W. Boss, A. Canela, H. Pan, Y. Jiang, C. Zhao, M. Jiang, D. Hu, X. Agirre, I. Niesvizky, J. E. Lee, H. T. Chen, D. Ennishi, D. W. Scott, A. Mottok, C. Hother, S. Liu, X. J. Cao, W. Tam, R. Shaknovich, B. A. Garcia, R. D. Gascoyne, K. Ge, A. Shilatifard, O. Elemento, A. Nussenzweig, A. M. Melnick, and H. G. Wendel. 2015. The histone lysine methyltransferase KMT2D sustains a gene expression program that represses B cell lymphoma development. *Nature medicine* 21: 1199-1208.

45. Lohr, J. G., P. Stojanov, M. S. Lawrence, D. Auclair, B. Chapuy, C. Sougnez, P. Cruz-Gordillo, B. Knoechel, Y. W. Asmann, S. L. Slager, A. J. Novak, A. Dogan, S. M. Ansell, B. K. Link, L. Zou, J. Gould, G. Saksena, N. Stransky, C. Rangel-Escareno, J. C. Fernandez-Lopez, A. Hidalgo-Miranda, J. Melendez-Zajgla, E. Hernandez-Lemus, A. Schwarz-Cruz y Celis, I. Imaz-Rosshandler, A. I. Ojesina, J. Jung, C. S. Pedamallu, E. S. Lander, T. M. Habermann, J. R. Cerhan, M. A. Shipp, G. Getz, and T. R. Golub. 2012. Discovery and prioritization of somatic mutations in diffuse large B-cell lymphoma (DLBCL) by whole-exome sequencing. *Proc Natl Acad Sci U S A* 109: 3879-3884.

46. Cerami, E., J. Gao, U. Dogrusoz, B. E. Gross, S. O. Sumer, B. A. Aksoy, A. Jacobsen, C. J. Byrne, M. L. Heuer, E. Larsson, Y. Antipin, B. Reva, A. P. Goldberg, C. Sander, and N. Schultz. 2012. The cBio cancer genomics portal: an open platform for exploring multidimensional cancer genomics data. *Cancer discovery* 2: 401-404.

47. Gao, J., B. A. Aksoy, U. Dogrusoz, G. Dresdner, B. Gross, S. O. Sumer, Y. Sun, A. Jacobsen, R. Sinha, E. Larsson, E. Cerami, C. Sander, and N. Schultz. 2013.

Integrative analysis of complex cancer genomics and clinical profiles using the cBioPortal. *Science signaling* 6: pl1.

48. Shi, J., and C. R. Vakoc. 2014. The mechanisms behind the therapeutic activity of BET bromodomain inhibition. *Molecular cell* 54: 728-736.

49. Chapuy, B., M. R. McKeown, C. Y. Lin, S. Monti, M. G. Roemer, J. Qi, P. B. Rahl, H. H. Sun, K. T. Yeda, J. G. Doench, E. Reichert, A. L. Kung, S. J. Rodig, R. A. Young, M. A. Shipp, and J. E. Bradner. 2013. Discovery and characterization of super-enhancer-associated dependencies in diffuse large B cell lymphoma. *Cancer cell* 24: 777-790.

50. Boi, M., E. Gaudio, P. Bonetti, I. Kwee, E. Bernasconi, C. Tarantelli, A. Rinaldi, M. Testoni, L. Cascione, M. Ponzoni, A. A. Mensah, A. Stathis, G. Stussi, M. E. Riveiro, P. Herait, G. Inghirami, E. Cvitkovic, E. Zucca, and F. Bertoni. 2015. The BET Bromodomain Inhibitor OTX015 Affects Pathogenetic Pathways in Preclinical B-cell Tumor Models and Synergizes with Targeted Drugs. *Clin Cancer Res* 21: 1628-1638.

51. Mottok, A., and R. D. Gascoyne. 2015. Bromodomain inhibition in diffuse large B-cell lymphoma--giving MYC a brake. *Clin Cancer Res* 21: 4-6.

52. Trabucco, S. E., R. M. Gerstein, A. M. Evens, J. E. Bradner, L. D. Shultz, D. L. Greiner, and H. Zhang. 2015. Inhibition of bromodomain proteins for the treatment of human diffuse large B-cell lymphoma. *Clin Cancer Res* 21: 113-122.

53. Morin, R. D., N. A. Johnson, T. M. Severson, A. J. Mungall, J. An, R. Goya, J. E. Paul, M. Boyle, B. W. Woolcock, F. Kuchenbauer, D. Yap, R. K. Humphries, O. L. Griffith, S. Shah, H. Zhu, M. Kimbara, P. Shashkin, J. F. Charlot, M. Tcherpakov, R. Corbett, A. Tam, R. Varhol, D. Smailus, M. Moksa, Y. Zhao, A. Delaney, H. Qian, I. Birol, J. Schein, R. Moore, R. Holt, D. E. Horsman, J. M. Connors, S. Jones, S. Aparicio, M. Hirst, R. D. Gascoyne, and M. A. Marra. 2010. Somatic mutations altering EZH2

(Tyr641) in follicular and diffuse large B-cell lymphomas of germinal-center origin. *Nature genetics* 42: 181-185.

54. Bodor, C., C. O'Riain, D. Wrench, J. Matthews, S. Iyengar, H. Tayyib, M. Calaminici, A. Clear, S. Iqbal, H. Quentmeier, H. G. Drexler, S. Montoto, A. T. Lister, J. G. Gribben, A. Matolcsy, and J. Fitzgibbon. 2011. EZH2 Y641 mutations in follicular lymphoma. *Leukemia* 25: 726-729.

55. McCabe, M. T., A. P. Graves, G. Ganji, E. Diaz, W. S. Halsey, Y. Jiang, K. N. Smitheman, H. M. Ott, M. B. Pappalardi, K. E. Allen, S. B. Chen, A. Della Pietra, 3rd, E. Dul, A. M. Hughes, S. A. Gilbert, S. H. Thrall, P. J. Tummino, R. G. Kruger, M. Brandt, B. Schwartz, and C. L. Creasy. 2012. Mutation of A677 in histone methyltransferase EZH2 in human B-cell lymphoma promotes hypertrimethylation of histone H3 on lysine 27 (H3K27). *Proc Natl Acad Sci U S A* 109: 2989-2994.

56. Majer, C. R., L. Jin, M. P. Scott, S. K. Knutson, K. W. Kuntz, H. Keilhack, J. J. Smith, M. P. Moyer, V. M. Richon, R. A. Copeland, and T. J. Wigle. 2012. A687V EZH2 is a gain-of-function mutation found in lymphoma patients. *FEBS letters* 586: 3448-3451.

57. Kirmizis, A., S. M. Bartley, A. Kuzmichev, R. Margueron, D. Reinberg, R. Green, and P. J. Farnham. 2004. Silencing of human polycomb target genes is associated with methylation of histone H3 Lys 27. *Genes Dev* 18: 1592-1605.

58. Sneeringer, C. J., M. P. Scott, K. W. Kuntz, S. K. Knutson, R. M. Pollock, V. M. Richon, and R. A. Copeland. 2010. Coordinated activities of wild-type plus mutant EZH2 drive tumor-associated hypertrimethylation of lysine 27 on histone H3 (H3K27) in human B-cell lymphomas. *Proc Natl Acad Sci U S A* 107: 20980-20985.

59. Yap, D. B., J. Chu, T. Berg, M. Schapira, S. W. Cheng, A. Moradian, R. D. Morin, A. J. Mungall, B. Meissner, M. Boyle, V. E. Marquez, M. A. Marra, R. D. Gascoyne, R. K. Humphries, C. H. Arrowsmith, G. B. Morin, and S. A. Aparicio. 2011. Somatic

mutations at EZH2 Y641 act dominantly through a mechanism of selectively altered PRC2 catalytic activity, to increase H3K27 trimethylation. *Blood* 117: 2451-2459.

60. McCabe, M. T., H. M. Ott, G. Ganji, S. Korenchuk, C. Thompson, G. S. Van Aller, Y. Liu, A. P. Graves, A. Della Pietra, 3rd, E. Diaz, L. V. LaFrance, M. Mellinger, C. Duquenne, X. Tian, R. G. Kruger, C. F. McHugh, M. Brandt, W. H. Miller, D. Dhanak, S. K. Verma, P. J. Tummino, and C. L. Creasy. 2012. EZH2 inhibition as a therapeutic strategy for lymphoma with EZH2-activating mutations. *Nature* 492: 108-112.

61. Knutson, S. K., T. J. Wigle, N. M. Warholic, C. J. Sneeringer, C. J. Allain, C. R. Klaus, J. D. Sacks, A. Raimondi, C. R. Majer, J. Song, M. P. Scott, L. Jin, J. J. Smith, E. J. Olhava, R. Chesworth, M. P. Moyer, V. M. Richon, R. A. Copeland, H. Keilhack, R. M. Pollock, and K. W. Kuntz. 2012. A selective inhibitor of EZH2 blocks H3K27 methylation and kills mutant lymphoma cells. *Nature chemical biology* 8: 890-896.

62. Konze, K. D., A. Ma, F. Li, D. Barsyte-Lovejoy, T. Parton, C. J. Macnevin, F. Liu, C. Gao, X. P. Huang, E. Kuznetsova, M. Rougie, A. Jiang, S. G. Pattenden, J. L. Norris, L. I. James, B. L. Roth, P. J. Brown, S. V. Frye, C. H. Arrowsmith, K. M. Hahn, G. G. Wang, M. Vedadi, and J. Jin. 2013. An orally bioavailable chemical probe of the Lysine Methyltransferases EZH2 and EZH1. *ACS chemical biology* 8: 1324-1334.

63. Knutson, S. K., S. Kawano, Y. Minoshima, N. M. Warholic, K. C. Huang, Y. Xiao, T. Kadowaki, M. Uesugi, G. Kuznetsov, N. Kumar, T. J. Wigle, C. R. Klaus, C. J. Allain, A. Raimondi, N. J. Waters, J. J. Smith, M. Porter-Scott, R. Chesworth, M. P. Moyer, R. A. Copeland, V. M. Richon, T. Uenaka, R. M. Pollock, K. W. Kuntz, A. Yokoi, and H. Keilhack. 2014. Selective inhibition of EZH2 by EPZ-6438 leads to potent antitumor activity in EZH2-mutant non-Hodgkin lymphoma. *Mol Cancer Ther* 13: 842-854.

64. Song, X., L. Zhang, T. Gao, T. Ye, Y. Zhu, Q. Lei, Q. Feng, B. He, H. Deng, and L. Yu. 2016. Selective inhibition of EZH2 by ZLD10A blocks H3K27 methylation and kills

mutant lymphoma cells proliferation. *Biomedicine & pharmacotherapy = Biomedecine & pharmacotherapie* 81: 288-294.

65. Bradley, W. D., S. Arora, J. Busby, S. Balasubramanian, V. S. Gehling, C. G. Nasveschuk, R. G. Vaswani, C. C. Yuan, C. Hatton, F. Zhao, K. E. Williamson, P. Iyer, J. Mendez, R. Campbell, N. Cantone, S. Garapaty-Rao, J. E. Audia, A. S. Cook, L. A. Dakin, B. K. Albrecht, J. C. Harmange, D. L. Daniels, R. T. Cummings, B. M. Bryant, E. Normant, and P. Trojer. 2014. EZH2 inhibitor efficacy in non-Hodgkin's lymphoma does not require suppression of H3K27 monomethylation. *Chemistry & biology* 21: 1463-1475.

66. Weiner, G. J. 2010. Rituximab: mechanism of action. *Seminars in hematology* 47: 115-123.

67. Davis, R. E., V. N. Ngo, G. Lenz, P. Tolar, R. M. Young, P. B. Romesser, H. Kohlhammer, L. Lamy, H. Zhao, Y. Yang, W. Xu, A. L. Shaffer, G. Wright, W. Xiao, J. Powell, J. K. Jiang, C. J. Thomas, A. Rosenwald, G. Ott, H. K. Muller-Hermelink, R. D. Gascoyne, J. M. Connors, N. A. Johnson, L. M. Rimsza, E. Campo, E. S. Jaffe, W. H. Wilson, J. Delabie, E. B. Smeland, R. I. Fisher, R. M. Braziel, R. R. Tubbs, J. R. Cook, D. D. Weisenburger, W. C. Chan, S. K. Pierce, and L. M. Staudt. 2010. Chronic active B-cell-receptor signalling in diffuse large B-cell lymphoma. *Nature* 463: 88-92.

68. Wang, Y., L. L. Zhang, R. E. Champlin, and M. L. Wang. 2015. Targeting Bruton's tyrosine kinase with ibrutinib in B-cell malignancies. *Clinical pharmacology and therapeutics* 97: 455-468.

69. Blum, K. A. 2015. B-cell receptor pathway modulators in NHL. *Hematology. American Society of Hematology. Education Program* 2015: 82-91.

70. Alinari, L., C. Quinion, and K. A. Blum. 2015. Bruton's tyrosine kinase inhibitors in B-cell non-Hodgkin's lymphomas. *Clinical pharmacology and therapeutics* 97: 469-477.

71. Maffei, R., S. Fiorcari, S. Martinelli, L. Potenza, M. Luppi, and R. Marasca. 2015. Targeting neoplastic B cells and harnessing microenvironment: the "double face" of ibrutinib and idelalisib. *Journal of hematology & oncology* 8: 60.

72. Cheah, C. Y., and N. H. Fowler. 2016. Idelalisib in the management of lymphoma. *Blood* 128: 331-336.

73. Yap, T. A., L. Bjerke, P. A. Clarke, and P. Workman. 2015. Drugging PI3K in cancer: refining targets and therapeutic strategies. *Current opinion in pharmacology* 23: 98-107.

74. Sehn, L. H., and R. D. Gascoyne. 2015. Diffuse large B-cell lymphoma: optimizing outcome in the context of clinical and biologic heterogeneity. *Blood* 125: 22-32.

75. Pfeifer, M., M. Grau, D. Lenze, S. S. Wenzel, A. Wolf, B. Wollert-Wulf, K. Dietze, H. Nogai, B. Storek, H. Madle, B. Dorken, M. Janz, S. Dirnhofer, P. Lenz, M. Hummel, A. Tzankov, and G. Lenz. 2013. PTEN loss defines a PI3K/AKT pathway-dependent germinal center subtype of diffuse large B-cell lymphoma. *Proc Natl Acad Sci U S A* 110: 12420-12425.

76. Rolf, M. G., J. O. Curwen, M. Veldman-Jones, C. Eberlein, J. Wang, A. Harmer, C. J. Hellawell, and M. Braddock. 2015. In vitro pharmacological profiling of R406 identifies molecular targets underlying the clinical effects of fostamatinib. *Pharmacology research & perspectives* 3: e00175.

77. Spurgeon, S. E., G. Coffey, L. B. Fletcher, R. Burke, J. W. Tyner, B. J. Druker, A. Betz, F. DeGuzman, Y. Pak, D. Baker, A. Pandey, S. J. Hollenbach, U. Sinha, and M. M. Loriaux. 2013. The selective SYK inhibitor P505-15 (PRT062607) inhibits B cell signaling and function in vitro and in vivo and augments the activity of fludarabine in chronic lymphocytic leukemia. *The Journal of pharmacology and experimental therapeutics* 344: 378-387.

78. Lam, B., Y. Arikawa, J. Cramlett, Q. Dong, R. de Jong, V. Feher, C. E. Grimshaw, P. J. Farrell, I. D. Hoffman, A. Jennings, B. Jones, J. Matuszkiewicz, J. Miura, H. Miyake, S. R. Natala, L. Shi, M. Takahashi, E. Taylor, C. Wyrick, J. Yano, J. Zalevsky, and Z. Nie. 2016. Discovery of TAK-659 an orally available investigational inhibitor of Spleen Tyrosine Kinase (SYK). *Bioorganic & medicinal chemistry letters* 26: 5947-5950.

79. Purroy, N., J. Carabia, P. Abrisqueta, L. Egia, M. Aguilo, C. Carpio, C. Palacio, M. Crespo, and F. Bosch. 2017. Inhibition of BCR signaling using the Syk inhibitor TAK-659 prevents stroma-mediated signaling in chronic lymphocytic leukemia cells. *Oncotarget* 8: 742-756.

80. Cheng, S., G. Coffey, X. H. Zhang, R. Shaknovich, Z. Song, P. Lu, A. Pandey, A. M. Melnick, U. Sinha, and Y. L. Wang. 2011. SYK inhibition and response prediction in diffuse large B-cell lymphoma. *Blood* 118: 6342-6352.

81. Seiler, T., G. Hutter, and M. Dreyling. 2016. The Emerging Role of PI3K Inhibitors in the Treatment of Hematological Malignancies: Preclinical Data and Clinical Progress to Date. *Drugs* 76: 639-646.

82. Akinleye, A., Y. Chen, N. Mukhi, Y. Song, and D. Liu. 2013. Ibrutinib and novel BTK inhibitors in clinical development. *Journal of hematology & oncology* 6: 59.

83. Herman, S. E., A. Montraveta, C. U. Niemann, H. Mora-Jensen, M. Gulrajani, F. Krantz, R. Mantel, L. L. Smith, F. McClanahan, B. K. Harrington, D. Colomer, T. Covey, J. C. Byrd, R. Izumi, A. Kaptein, R. Ulrich, A. J. Johnson, B. J. Lannutti, A. Wiestner, and J. A. Woyach. 2016. The Bruton Tyrosine Kinase (BTK) Inhibitor Acalabrutinib Demonstrates Potent On-Target Effects and Efficacy in Two Mouse Models of Chronic Lymphocytic Leukemia. *Clin Cancer Res*.

84. Byrd, J. C., B. Harrington, S. O'Brien, J. A. Jones, A. Schuh, S. Devereux, J. Chaves, W. G. Wierda, F. T. Awan, J. R. Brown, P. Hillmen, D. M. Stephens, P. Ghia, J. C. Barrientos, J. M. Pagel, J. Woyach, D. Johnson, J. Huang, X. Wang, A. Kaptein, B. J.

Lannutti, T. Covey, M. Fardis, J. McGreivy, A. Hamdy, W. Rothbaum, R. Izumi, T. G. Diacovo, A. J. Johnson, and R. R. Furman. 2016. Acalabrutinib (ACP-196) in Relapsed Chronic Lymphocytic Leukemia. *The New England journal of medicine* 374: 323-332.

85. Burki, T. K. 2016. Acalabrutinib for relapsed chronic lymphocytic leukaemia. *The Lancet. Oncology* 17: e48.

86. Wu, J., M. Zhang, and D. Liu. 2016. Acalabrutinib (ACP-196): a selective second-generation BTK inhibitor. *Journal of hematology & oncology* 9: 21.

87. Souers, A. J., J. D. Leverson, E. R. Boghaert, S. L. Ackler, N. D. Catron, J. Chen, B. D. Dayton, H. Ding, S. H. Enschede, W. J. Fairbrother, D. C. Huang, S. G. Hymowitz, S. Jin, S. L. Khaw, P. J. Kovar, L. T. Lam, J. Lee, H. L. Maecker, K. C. Marsh, K. D. Mason, M. J. Mitten, P. M. Nimmer, A. Oleksijew, C. H. Park, C. M. Park, D. C. Phillips, A. W. Roberts, D. Sampath, J. F. Seymour, M. L. Smith, G. M. Sullivan, S. K. Tahir, C. Tse, M. D. Wendt, Y. Xiao, J. C. Xue, H. Zhang, R. A. Humerickhouse, S. H. Rosenberg, and S. W. Elmore. 2013. ABT-199, a potent and selective BCL-2 inhibitor, achieves antitumor activity while sparing platelets. *Nature medicine* 19: 202-208.

88. Wensveen, F. M., E. Slinger, M. H. van Attekum, R. Brink, and E. Eldering. 2016. Antigen-affinity controls pre-germinal centser B cell selection by promoting Mcl-1 induction through BAFF receptor signaling. *Scientific reports* 6: 35673.

89. Vikstrom, I., S. Carotta, K. Luthje, V. Peperzak, P. J. Jost, S. Glaser, M. Busslinger, P. Bouillet, A. Strasser, S. L. Nutt, and D. M. Tarlinton. 2010. Mcl-1 is essential for germinal center formation and B cell memory. *Science* 330: 1095-1099.

90. Vikstrom, I. B., A. Slomp, E. M. Carrington, L. M. Moesbergen, C. Chang, G. L. Kelly, S. P. Glaser, J. H. Jansen, J. H. Leusen, A. Strasser, D. C. Huang, A. M. Lew, V. Peperzak, and D. M. Tarlinton. 2016. MCL-1 is required throughout B-cell development and its loss sensitizes specific B-cell subsets to inhibition of BCL-2 or BCL-XL. *Cell death & disease* 7: e2345.

91. Ryan, R. J., M. Nitta, D. Borger, L. R. Zukerberg, J. A. Ferry, N. L. Harris, A. J. Iafrate, B. E. Bernstein, A. R. Sohani, and L. P. Le. 2011. EZH2 codon 641 mutations are common in BCL2-rearranged germinal center B cell lymphomas. *PloS one* 6: e28585.

92. Souroullas, G. P., W. R. Jeck, J. S. Parker, J. M. Simon, J. Y. Liu, J. Paulk, J. Xiong, K. S. Clark, Y. Fedoriw, J. Qi, C. E. Burd, J. E. Bradner, and N. E. Sharpless. 2016. An oncogenic Ezh2 mutation induces tumors through global redistribution of histone 3 lysine 27 trimethylation. *Nature medicine* 22: 632-640.

93. Yang, Y., and M. T. Bedford. 2013. Protein arginine methyltransferases and cancer. *Nat Rev Cancer* 13: 37-50.

94. Bedford, M. T., and S. G. Clarke. 2009. Protein arginine methylation in mammals: who, what, and why. *Molecular cell* 33: 1-13.

95. Teyssier, C., M. Le Romancer, S. Sentis, S. Jalaguier, L. Corbo, and V. Cavailles. 2010. Protein arginine methylation in estrogen signaling and estrogen-related cancers. *Trends in endocrinology and metabolism: TEM* 21: 181-189.

96. Di Lorenzo, A., and M. T. Bedford. 2011. Histone arginine methylation. *FEBS letters* 585: 2024-2031.

97. An, W., J. Kim, and R. G. Roeder. 2004. Ordered cooperative functions of PRMT1, p300, and CARM1 in transcriptional activation by p53. *Cell* 117: 735-748.

98. Kleinschmidt, M. A., G. Streubel, B. Samans, M. Krause, and U. M. Bauer. 2008. The protein arginine methyltransferases CARM1 and PRMT1 cooperate in gene regulation. *Nucleic acids research* 36: 3202-3213.

99. Jacques, S. L., K. P. Aquino, J. Gureasko, P. A. Boriack-Sjodin, M. Porter Scott, R. A. Copeland, and T. V. Riera. 2016. CARM1 Preferentially Methylates H3R17 over H3R26 through a Random Kinetic Mechanism. *Biochemistry* 55: 1635-1644.

100. Iberg, A. N., A. Espejo, D. Cheng, D. Kim, J. Michaud-Levesque, S. Richard, and M. T. Bedford. 2008. Arginine methylation of the histone H3 tail impedes effector binding. *The Journal of biological chemistry* 283: 3006-3010.

101. Guccione, E., C. Bassi, F. Casadio, F. Martinato, M. Cesaroni, H. Schuchlautz, B. Luscher, and B. Amati. 2007. Methylation of histone H3R2 by PRMT6 and H3K4 by an MLL complex are mutually exclusive. *Nature* 449: 933-937.

102. Wang, L., Z. Zhao, M. B. Meyer, S. Saha, M. Yu, A. Guo, K. B. Wisinski, W. Huang, W. Cai, J. W. Pike, M. Yuan, P. Ahlquist, and W. Xu. 2014. CARM1 methylates chromatin remodeling factor BAF155 to enhance tumor progression and metastasis. *Cancer cell* 25: 21-36.

103. Wang, L., H. Zeng, Q. Wang, Z. Zhao, T. G. Boyer, X. Bian, and W. Xu. 2015. MED12 methylation by CARM1 sensitizes human breast cancer cells to chemotherapy drugs. *Science advances* 1: e1500463.

104. Vu, L. P., F. Perna, L. Wang, F. Voza, M. E. Figueroa, P. Tempst, H. Erdjument-Bromage, R. Gao, S. Chen, E. Paietta, T. Deblasio, A. Melnick, Y. Liu, X. Zhao, and S. D. Nimer. 2013. PRMT4 blocks myeloid differentiation by assembling a methyl-RUNX1-dependent repressor complex. *Cell reports* 5: 1625-1638.

105. Xu, W., H. Chen, K. Du, H. Asahara, M. Tini, B. M. Emerson, M. Montminy, and R. M. Evans. 2001. A transcriptional switch mediated by cofactor methylation. *Science* 294: 2507-2511.

106. Lafleur, V. N., S. Richard, and D. E. Richard. 2014. Transcriptional repression of hypoxia-inducible factor-1 (HIF-1) by the protein arginine methyltransferase PRMT1. *Molecular biology of the cell* 25: 925-935.

107. Liao, H. W., J. M. Hsu, W. Xia, H. L. Wang, Y. N. Wang, W. C. Chang, S. T. Arold, C. K. Chou, P. H. Tsou, H. Yamaguchi, Y. F. Fang, H. J. Lee, H. H. Lee, S. K. Tai, M. H. Yang, M. P. Morelli, M. Sen, J. E. Ladbury, C. H. Chen, J. R. Grandis, S. Kopetz, and

M. C. Hung. 2015. PRMT1-mediated methylation of the EGF receptor regulates signaling and cetuximab response. *The Journal of clinical investigation* 125: 4529-4543.

108. Wang, Y., J. M. Hsu, Y. Kang, Y. Wei, P. C. Lee, S. J. Chang, Y. H. Hsu, J. L. Hsu, H. L. Wang, W. C. Chang, C. W. Li, H. W. Liao, S. S. Chang, W. Xia, H. W. Ko, C. K. Chou, J. B. Fleming, H. Wang, R. F. Hwang, Y. Chen, J. Qin, and M. C. Hung. 2016. Oncogenic Functions of Gli1 in Pancreatic Adenocarcinoma Are Supported by Its PRMT1-Mediated Methylation. *Cancer Res* 76: 7049-7058.

109. Gao, Y., Y. Zhao, J. Zhang, Y. Lu, X. Liu, P. Geng, B. Huang, Y. Zhang, and J. Lu. 2016. The dual function of PRMT1 in modulating epithelial-mesenchymal transition and cellular senescence in breast cancer cells through regulation of ZEB1. *Scientific reports* 6: 19874.

110. Takai, H., K. Masuda, T. Sato, Y. Sakaguchi, T. Suzuki, T. Suzuki, R. Koyama-Nasu, Y. Nasu-Nishimura, Y. Katou, H. Ogawa, Y. Morishita, H. Kozuka-Hata, M. Oyama, T. Todo, Y. Ino, A. Mukasa, N. Saito, C. Toyoshima, K. Shirahige, and T. Akiyama. 2014. 5-Hydroxymethylcytosine plays a critical role in glioblastomagenesis by recruiting the CHTOP-methylosome complex. *Cell reports* 9: 48-60.

111. Cheung, N., T. K. Fung, B. B. Zeisig, K. Holmes, J. K. Rane, K. A. Mowen, M. G. Finn, B. Lenhard, L. C. Chan, and C. W. So. 2016. Targeting Aberrant Epigenetic Networks Mediated by PRMT1 and KDM4C in Acute Myeloid Leukemia. *Cancer cell* 29: 32-48.

112. Dhar, S., V. Vemulapalli, A. N. Patananan, G. L. Huang, A. Di Lorenzo, S. Richard, M. J. Comb, A. Guo, S. G. Clarke, and M. T. Bedford. 2013. Loss of the major Type I arginine methyltransferase PRMT1 causes substrate scavenging by other PRMTs. *Scientific reports* 3: 1311.

113. Schapira, M., and R. Ferreira de Freitas. 2014. Structural biology and chemistry of protein arginine methyltransferases. *MedChemComm* 5: 1779-1788.

114. Yue, W. W., M. Hassler, S. M. Roe, V. Thompson-Vale, and L. H. Pearl. 2007. Insights into histone code syntax from structural and biochemical studies of CARM1 methyltransferase. *The EMBO journal* 26: 4402-4412.

115. Troffer-Charlier, N., V. Cura, P. Hassenboehler, D. Moras, and J. Cavarelli. 2007. Functional insights from structures of coactivator-associated arginine methyltransferase 1 domains. *The EMBO journal* 26: 4391-4401.

116. Scheffzek, K., and S. Welti. 2012. Pleckstrin homology (PH) like domains - versatile modules in protein-protein interaction platforms. *FEBS letters* 586: 2662-2673.

117. Shishkova, E., H. Zeng, F. Liu, N. W. Kwiecien, A. S. Hebert, J. J. Coon, and W. Xu. 2017. Global mapping of CARM1 substrates defines enzyme specificity and substrate recognition. *Nature communications* 8: 15571.

118. Kuhn, P., R. Chumanov, Y. Wang, Y. Ge, R. R. Burgess, and W. Xu. 2011. Automethylation of CARM1 allows coupling of transcription and mRNA splicing. *Nucleic acids research* 39: 2717-2726.

119. Mitchell, L. H., A. E. Drew, S. A. Ribich, N. Rioux, K. K. Swinger, S. L. Jacques, T. Lingaraj, P. A. Boriack-Sjodin, N. J. Waters, T. J. Wigle, O. Moradei, L. Jin, T. Riera, M. Porter-Scott, M. P. Moyer, J. J. Smith, R. Chesworth, and R. A. Copeland. 2015. Aryl Pyrazoles as Potent Inhibitors of Arginine Methyltransferases: Identification of the First PRMT6 Tool Compound. *ACS medicinal chemistry letters* 6: 655-659.

120. Eram, M. S., Y. Shen, M. M. Szewczyk, H. Wu, G. Senisterra, F. Li, K. V. Butler, H. U. Kaniskan, B. A. Speed, C. dela Sena, A. Dong, H. Zeng, M. Schapira, P. J. Brown, C. H. Arrowsmith, D. Barsyte-Lovejoy, J. Liu, M. Vedadi, and J. Jin. 2016. A Potent, Selective, and Cell-Active Inhibitor of Human Type I Protein Arginine Methyltransferases. *ACS chemical biology* 11: 772-781.

121. Shen, Y., M. M. Szewczyk, M. S. Eram, D. Smil, H. U. Kaniskan, R. Ferreira de Freitas, G. Senisterra, F. Li, M. Schapira, P. J. Brown, C. H. Arrowsmith, D. Barsyte-Lovejoy,

J. Liu, M. Vedadi, and J. Jin. 2016. Discovery of a Potent, Selective, and Cell-Active Dual Inhibitor of Protein Arginine Methyltransferase 4 and Protein Arginine Methyltransferase 6. *Journal of medicinal chemistry* 59: 9124-9139.

122. Kaniskan, H. U., M. M. Szewczyk, Z. Yu, M. S. Eram, X. Yang, K. Schmidt, X. Luo, M. Dai, F. He, I. Zang, Y. Lin, S. Kennedy, F. Li, E. Dobrovetsky, A. Dong, D. Smil, S. J. Min, M. Landon, J. Lin-Jones, X. P. Huang, B. L. Roth, M. Schapira, P. Atadja, D. Barsyte-Lovejoy, C. H. Arrowsmith, P. J. Brown, K. Zhao, J. Jin, and M. Vedadi. 2015. A potent, selective and cell-active allosteric inhibitor of protein arginine methyltransferase 3 (PRMT3). *Angewandte Chemie* 54: 5166-5170.

123. Cheng, D., N. Yadav, R. W. King, M. S. Swanson, E. J. Weinstein, and M. T. Bedford. 2004. Small molecule regulators of protein arginine methyltransferases. *The Journal of biological chemistry* 279: 23892-23899.

124. Ran, F. A., P. D. Hsu, J. Wright, V. Agarwala, D. A. Scott, and F. Zhang. 2013. Genome engineering using the CRISPR-Cas9 system. *Nature protocols* 8: 2281-2308.

125. Cong, L., F. A. Ran, D. Cox, S. Lin, R. Barretto, N. Habib, P. D. Hsu, X. Wu, W. Jiang, L. A. Marraffini, and F. Zhang. 2013. Multiplex genome engineering using CRISPR/Cas systems. *Science* 339: 819-823.

126. Hsu, P. D., D. A. Scott, J. A. Weinstein, F. A. Ran, S. Konermann, V. Agarwala, Y. Li, E. J. Fine, X. Wu, O. Shalem, T. J. Cradick, L. A. Marraffini, G. Bao, and F. Zhang. 2013. DNA targeting specificity of RNA-guided Cas9 nucleases. *Nature biotechnology* 31: 827-832.

127. Forbes, S. A., D. Beare, H. Boutselakis, S. Bamford, N. Bindal, J. Tate, C. G. Cole, S. Ward, E. Dawson, L. Ponting, R. Stefancsik, B. Harsha, C. Y. Kok, M. Jia, H. Jubb, Z. Sondka, S. Thompson, T. De, and P. J. Campbell. 2017. COSMIC: somatic cancer genetics at high-resolution. *Nucleic acids research* 45: D777-D783.

128. Klanova, M., L. Andera, J. Brazina, J. Svadlenka, S. Benesova, J. Soukup, D. Prukova, D. Vejmelkova, R. Jaksa, K. Helman, P. Vockova, L. Lateckova, J. Molinsky, B. C. Maswabi, M. Alam, R. Kodet, R. Pytlik, M. Trneny, and P. Klener. 2016. Targeting of BCL2 Family Proteins with ABT-199 and Homoharringtonine Reveals BCL2- and MCL1-Dependent Subgroups of Diffuse Large B-Cell Lymphoma. *Clin Cancer Res* 22: 1138-1149.

129. Basso, K., A. A. Margolin, G. Stolovitzky, U. Klein, R. Dalla-Favera, and A. Califano. 2005. Reverse engineering of regulatory networks in human B cells. *Nature genetics* 37: 382-390.

130. Brune, V., E. Tiacci, I. Pfeil, C. Doring, S. Eckerle, C. J. van Noesel, W. Klapper, B. Falini, A. von Heydebreck, D. Metzler, A. Brauninger, M. L. Hansmann, and R. Kuppers. 2008. Origin and pathogenesis of nodular lymphocyte-predominant Hodgkin lymphoma as revealed by global gene expression analysis. *The Journal of experimental medicine* 205: 2251-2268.

131. Rhodes, D. R., S. Kalyana-Sundaram, V. Mahavisno, R. Varambally, J. Yu, B. B. Briggs, T. R. Barrette, M. J. Anstet, C. Kincead-Beal, P. Kulkarni, S. Varambally, D. Ghosh, and A. M. Chinnaiyan. 2007. Oncomine 3.0: genes, pathways, and networks in a collection of 18,000 cancer gene expression profiles. *Neoplasia* 9: 166-180.

132. Rosenwald, A., G. Wright, K. Leroy, X. Yu, P. Gaulard, R. D. Gascoyne, W. C. Chan, T. Zhao, C. Haioun, T. C. Greiner, D. D. Weisenburger, J. C. Lynch, J. Vose, J. O. Armitage, E. B. Smeland, S. Kvaloy, H. Holte, J. Delabie, E. Campo, E. Montserrat, A. Lopez-Guillermo, G. Ott, H. K. Muller-Hermelink, J. M. Connors, R. Braziel, T. M. Grogan, R. I. Fisher, T. P. Miller, M. LeBlanc, M. Chiorazzi, H. Zhao, L. Yang, J. Powell, W. H. Wilson, E. S. Jaffe, R. Simon, R. D. Klausner, and L. M. Staudt. 2003. Molecular diagnosis of primary mediastinal B cell lymphoma identifies a clinically favorable

subgroup of diffuse large B cell lymphoma related to Hodgkin lymphoma. *The Journal of experimental medicine* 198: 851-862.

133. Lenz, G., G. Wright, S. S. Dave, W. Xiao, J. Powell, H. Zhao, W. Xu, B. Tan, N. Goldschmidt, J. Iqbal, J. Vose, M. Bast, K. Fu, D. D. Weisenburger, T. C. Greiner, J. O. Armitage, A. Kyle, L. May, R. D. Gascoyne, J. M. Connors, G. Troen, H. Holte, S. Kvaloy, D. Dierickx, G. Verhoef, J. Delabie, E. B. Smeland, P. Jares, A. Martinez, A. Lopez-Guillermo, E. Montserrat, E. Campo, R. M. Braziel, T. P. Miller, L. M. Rimsza, J. R. Cook, B. Pohlman, J. Sweetenham, R. R. Tubbs, R. I. Fisher, E. Hartmann, A. Rosenwald, G. Ott, H. K. Muller-Hermelink, D. Wrench, T. A. Lister, E. S. Jaffe, W. H. Wilson, W. C. Chan, L. M. Staudt, and P. Lymphoma/Leukemia Molecular Profiling. 2008. Stromal gene signatures in large-B-cell lymphomas. *The New England journal of medicine* 359: 2313-2323.

134. Shipp, M. A., K. N. Ross, P. Tamayo, A. P. Weng, J. L. Kutok, R. C. Aguiar, M. Gaasenbeek, M. Angelo, M. Reich, G. S. Pinkus, T. S. Ray, M. A. Koval, K. W. Last, A. Norton, T. A. Lister, J. Mesirov, D. S. Neuberg, E. S. Lander, J. C. Aster, and T. R. Golub. 2002. Diffuse large B-cell lymphoma outcome prediction by gene-expression profiling and supervised machine learning. *Nature medicine* 8: 68-74.

135. Abou El Hassan, M., K. Huang, M. B. Eswara, M. Zhao, L. Song, T. Yu, Y. Liu, J. C. Liu, S. McCurdy, A. Ma, J. Wither, J. Jin, E. Zacksenhaus, J. L. Wrana, and R. Bremner. 2015. Cancer Cells Hijack PRC2 to Modify Multiple Cytokine Pathways. *PloS one* 10: e0126466.

136. Chung, E. Y., J. N. Psathas, D. Yu, Y. Li, M. J. Weiss, and A. Thomas-Tikhonenko. 2012. CD19 is a major B cell receptor-independent activator of MYC-driven B-lymphomagenesis. *The Journal of clinical investigation* 122: 2257-2266.

137. Yuan, W., M. Xu, C. Huang, N. Liu, S. Chen, and B. Zhu. 2011. H3K36 methylation antagonizes PRC2-mediated H3K27 methylation. *The Journal of biological chemistry* 286: 7983-7989.

138. Simandi, Z., E. Czipa, A. Horvath, A. Koszeghy, C. Bordas, S. Poliska, I. Juhasz, L. Imre, G. Szabo, B. Dezso, E. Barta, S. Sauer, K. Karolyi, I. Kovacs, G. Hutoczki, L. Bognar, A. Klekner, P. Szucs, B. L. Balint, and L. Nagy. 2015. PRMT1 and PRMT8 regulate retinoic acid-dependent neuronal differentiation with implications to neuropathology. *Stem cells* 33: 726-741.

139. Picaud, S., O. Fedorov, A. Thanasopoulou, K. Leonards, K. Jones, J. Meier, H. Olzscha, O. Monteiro, S. Martin, M. Philpott, A. Tumber, P. Filippakopoulos, C. Yapp, C. Wells, K. H. Che, A. Bannister, S. Robson, U. Kumar, N. Parr, K. Lee, D. Lugo, P. Jeffrey, S. Taylor, M. L. Vecellio, C. Bountra, P. E. Brennan, A. O'Mahony, S. Velichko, S. Muller, D. Hay, D. L. Daniels, M. Urh, N. B. La Thangue, T. Kouzarides, R. Prinjha, J. Schwaller, and S. Knapp. 2015. Generation of a Selective Small Molecule Inhibitor of the CBP/p300 Bromodomain for Leukemia Therapy. *Cancer Res* 75: 5106-5119.

140. Hornbeck, P. V., I. Chabra, J. M. Kornhauser, E. Skrzypek, and B. Zhang. 2004. PhosphoSite: A bioinformatics resource dedicated to physiological protein phosphorylation. *Proteomics* 4: 1551-1561.

141. Gonzalez, I., R. Munita, E. Agirre, T. A. Dittmer, K. Gysling, T. Misteli, and R. F. Luco. 2015. A lncRNA regulates alternative splicing via establishment of a splicing-specific chromatin signature. *Nature structural & molecular biology* 22: 370-376.

VITA

Aarthi Goverdhan was born in Chennai, India. After completing her high school education in India, she attended college at the University of Arizona in Tucson, Arizona. She graduated from college in May 2009, and received a degree in Bachelor of Science with a double-major in Biochemistry and Molecular Biophysics, and Molecular and Cellular Biology. For one year, she worked as a research technician in a lab at the Arizona Cancer Center. In Fall 2010, she enrolled in the PhD program at The University of Texas MD Anderson Cancer Center UTHealth Graduate School of Biomedical Sciences, Houston, Texas.